FIRE DETECTION ALGORITHMS USING MULTIMODAL SIGNAL AND IMAGE ANALYSIS

A DISSERTATION SUBMITTED TO
THE DEPARTMENT OF ELECTRICAL AND ELECTRONICS ENGINEERING
AND THE INSTITUTE OF ENGINEERING AND SCIENCE
OF BİLKENT UNIVERSITY
IN PARTIAL FULFILLMENT OF THE REQUIREMENTS
FOR THE DEGREE OF
DOCTOR OF PHILOSOPHY

By
Behçet Uğur Töreyin
January, 2009

I certify that I have read this thesis and that in my opinion it is fully adequate, in scope and in quality, as a dissertation for the degree of doctor of philosophy.

Prof. Dr. A. Enis Çetin (Supervisor)

I certify that I have read this thesis and that in my opinion it is fully adequate, in scope and in quality, as a dissertation for the degree of doctor of philosophy.

Prof. Dr. Orhan Arıkan

I certify that I have read this thesis and that in my opinion it is fully adequate, in scope and in quality, as a dissertation for the degree of doctor of philosophy.

Assoc. Prof. Dr. A. Aydın Alatan

I certify that I have read this thesis and that in my opinion it is fully adequate, in scope and in quality, as a dissertation for the degree of doctor of philosophy.

Assoc. Prof. Dr. Uğur Güdükbay

I certify that I have read this thesis and that in my opinion it is fully adequate, in scope and in quality, as a dissertation for the degree of doctor of philosophy.

Asst. Prof. Dr. Sinan Gezici

Approved for the Institute of Engineering and Science:

Prof. Dr. Mehmet B. Baray
Director of the Institute

ABSTRACT

FIRE DETECTION ALGORITHMS USING MULTIMODAL SIGNAL AND IMAGE ANALYSIS

Behçet Uğur Töreyin
Ph.D. in Electrical and Electronics Engineering
Supervisor: Prof. Dr. A. Enis Çetin
January, 2009

Dynamic textures are common in natural scenes. Examples of dynamic textures in video include fire, smoke, clouds, volatile organic compound (VOC) plumes in infra-red (IR) videos, trees in the wind, sea and ocean waves, etc. Researchers extensively studied 2-D textures and related problems in the fields of image processing and computer vision. On the other hand, there is very little research on dynamic texture detection in video. In this dissertation, signal and image processing methods developed for detection of a specific set of dynamic textures are presented.

Signal and image processing methods are developed for the detection of flames and smoke in open and large spaces with a range of up to 30m to the camera in visible-range (IR) video. Smoke is semi-transparent at the early stages of fire. Edges present in image frames with smoke start loosing their sharpness and this leads to an energy decrease in the high-band frequency content of the image. Local extrema in the wavelet domain correspond to the edges in an image. The decrease in the energy content of these edges is an important indicator of smoke in the viewing range of the camera. Image regions containing flames appear as fire-colored (bright) moving regions in (IR) video. In addition to motion and color (brightness) clues, the flame flicker process is also detected by using a Hidden Markov Model (HMM) describing the temporal behavior. Image frames are also analyzed spatially. Boundaries of flames are represented in wavelet domain. High frequency nature of the boundaries of fire regions is also used as a clue to model the flame flicker. Temporal and spatial clues extracted from the video are combined to reach a final decision.

Signal processing techniques for the detection of flames with pyroelectric (passive) infrared (PIR) sensors are also developed. The flame flicker process of an uncontrolled fire and ordinary activity of human beings and other objects are modeled using a set of Markov models, which are trained using the wavelet transform of the PIR sensor signal. Whenever there is an activity within the viewing range of the PIR sensor, the sensor signal is analyzed in the wavelet domain and the wavelet signals are fed to a set of Markov models. A fire or no fire decision is made according to the Markov model producing the highest probability.

Smoke at far distances ($>$ 100m to the camera) exhibits different temporal and spatial characteristics than nearby smoke and fire. This demands specific methods explicitly developed for smoke detection at far distances rather than using nearby smoke detection methods. An algorithm for vision-based detection of smoke due to wild fires is developed. The main detection algorithm is composed of four sub-algorithms detecting (i) slow moving objects, (ii) smoke-colored regions, (iii) rising regions, and (iv) shadows. Each sub-algorithm yields its own decision as a zero-mean real number, representing the confidence level of that particular sub-algorithm. Confidence values are linearly combined for the final decision.

Another contribution of this thesis is the proposal of a framework for active fusion of sub-algorithm decisions. Most computer vision based detection algorithms consist of several sub-algorithms whose individual decisions are integrated to reach a final decision. The proposed adaptive fusion method is based on the least-mean-square (LMS) algorithm. The weights corresponding to individual sub-algorithms are updated on-line using the adaptive method in the training (learning) stage. The error function of the adaptive training process is defined as the difference between the weighted sum of decision values and the decision of an oracle who may be the user of the detector. The proposed decision fusion method is used in wildfire detection.

Keywords: fire detection, flame detection, smoke detection, wildfire detection, computer vision, pyroelectric infra-red (PIR) sensor, dynamic textures, wavelet transform, Hidden Markov Models, the least-mean-square (LMS) algorithm, supervised learning, on-line learning, active learning.

ÖZET

ÇOKKİPLİ İŞARET VE İMGE ÇÖZÜMLEME TABANLI YANGIN TESPİT ALGORİTMALARI

Behçet Uğur Töreyin
Elektrik ve Elektronik Mühendisliği, Doktora
Tez Yöneticisi: Prof. Dr. A. Enis Çetin
Ocak, 2009

Dinamik dokular doğa görüntülerinde yaygın olarak bulunmaktadır. Videodaki dinamik doku örnekleri arasında ateş, duman, bulutlar, kızılberisi videoda uçucu organik bileşik gazları, rüzgarda sallanan ağaçlar, deniz ve okyanuslardaki dalgalar, vb. sayılabilir. Görüntü işleme ve bilgisayarlı görü alanlarındaki araştırmacılar yaygın olarak iki boyutlu dokular ve ilgili problemleri çalışmışlardır. Öte yandan, videodaki dinamik dokularla ilgili çalışma çok azdır. Bu tezde, özel bir çeşit dinamik doku tespiti için geliştirilen işaret ve imge işleme yöntemleri sunulmaktadır.

Görünür ve kızılberisi videoda, kameraya en fazla 30m mesafade bulunan açık ve geniş alanlardaki alev ve dumanın tespiti için işaret ve imge işleme yöntemleri geliştirilmiştir. Duman, yangınların ilk safhalarında yarı saydamdır. Duman içeren imge çerçevelerindeki ayrıtlar keskinliklerini kaybetmeye başlar ve bu da imgenin yüksek bant sıklık içeriğinde bir enerji azalmasına yol açar. Dalgacık etki alanındaki yerel en büyük değerler bir imgedeki ayrıtlara karşılık gelmektedir. Bu ayrıtlarda meydana gelen enerji düşmesi, kameranın görüş alanı içinde duman olduğunun önemli bir göstergesidir. Alev içeren imge bölgeleri (kızılberisi) videoda (parlak) ateş-renginde görünür. Hareket ve renk (parlaklık) özelliklerine ek olarak, alevdeki kırpışma, alevin zamansal hareketini betimleyen bir saklı Markov model kullanılarak tespit edilmektedir. İmge çerçeveleri uzamsal olarak da çözümlenmektedir. Alev çevritleri dalgacık domeninde temsil edilmektedir. Alevdeki kırpışmanın modellenmesi için ateş çevritinin yüksek sıklık özelliği de bir ipucu olarak kullanılmaktadır. Videodan çıkarılan zamansal ve uzamsal ipuçları son kararın alınması için birleştirilmektedir.

Alevin pyro-elektrik kızılberisi algılayıcılar (PIR) tarafından tespit edilebilmesi

için de işaret işleme yöntemleri geliştirilmiştir. Denetimsiz bir yangının alevlerindeki kırpışma süreci ile insan ve diğer sıcak nesneler tarafından yapılan sıradan hareketler, PIR algılayıcısı işaretine ait dalgacık dönüşümü katsayılarıyla eğitilen saklı Markov modelleriyle modellenmektedir. PIR algılayıcısının görüş alanı içinde bir hareketlilik meydana geldiğinde, algılayıcı işareti dalgacık etki alanında çözümlenmekte ve dalgacık işaretleri bir dizi Markov modeline beslenmektedir. Yangın var ya da yok kararı en yüksek olasılık değerini üreten Markov modeline göre alınmaktadır.

Uzak mesafedeki (kameraya mesafesi 100m'den büyük) duman, kameraya daha yakında cereyan eden bir yangın neticesinde oluşan dumandan daha farklı zamansal ve uzamsal özellikler sergilemektedir. Bu da yakın mesafe dumanlarının tespiti için geliştirilen yöntemleri kullanmak yerine, uzak mesafedeki duman tespiti için özel yöntemler geliştirilmesi gereğini doğurmaktadır. Orman yangınlarından kaynaklanan dumanın tespit edilmesi için görüntü tabanlı bir algoritma geliştirilmiştir. Ana tespit algoritması (i) yavaş hareket eden nesneleri, (ii) duman rengindeki bölgeleri, (iii) yükselen bölgeleri, ve (iv) gölgeleri tespit eden dört alt-algoritmadan oluşmaktadır. Herbir alt-algoritma kendi kararını, güven seviyesinin bir göstergesi olarak sıfır ortalamalı gerçel bir sayı şeklinde üretmektedir. Bu güven değerleri son kararın verilmesi için doğrusal olarak birleştirilmektedir.

Bu tezin bir diğer katkısı da alt-algoritma kararlarının etkin bir şekilde birleştirilmesi için bir çerçeve yapı önermesidir. Bilgisayarlı görü tabanlı pekçok tespit algoritması, son kararın verilmesinde ayrı ayrı kararlarının birleştirildiği çeşitli alt-algoritmalardan oluşmaktadır. Önerilen uyarlanır birleştirme yöntemi en küçük-ortalama-kare algoritmasına dayanmaktadır. Herbir alt-algoritmaya ait ağırlık, eğitim (öğrenme) aşamasında çevrimiçi olarak uyarlanır yöntemle güncellenmektedir. Uyarlanır eğitim sürecindeki hata fonksiyonu, karar değerlerinin ağırlıklı toplamıyla kullanıcının kararı arasındaki fark olarak tanımlanmıştır. Önerilen karar birleştirme yöntemi orman yangını tespitinde kullanılmıştır.

Anahtar sözcükler: yangın tespiti, alev tespiti, duman tespiti, orman yangını tespiti, bilgisayarlı görü, pyro-elektrik kızılberisi algılayıcı, dinamik dokular, dalgacık dönüşümü, saklı Markov modelleri, en küçük-ortalama-kare algoritması, güdümlü öğrenme, çevrimiçi öğrenme, etkin öğrenme.

Acknowledgement

I would like to express my gratitude to my supervisor Prof. Enis Çetin for his guidance and contributions at all stages of this work. He was much more than an academic advisor. I was very fortunate to have such a wise person as my supervisor.

I am also very grateful to Prof. Uğur Güdükbay and Prof. Orhan Arıkan for their support, suggestions and encouragement during the development of this thesis and throughout my PhD studies.

I would also like to express my sincere thanks to Prof. Aydın Alatan and Prof. Sinan Gezici for accepting to read and review this thesis and providing useful comments.

I want to thank Dr. Bilgay Akhan for drawing our attention to fire detection problems in video, in the early days of my graduate studies.

I wish to thank all of my friends and colleagues at İSYAM and our department for their collaboration and support. My special thanks go to Erdem Dengel, Yiğithan Dedeoğlu, Birey Soyer, İbrahim Onaran, Kıvanç Köse, Onay Urfalıoğlu, Osman Günay, and Kasım Taşdemir. I would also like to thank our department's legendary secretary Mürüvet Parlakay for her assistance during my years in Bilkent.

I would like to extend my thanks to the administrative staff and personnel of General Directorate of Forestry: Mr. Osman Kahveci, Mr. Nurettin Doğan, Mr. İlhami Aydın, Mr. İsmail Belen, and Mr. Ahmet Ulukanlıgil for their collaboration.

I am indebted to my parents, my sister and my brother for their continuous support and encouragement throughout my life.

It is a pleasure to express my special thanks to my wife and my son for their endless love and understanding at all stages of my graduate studies.

This work was supported in part by the Scientific and Technical Research Council of Turkey, TÜBİTAK with grant numbers 105E065, 105E121, and 106G126 and in part by the European Commission with grant no. FP6-507752 MUSCLE NoE project.

Contents

List of Figures

List of Tables

Chapter 1

Introduction

Dynamic textures are common in many image sequences of natural scenes. Examples of dynamic textures in video include fire, smoke, clouds, volatile organic compound (VOC) plumes in infra-red (IR) videos, trees in the wind, sea and ocean waves, as well as traffic scenes, motion of crowds, all of which exhibit some sort of spatio-temporal stationarity. They are also named as temporal or 3-D textures in the literature. Researchers extensively studied 2-D textures and related problems in the fields of image processing and computer vision [32], [30]. On the other hand, there is comparably less research conducted on dynamic texture detection in video [18], [63], [12].

There are several approaches in the computer vision literature aiming at recognition and synthesis of dynamic textures in video independent of their types [71], [15], [16], [50], [29], [51], [33], [35], [89], [48], [49], [57], [79], [55], [96], [62], [75], [28], [68], [90]. Some of these approaches model the dynamic textures as linear dynamical systems [71], [15], [16], [50], some others use spatio-temporal auto-regressive models [48], [79]. Other researchers in the field analyze and model the optical flow vectors for the recognition of generic dynamic textures in video [29], [89]. In this dissertation, we do not attempt to characterize all dynamic textures but we present smoke and fire detection methods by taking advantage of specific properties of smoke and fire.

The motivation behind attacking a specific kind of recognition problem is influenced by the notion of 'weak' Artificial Intelligence (AI) framework which was first introduced by Hubert L. Dreyfus in his critique of the so called 'generalized' AI [25], [26]. Dreyfus presents solid philosophical and scientific arguments on why the search for 'generalized' AI is futile [61]. Current content based general image and video content understanding methods are not robust enough to be deployed for fire detection [21], [53], [43], [54]. Instead, each specific problem should be addressed as an individual engineering problem which has its own characteristics. In this study, both temporal and spatial characteristics related to flames and smoke are utilized as clues for developing solutions to the detection problem.

Another motivation for video and pyroelectric infra-red (PIR) sensor based fire detection is that conventional point smoke and fire detectors typically detect the presence of certain particles generated by smoke and fire by ionization or photometry. An important weakness of point detectors is that they cannot provide quick responses in large spaces. Furthermore, conventional point detectors cannot be utilized to detect smoldering fires in open areas.

In this thesis, novel image processing methods are proposed for the detection of flames and smoke in open and large spaces with ranges up to 30m. Flicker process inherent in fire is used as a clue for detection of flames and smoke in (IR) video. A similar technique modeling flame flicker is developed for the detection of flames using PIR sensors. Wildfire smoke appearing far away from the camera has different spatio-temporal characteristics than nearby smoke. The algorithms for detecting smoke due to wildfire are also proposed.

Each detection algorithm consists of several sub-algorithms each of which tries to estimate a specific feature of the problem at hand. For example, long distance smoke detection algorithm consists of four sub-algorithms: (i) slow moving video object detection, (ii) smoke-colored region detection, (iii) rising video object detection, (iv) shadow detection and elimination. A framework for active fusion of decisions from these sub-algorithms is developed based on the least-mean-square (LMS) adaptation algorithm.

No fire detection experiments were carried out using other sensing modalities such as ultra-violet (UV) sensors, near infrared (NIR) or middle wave-length infrared (MWIR) cameras, in this study. As a matter of fact, MWIR cameras are even more expensive than LWIR cameras. Therefore, deploying MWIR cameras for fire monitoring turns out to be an unfeasible option for most practical applications.

There are built-in microphones in most of the off-the-shelf surveillance cameras. Audio data captured from these microphones can be also analyzed along with the video data in fire monitoring applications. One can develop fire detection methods exploiting data coming from several sensing modalities similar to methods described in [31], [85], [88], [24].

1.1 Contribution of this Thesis

The major contributions of this thesis can be divided into two main categories.

1.1.1 Markov Models Using Wavelet Domain Features for Short Range Flame and Smoke Detection

A common feature of all the algorithms developed in this thesis is the use of wavelets and Markov models. In the proposed approach wavelets or sub-band analysis are used in dynamic texture modeling. This leads to computationally efficient algorithms for texture feature analysis, because computing wavelet coefficients is an Order-(N) type operation. In addition, we do not try to determine edges or corners in a given scene. We simply monitor the decay or increase in wavelet coefficients' sub-band energies both temporally and spatially.

Another important feature of the proposed smoke and fire detection methods is the use of Markov models to characterize temporal motion in the scene. Turbulent fire behavior is a random phenomenon which can be conveniently modeled in a

Markovian setting.

In the following sub-sections, the general overview of the proposed algorithms are developed. In all methods, it is assumed that a stationary camera monitors the scene.

1.1.1.1 Flame Detection in Visible Range Video

Novel real-time signal processing techniques are developed to detect flames by processing the video data generated by a visible range camera. In addition to motion and color clues used by [64], flame flicker is detected by analyzing the video in wavelet domain. Turbulent behavior in flame boundaries is detected by performing temporal wavelet transform. Wavelet coefficients are used as feature parameters in Hidden Markov Models (HMMs). A Markov model is trained with flames and another is trained with ordinary activity of human beings and other flame colored moving objects. Flame flicker process is also detected by using an HMM. Markov models representing the flame and flame colored ordinary moving objects are used to distinguish flame flicker process from motion of flame colored moving objects.

Other clues used in the fire detection algorithm include irregularity of the boundary of the fire colored region and the growth of such regions in time. All these clues are combined to reach a final decision. The main contribution of the proposed video based fire detection method is the analysis of the flame flicker and integration of this clue as a fundamental step in the detection process.

1.1.1.2 Flame Detection in IR Video

A novel method to detect flames in videos captured with Long-Wavelength Infra-Red (LWIR) cameras is proposed, as well. These cameras cover 8-12μm range in the electromagnetic spectrum. Image regions containing flames appear as bright regions in IR video. In addition to motion and brightness clues, flame flicker process is also detected by using an HMM describing the temporal behavior as in

the previous algorithm. IR image frames are also analyzed spatially. Boundary of flames are represented in wavelet domain and high frequency nature of the boundaries of fire regions is also used as a clue to model the flame flicker.

All of the temporal and spatial clues extracted from the IR video are combined to reach a final decision. False alarms due to ordinary bright moving objects are greatly reduced because of the HMM based flicker modeling and wavelet domain boundary modeling. The contribution of this work is the introduction of a novel sub-band energy based feature for the analysis of flame region boundaries.

1.1.1.3 Short-range Smoke Detection in Video

Smoldering smoke appears first, even before flames, in most fires. Contrary to the common belief, smoke cannot be visualized in LWIR (8-12μm range) video. A novel method to detect smoke in video is developed.

The smoke is semi-transparent at the early stages of a fire. Therefore edges present in image frames start loosing their sharpness and this leads to a decrease in the high frequency content of the image. The background of the scene is estimated and decrease of high frequency energy of the scene is monitored using the spatial wavelet transforms of the current and the background images.

Edges of the scene produce local extrema in the wavelet domain and a decrease in the energy content of these edges is an important indicator of smoke in the viewing range of the camera. Moreover, scene becomes grayish when there is smoke and this leads to a decrease in chrominance values of pixels. Random behavior in smoke boundaries is also analyzed using an HMM mimicking the temporal behavior of the smoke. In addition, boundaries of smoke regions are represented in wavelet domain and high frequency nature of the boundaries of smoke regions is also used as a clue to model the smoke flicker. All these clues are combined to reach a final decision.

Monitoring the decrease in the sub-band image energies corresponding to smoke regions in video constitutes the main contribution of this work.

1.1.1.4 Flame Detection Using PIR sensors

A flame detection system based on a pyroelectric (or passive) infrared (PIR) sensor is developed. This algorithm is similar to the video flame detection algorithm. The PIR sensor can be considered as a single pixel camera. Therefore an algorithm for flame detection for PIR sensors can be developed by simply removing the spatial analysis steps of the video flame detection method.

The flame detection system can be used for fire detection in large rooms. The flame flicker process of an uncontrolled fire and ordinary activity of human beings and other objects are modeled using a set of Hidden Markov Models (HMM), which are trained using the wavelet transform of the PIR sensor signal. Whenever there is an activity within the viewing range of the PIR sensor system, the sensor signal is analyzed in the wavelet domain and the wavelet signals are fed to a set of HMMs. A fire or no fire decision is made according to the HMM producing the highest probability.

1.1.2 Wildfire Detection with Active Learning Based on the LMS Algorithm

Wildfire smoke has different spatio-temporal characteristics than nearby smoke, because wildfire usually starts far away from forest look-out towers. The main wildfire (long-range smoke) detection algorithm is composed of four sub-algorithms detecting (i) slow moving objects, (ii) smoke-colored regions, (iii) rising regions, and (iv) shadows. Each sub-algorithm yields its own decision as a zero-mean real number, representing the confidence level of that particular sub-algorithm. Confidence values are linearly combined with weights determined according to a novel active fusion method based on the least-mean-square (LMS) algorithm which is a widely used technique in adaptive filtering. Weights are updated on-line using the LMS method in the training (learning) stage. The error function of the LMS based training process is defined as the difference between the weighted sum of decision values and the decision of an oracle, who is the

security guard of the forest look-out tower.

The contribution of this work is twofold; a novel video based wildfire detection method and a novel active learning framework based on the LMS algorithm. The proposed adaptive fusion strategy can be used in many supervised learning based computer vision applications comprising of several sub-algorithms.

1.2 Thesis Outline

The outline of the thesis is as follows. In Chapters 2 and 3, wavelet and HMM based methods for flame detection in visible and IR range video are presented, respectively. The short-range smoke detection algorithm is presented in Chapter 4. Detection of flames using PIR sensors is discussed in Chapter 5. In Chapter 6, wildfire (long-range smoke) detection with active learning based on the LMS algorithm is described. Finally Chapter 7 concludes this thesis by providing an overall summary of the results. Possible research areas in the future are provided, as well.

The organization of this thesis is presented in Table 1.1. Note that, smoke detection methods could only be developed for visible range cameras due to the fact that smoke cannot be visualized with PIR sensors and LWIR cameras.

Table 1.1: Organization of this thesis.

Sensor type	Flame	Short-range ($< 30m$) Smoke	Long distance ($> 100m$) Smoke
Visible Range Camera	Chapter 2	Chapter 4	Chapter 6
LWIR Camera	Chapter 3	N/A	N/A
PIR Sensor	Chapter 5	N/A	N/A

Chapter 2

Flame Detection in Visible Range Video

In this chapter, the previous work in the literature on video based fire detection is summarized, first. Then, the proposed wavelet analysis and Markov model based detection method characterizing the flame flicker process is described. Markov model based approach reduces the number of false alarms issued to ordinary fire-colored moving objects as compared to the methods using only motion and color clues. Experimental results show that the proposed method is successful in detecting flames.

2.1 Related Work

Video based fire detection systems can be useful for detecting fire in covered areas including auditoriums, tunnels, atriums, etc., in which conventional chemical fire sensors cannot provide quick responses to fire. Furthermore, closed circuit television (CCTV) surveillance systems are currently installed in various public places monitoring indoors and outdoors. Such systems may gain an early fire detection capability with the use of a fire detection software processing the outputs of CCTV cameras in real time.

There are several video-based fire and flame detection algorithms in the literature [64], [17], [48], [78], [38], [81], [80], [94]. These methods make use of various visual signatures including color, motion and geometry of fire regions. Healey et al. [38] use only color clues for flame detection. Phillips et al. [64] use pixel colors and their temporal variations. Chen et al. [17] utilize a change detection scheme to detect flicker in fire regions. In [78], Fast Fourier Transforms (FFT) of temporal object boundary pixels are computed to detect peaks in Fourier domain, because it is claimed that turbulent flames flicker with a characteristic flicker frequency of around 10 Hz independent of the burning material and the burner in a mechanical engineering paper [1], [14]. We observe that flame flicker process is a wide-band activity below 12.5 Hz in frequency domain for a pixel at the boundary of a flame region in a color-video clip recorded at 25 fps (cf. Fig. 2.1). Liu and Ahuja [48] also represent the shapes of fire regions in Fourier domain. However, an important weakness of Fourier domain methods is that flame flicker is not purely sinusoidal but it's random in nature. Therefore, there may not be any peaks in FFT plots of fire regions. In addition, Fourier Transform does not have any time information. Therefore, Short-Time Fourier Transform (STFT) can be used requiring a temporal analysis window. In this case, temporal window size becomes an important parameter for detection. If the window size is too long, one may not observe peakiness in the FFT data. If it is too short, one may completely miss cycles and therefore no peaks can be observed in the Fourier domain.

Our method not only detects fire and flame colored moving regions in video but also analyzes the motion of such regions in wavelet domain for flicker estimation. The appearance of an object whose contours, chrominance or luminosity values oscillate at a frequency higher than 0.5 Hz in video is an important sign of the possible presence of flames in the monitored area [78].

High-frequency analysis of moving pixels is carried out in wavelet domain in our work. There is an analogy between the proposed wavelet domain motion analysis and the temporal templates of [21] and the motion recurrence images of [43], which are ad hoc tools used by computer scientists to analyze dancing people and periodically moving objects and body parts. However, temporal templates

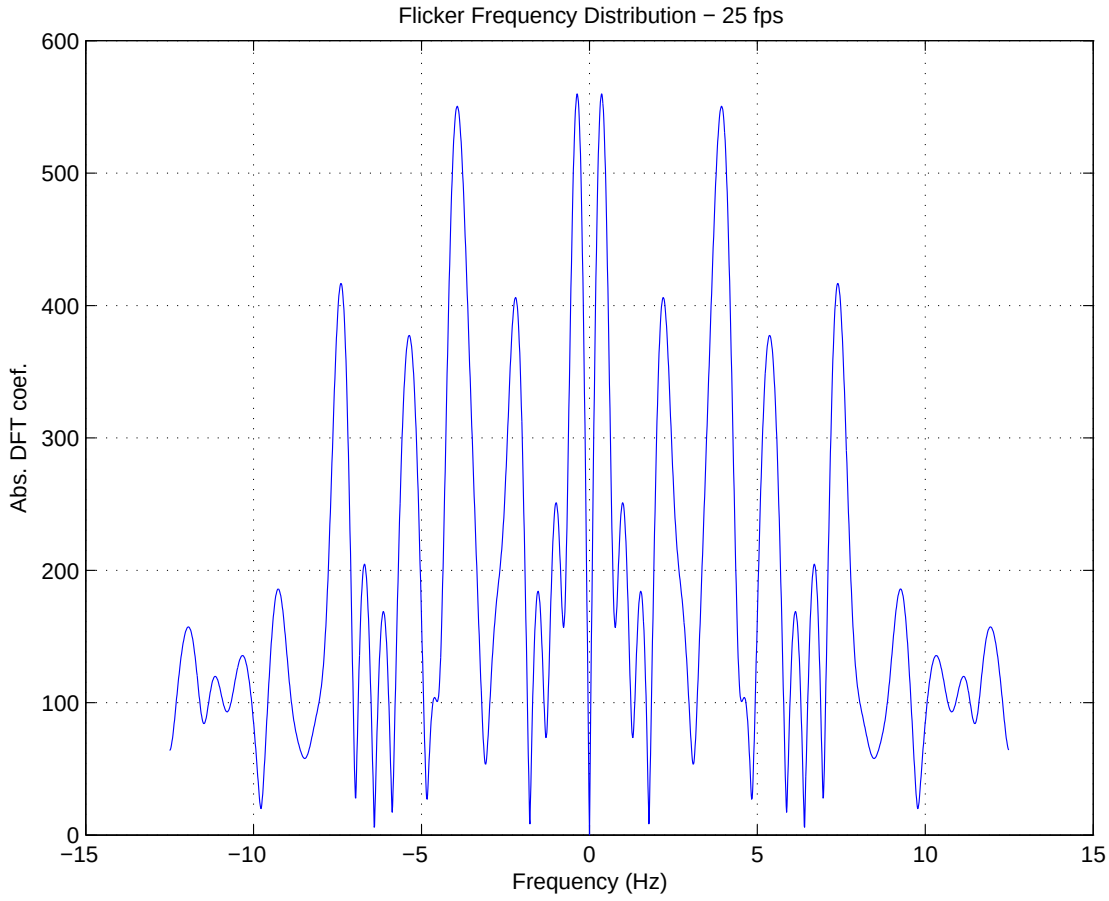

Figure 2.1: Flicker frequency distribution for a pixel at the boundary of a flame region in a color-video clip recorded at 25 fps. This frequency distribution is obtained by analyzing the temporal variations in the red channel value of the pixel.

and motion recurrence images do not provide a quantitative frequency domain measure. On the other hand, wavelet transform is a time-frequency analysis tool providing both partial frequency and time information about the signal. One can examine an entire frequency band in the wavelet domain without completely loosing the time information [10], [52]. Since the wavelet transform is computed using a subband decomposition filter bank, it does not require any batch processing. It is ideally suited to determine an increase in high-frequency activity in fire and flame colored moving objects by detecting zero crossings of the wavelet transform coefficients.

In practice, flame flicker process is time-varying and it is far from being periodic. This stochastic behavior in flicker frequency is especially valid for uncontrolled fires. Therefore, a random model based modeling of flame flicker process produces more robust performance compared to frequency domain based methods which try to detect peaks around 10 Hz in the Fourier domain. In [84], fire and flame flicker is modeled by using HMMs trained with pixel domain features in video. In this thesis, temporal wavelet coefficients are used as feature parameters in Markov models.

Turbulent high-frequency behaviors exist not only on the boundary but also inside a fire region. Another novelty of the proposed method is the analysis of the spatial variations inside fire and flame colored regions. The method described in [78] does not take advantage of such color variations. Spatial wavelet analysis makes it possible to detect high-frequency behavior inside fire regions. Variation in energy of wavelet coefficients is an indicator of activity within the region. On the other hand, a fire colored moving object will not exhibit any change in values of wavelet coefficients because there will not be any variation in fire colored pixel values. Spatial wavelet coefficients are also used in Markov models to characterize the turbulent behavior within fire regions.

2.2 Steps of Video Flame Detection Algorithm

The proposed video-based fire detection algorithm consists of four sub-algorithms: (i) moving pixels or regions in the current frame of a video are determined, (ii) colors of moving pixels are checked to see if they match to pre-specified fire colors. Afterwards, wavelet analysis in (iii) temporal and (iv) spatial domains are carried out to determine high-frequency activity within these moving regions. Each step of the proposed algorithm is explained in detail in the sequel.

2.2.1 Moving Region Detection

Background subtraction is commonly used for segmenting out moving objects in a scene for surveillance applications. There are several methods in the literature [19], [3], [77]. The background estimation algorithm described in [19] uses a simple IIR filter applied to each pixel independently to update the background and use adaptively updated thresholds to classify pixels into foreground and background.

Stationary pixels in the video are the pixels of the background scene because the background can be defined as temporally stationary part of the video.If the scene is observed for some time, then pixels forming the entire background scene can be estimated because moving regions and objects occupy only some parts of the scene in a typical image of a video. A simple approach to estimate the background is to average the observed image frames of the video. Since moving objects and regions occupy only a part of the image, they conceal a part of the background scene and their effect is canceled over time by averaging. Our main concern is real-time performance of the system. In Video Surveillance and Monitoring (VSAM) Project at Carnegie Mellon University [19] a recursive background estimation method was developed from the actual image data using $\ell 1$-norm based calculations.

Let $I(x, n)$ represent the intensity value of the pixel at location x in the $n-th$ video frame I. Estimated background intensity value, $B(x, n+1)$, at the same

pixel position is calculated as follows:

$$B(x,n+1) = \begin{cases} aB(x,n) + (1-a)I(x,n) & \text{if } x \text{ is stationary} \\ B(x,n) & \text{if } x \text{ is a moving pixel} \end{cases} \tag{2.1}$$

where $B(x,n)$ is the previous estimate of the background intensity value at the same pixel position. The update parameter a is a positive real number close to one. Initially, $B(x,0)$ is set to the first image frame $I(x,0)$. A pixel positioned at x is assumed to be moving if:

$$|I(x,n) - I(x,n-1)| > T(x,n) \tag{2.2}$$

where $I(x,n-1)$ is the intensity value of the pixel at location x in the $(n-1)-th$ video frame I and $T(x,n)$ is a recursively updated threshold at each frame n, describing a statistically significant intensity change at pixel position x:

$$T(x,n+1) = \begin{cases} aT(x,n) + (1-a)(c|I(x,n) - B(x,n)|) & \text{if } x \text{ is stationary} \\ T(x,n) & \text{if } x \text{ is a moving pixel} \end{cases} \tag{2.3}$$

where c is a real number greater than one and the update parameter a is a positive number close to one. Initial threshold values are set to a pre-determined non-zero value.

Both the background image $B(x,n)$ and the threshold image $T(x,n)$ are statistical blue prints of the pixel intensities observed from the sequence of images $\{I(x,k)\}$ for $k < n$. The background image $B(x,n)$ is analogous to a local temporal average of intensity values, and $T(x,n)$ is analogous to c times the local temporal standard deviation of intensity in $\ell 1$-norm [19].

As it can be seen from Eq. 2.3, the higher the parameter c, higher the threshold or lower the sensitivity of detection scheme. It is assumed that regions significantly different from the background are moving regions. Estimated background image is subtracted from the current image to detect moving regions which corresponds to the set of pixels satisfying:

$$|I(x,n) - B(x,n)| > T(x,n) \tag{2.4}$$

are determined. These pixels are grouped into connected regions (blobs) and labeled by using a two-level connected component labeling algorithm [40]. The

output of the first step of the algorithm is a binary pixel map *Blobs(x,n)* that indicates whether or not the pixel at location x in $n-th$ frame is moving.

Other more sophisticated methods, including the ones developed by Bagci et al. [3] and Stauffer and Grimson [77], can also be used for moving pixel estimation. In our application, accurate detection of moving regions is not as critical as in other object tracking and estimation problems; we are mainly concerned with real-time detection of moving regions as an initial step in the fire and flame detection system. We choose to implement the method suggested by Collins et al. [19], because of its computational efficiency.

2.2.2 Detection of Fire Colored Pixels

Color values of moving pixels are compared with a pre-determined color distribution, which represents possible flame colors in video in RGB color space. The flame color distribution is obtained from sample images containing flame regions. The cloud is represented by using mixture of Gaussians in the RGB color space as described in [69] and [77].

Similar to the model in [77], the values of a particular pixel corresponding to a flame region is considered as a 'flame pixel process'. The 'flame pixel process' is a time series of RGB vectors of pixels in a flame region. Let $I(x,n)$ be a pixel at location x of the image frame at time step n with color values $r_I(x,n)$, $g_I(x,n)$, and $b_I(x,n)$ corresponding to red, green and blue channels. At any time step n, the history of the pixel vectors are known:

$$\{Q_1, ..., Q_n\} = \{[r_I(x,m), g_I(x,m), b_I(x,m)] : 1 \leq m \leq n\} \tag{2.5}$$

where $Q_m = [r_I(x,m), g_I(x,m), b_I(x,m)]$, represents the RGB color vector for the pixel at location x and time step m.

A sample 'flame pixel process' is shown in Fig. 2.2 (a). It represents a flame color distribution in RGB color space corresponding to a particular fire. Different color distributions and flame pixel processes can be obtained by observing different types of fire depending on the burning material.

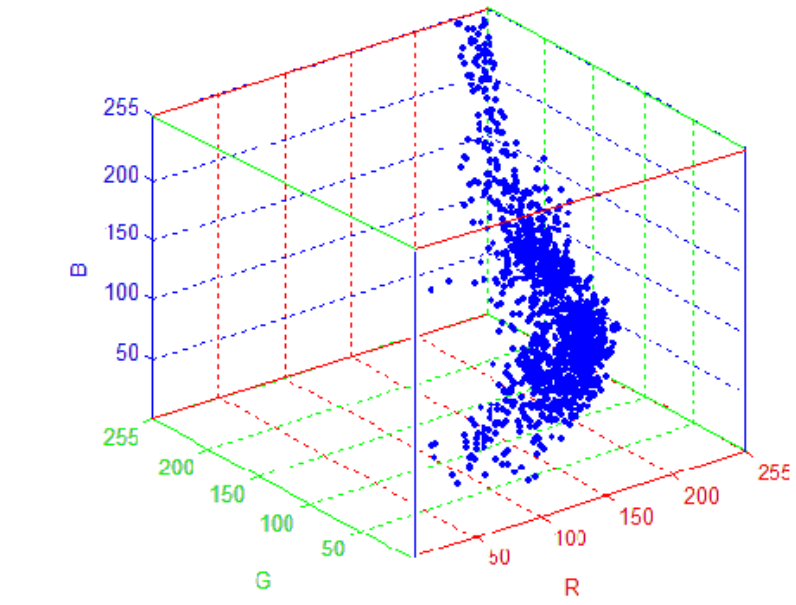

(a)

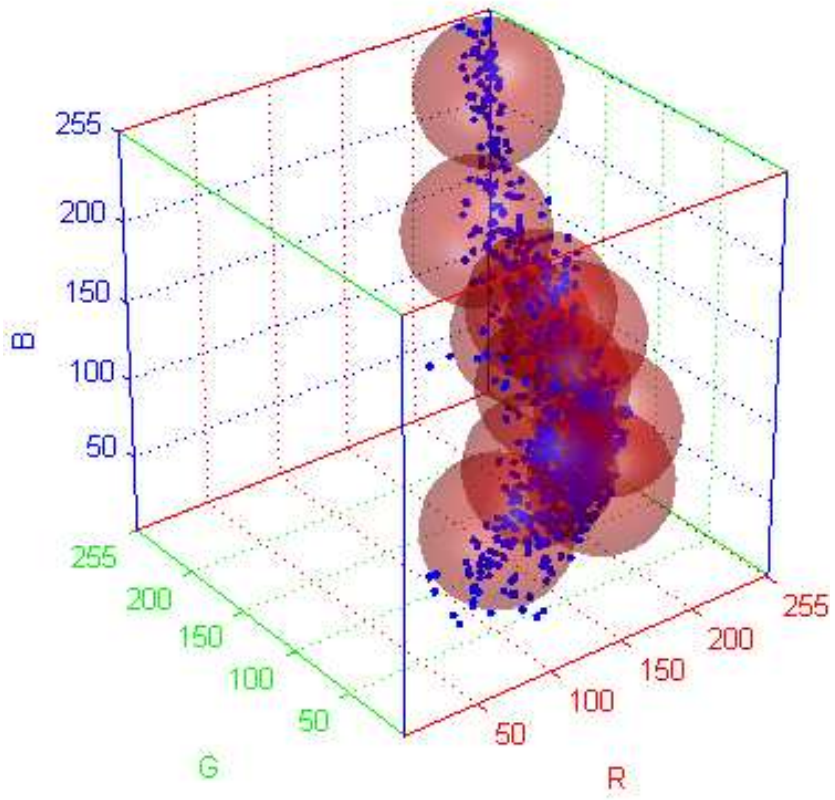

(b)

Figure 2.2: (a) A sample flame pixel process in *RGB* space, and (b) the spheres centered at the means of the Gaussian distributions with radius twice the standard deviation.

A Gaussian mixture model with D Gaussian distributions is used to model the past observations $\{Q_1, ..., Q_n\}$

$$P(Q_n) = \sum_{d=1}^{D} \eta(Q_n|\mu_{d,n}, \Sigma_{d,n}) \tag{2.6}$$

where D is the number of distributions, $\mu_{d,n}$ is the mean value of the d-th Gaussian in the mixture at time step n, $\Sigma_{d,n}$ is the covariance matrix of the d-th Gaussian in the mixture at time step n, and η is a Gaussian probability density function

$$\eta(Q|\mu, \Sigma) = \frac{1}{(2\pi)^{\frac{n}{2}}|\Sigma|^{\frac{1}{2}}} e^{-\frac{1}{2}(Q-\mu)^T\Sigma^{-1}(Q-\mu)} \tag{2.7}$$

In our implementation, we model the flame color distribution with $D = 10$ Gaussians. In order to lower computational cost, red, blue and green channel values of pixels are assumed to be independent and have the same variance [77]. This assumption results in a covariance matrix of the form:

$$\Sigma_{d,n} = \sigma_d^2 \mathbf{I} \tag{2.8}$$

where $\mathbf{I}$ is the 3-by-3 identity matrix.

In the training phase, each observation vector, Q_n, is checked with the existing D distributions for a possible match. In the preferred embodiment, a match is defined as an RGB vector within 2 standard deviations of a distribution. If none of the D distributions match the current observation vector, Q_n, the least probable distribution is replaced with a distribution with the current observation vector as its mean value and a high initial variance.

The mean and the standard deviation values of the un-matched distributions are kept the same. However, both the mean and the variance of the matching distribution with the current observation vector, Q_n, are updated. Let the matching distribution with the current observation vector, Q_n, be the d-th Gaussian with mean $\mu_{d,n}$ and standard deviation $\sigma_{d,n}$. The mean, $\mu_{d,n}$, of the matching distribution is updated as:

$$\mu_{d,n} = (1 - c)\mu_{d,n-1} + cQ_n \tag{2.9}$$

and the variance, $\sigma_{d,n}^2$, is updated as:

$$\sigma_{d,n}^2 = (1 - c)\sigma_{d,n-1}^2 + c(Q_n - \mu_{d,n})^T(Q_n - \mu_{d,n}) \tag{2.10}$$

Table 2.1: The mean red, green and blue channel values and variances of ten Gaussian distributions modeling flame color in Fig. 2.2 (b) are listed.

Distribution	Red	Green	Blue	Variance
1	121.16	76.87	43.98	101.16
2	169.08	84.14	35.20	102.77
3	177.00	104.00	62.00	100.00
4	230.42	113.78	43.71	107.22
5	254.47	214.66	83.08	100.11
6	254.97	159.06	151.00	100.08
7	254.98	140.98	141.93	100.39
8	254.99	146.95	102.99	99.57
9	255.00	174.08	175.01	101.01
10	255.00	217.96	176.07	100.78

where

$$c = \eta(Q_n|\mu_{d,n}, \Sigma_{d,n}) \tag{2.11}$$

A Gaussian mixture model with ten Gaussian distributions is presented in Fig. 2.2 (b). In this figure, spheres centered at the mean values of Gaussians have radii twice the corresponding standard deviations. The mean red, green and blue values and variances of Gaussian distributions in Fig. 2.2 (b) are listed in Table 2.1.

Once flame pixel process is modeled and fixed in the training phase, the *RGB* color vector of a pixel is checked whether the pixel lies within two standard deviations of the centers of the Gaussians to determine its nature. In other words, if a given pixel color value is inside one of the spheres shown in Fig. 2.2 (b), then it is assumed to be a fire colored pixel. We set a binary mask, called *FireColored*, which returns whether a given pixel is fire colored or not. The intersection of this mask with *Blobs* formed in the first step is fed into the next step as a new binary mask called *Fire*.

2.2.3 Temporal Wavelet Analysis

The third step of our fire detection algorithm is to keep track of the frequency history of pixels in the fire colored region and analyze the history. In order to detect flicker or oscillations in pixels due to fire in a reliable manner, the video capture rate should be high enough to capture high-frequency flicker in flames. To capture 10 Hz flicker, the video should capture at least 20 frames per second (fps). However, in some surveillance systems, the video capture rate is below 20 Hz. If the video is available at a lower capture rate, aliasing occurs but flicker due to flames can still be observed in the video. For example, 8 Hz sinusoid appears as 2 Hz sinusoid in a 10 fps video.

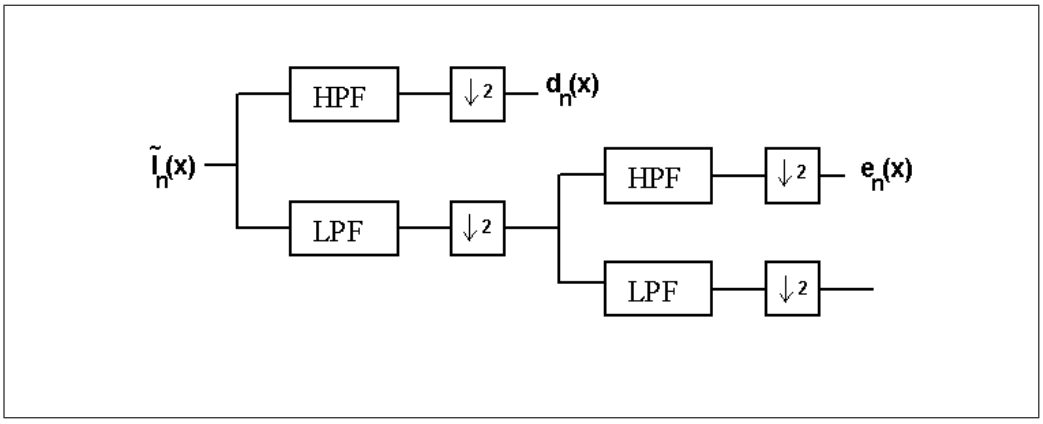

Figure 2.3: A two-stage filter bank. HPF and LPF represent half-band high-pass and low-pass filters, with filter coefficients $\{-\frac{1}{4}, \frac{1}{2}, -\frac{1}{4}\}$ and $\{\frac{1}{4}, \frac{1}{2}, \frac{1}{4}\}$, respectively. This filter bank is used for wavelet analysis.

Each pixel $I(x, n)$ at location x in the image frame at time step n which also belongs to the binary mask *Fire* is fed to a two stage-filter bank as shown in Fig. 2.3. The signal $\tilde{I}_n(x)$ is a one-dimensional signal representing the temporal variations in color values of the pixel $I(x, n)$ at location x in the $n - th$ image frame. Temporal wavelet analysis can be carried out using either the luminance (Y component) in YUV color representation or the red component in RGB color representation. In our implementation the red channel values of the pixels are used. The two-channel subband decomposition filter bank is composed of half-band high-pass and low-pass filters with filter coefficients $\{-\frac{1}{4}, \frac{1}{2}, -\frac{1}{4}\}$ and

$\{\frac{1}{4}, \frac{1}{2}, \frac{1}{4}\}$, respectively, as shown in Fig. 2.3. The filter bank produces wavelet subsignals $d_n(x)$ and $e_n(x)$. If there is high frequency activity at pixel location x, high-band subsignals d and e get non-zero values. However, in a stationary pixel, the values of these two subsignals should be equal to zero or very close to zero because of high-pass filters used in subband analysis. If the pixel is part of a flame boundary at some time (see Fig. 2.4), then there will be several spikes in one second due to transitions from background colors to flame colors and vice versa. If there is an ordinary fire-colored moving object going through pixel at location x, then there will be a single spike in one of these wavelet subsignals because of the transition from the background pixel to the object pixel as shown in Fig. 2.5. The number of zero crossings of the subband signals d_n and e_n in a few seconds can be used to discriminate between a flame pixel and an ordinary fire colored object pixel. If this number is above some threshold, then an alarm can be issued for this pixel.

The temporal history of the red channel of a pixel at location $x = (111,\ 34)$ which is part of a flame, and the corresponding wavelet signals are shown in Fig. 2.4. A flicker in the red channel values of this flame pixel is obvious from the figure. The pixel is part of a flame for image frames with time steps n=1, 2, 3, 19, 23, 24, 41 and 50. It becomes part of the background for n=12,...,17, 20, 21, 26, 27, 31,...,39, 45, 52,..., and 60. Wavelet domain subsignals d_n and e_n reveal the fluctuations of the pixel at location $x = (111,\ 34)$ with several zero crossings. Due to a down-sampling operation during wavelet computation, the length of wavelet signals are halved after each stage of subband filtering. As a result, the value of a sample in a subband signal corresponds to several samples in the original signal, e.g., the value of $d_5(111, 34)$ corresponds to the values of $\tilde{I}_{10}(111, 34)$ and $\tilde{I}_{11}(111, 34)$, and the value of $e_4(111, 34)$ corresponds to the values of $\tilde{I}_{12}(111, 34)$, $\tilde{I}_{13}(111, 34)$, $\tilde{I}_{14}(111, 34)$ and $\tilde{I}_{15}(111, 34)$, in the original signal.

The temporal history of the red channel of a pixel at location $x = (18,\ 34)$, which is part of a fire colored object, and the corresponding wavelet signals are shown in Fig. 2.5. As shown in this figure, neither the original nor the wavelet signals exhibit oscillatory behavior. The pixel is part of a white-colored background for n=1, 2, and 3, becomes part of a fire colored object for n=4, 5, 6, 7,

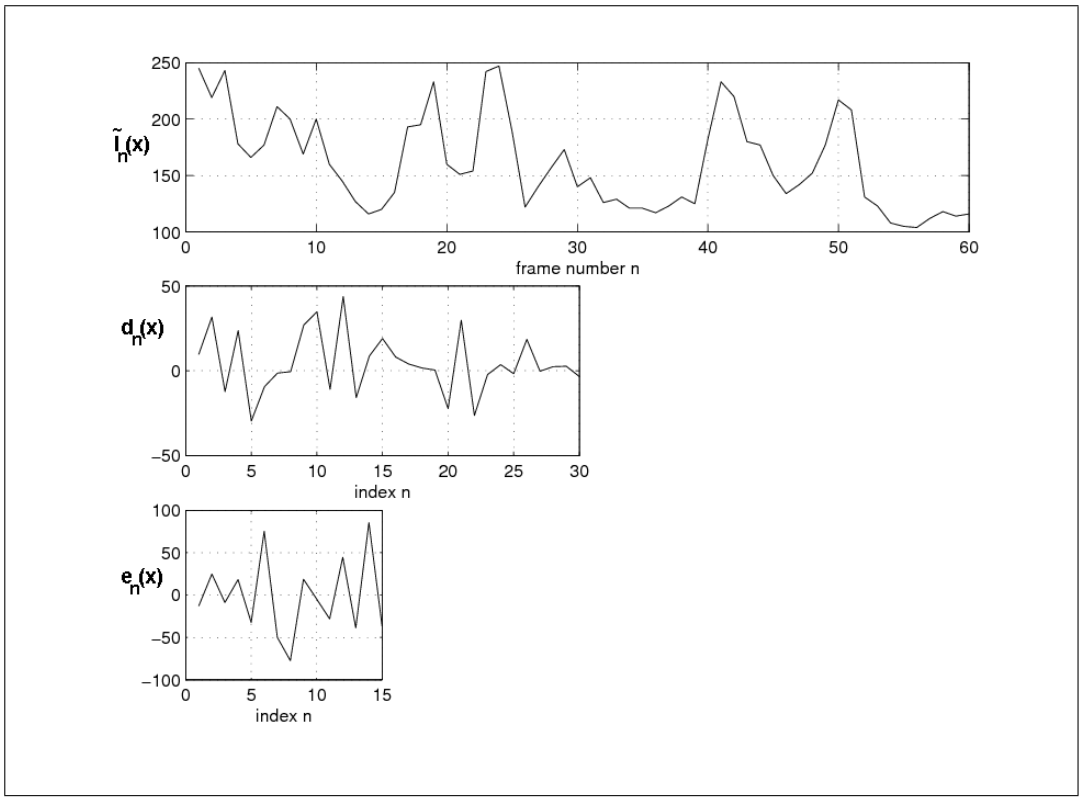

Figure 2.4: (a) Temporal variation of image pixel at location $x = (111,\ 34)$, $\tilde{I}_n(x)$. The pixel at $x = (111,\ 34)$ is part of a flame for image frames $I(x, n)$, n=1, 2, 3, 19, 23, 24, 41 and 50. It becomes part of the background for n = 12,..., 17, 20, 21, 26, 27, 31,..., 39, 45, 52,..., and 60. Wavelet domain subsignals (b) d_n and (c) e_n reveal the fluctuations of the pixel at location $x = (111,\ 34)$.

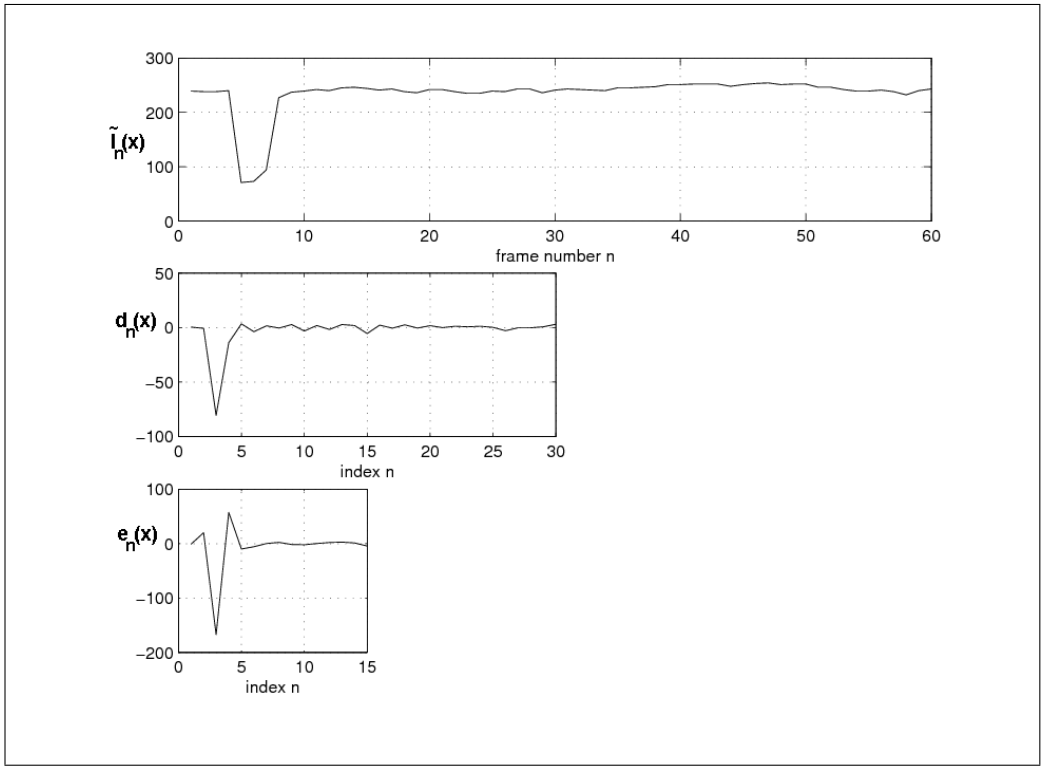

Figure 2.5: (a) Temporal history of the pixel at location $x = (18,\ 34)$. It is part of a fire-colored object for n = 4, 5, 6, 7, and 8, and it becomes part of the background afterwards. Corresponding subsignals (b) d_n and (c) e_n exhibit stationary behavior for $n > 8$.

and 8, then it becomes part of the background again for $n > 8$. Corresponding wavelet signals d_n and e_n do not exhibit oscillatory behavior as shown in Fig. 2.5. Small variations due to noise around zero after the $10 - th$ frame are ignored by setting up a threshold.

The number of wavelet stages needed for used in flame flicker analysis is determined by the video capture rate. In the first stage of dyadic wavelet decomposition, the low-band subsignal and the high-band wavelet subsignal $d_n(x)$ of the signal $\tilde{I}_n(x)$ are obtained. The subsignal $d_n(x)$ contains [2.5 Hz, 5 Hz] frequency band information of the original signal $\tilde{I}_n(x)$ in 10 Hz video frame rate. In the second stage the low-band subsignal is processed once again using a dyadic filter bank, and the wavelet subsignal $e_n(x)$ covering the frequency band [1.25 Hz, 2.5 Hz] is obtained. Thus by monitoring wavelet subsignals $e_n(x)$ and $d_n(x)$, one can detect fluctuations between 1.25 to 5 Hz in the pixel at location x.

Flame flicker can be detected in low-rate image sequences obtained with a rate of less than 20 Hz as well in spite of the aliasing phenomenon. To capture 10 Hz flicker, the video should capture at least 20 frames per second (fps). However, in some surveillance systems, the video capture rate is below 20 Hz. If the video is available at a lower capture rate, aliasing occurs but flicker due to flames can still be observed in the video. For example, 8 Hz sinusoid appears as 2 Hz sinusoid in a 10 fps video [87]. Aliased version of flame flicker signal is also a wide-band signal in discrete-time Fourier Transform domain. This characteristic flicker behavior is very well suited to be modeled as a random Markov model which is extensively used in speech recognition systems and recently these models have been used in computer vision applications [6].

Three-state Markov models are trained off-line for both flame and non-flame pixels to represent the temporal behavior (cf. Fig.4.3). These models are trained by using first-level wavelet coefficients $d_n(x)$ corresponding to the intensity values $\tilde{I}_n(x)$ of the flame-colored moving pixel at location x as the feature signal. A single-level decomposition of the intensity variation signal $\tilde{I}_n(x)$ is sufficient to characterize the turbulent nature of flame flicker. One may use higher-order wavelet coefficients such as, $e_n(x)$, for flicker characterization, as well. However,

this may incur additional delays in detection.

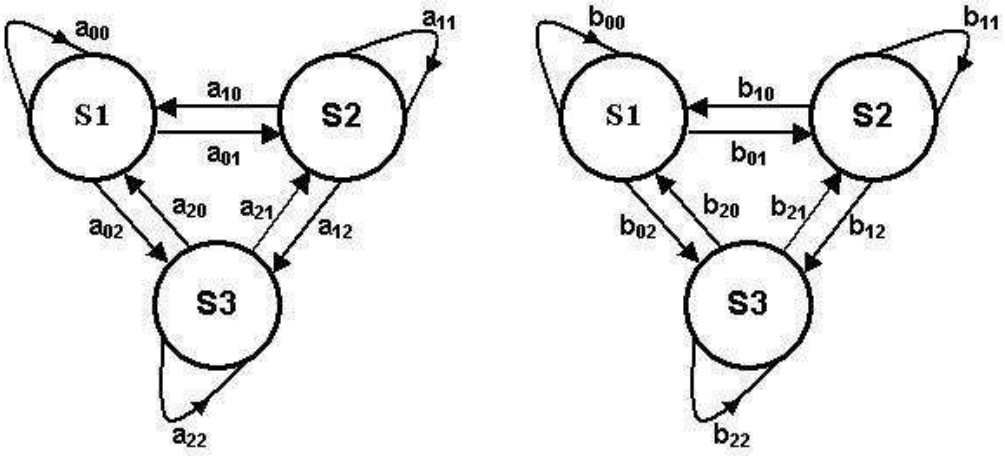

Figure 2.6: Three-state Markov models for a) flame and b) non-flame moving flame-colored pixels.

Wavelet signals can easily reveal the random characteristic of a given signal which is an intrinsic nature of flame pixels. That is why the use of wavelets instead of actual pixel values lead to more robust detection of flames in video. Since, wavelet signals are high-pass filtered signals, slow variations in the original signal lead to zero-valued wavelet coefficients. Hence it is easier to set thresholds in the wavelet domain to distinguish slow varying signals from rapidly changing signals. Non-negative thresholds $T_1 < T_2$ are introduced in wavelet domain to define the three states of the Hidden Markov Models for flame and non-flame moving bright objects. For the pixels of regular hot objects like walking people, engine of a moving car, etc., no rapid changes take place in the pixel values. Therefore, the temporal wavelet coefficients ideally should be zero but due to thermal noise of the camera the wavelet coefficients wiggle around zero. The lower threshold T_1 basically determines a given wavelet coefficient being close to zero. The second threshold T_2 indicates that the wavelet coefficient is significantly higher than zero. When the wavelet coefficients fluctuate between values above the higher threshold T_2 and below the lower threshold T_1 in a frequent manner this indicates the existence of flames in the viewing range of the camera.

The states of HMMs are defined as follows: at time n, if $|w(n)| < T_1$, the state is in $S1$; if $T_1 < |w(n)| < T_2$, the state is $S2$; else if $|w(n)| > T_2$, the state $S3$ is attained. For the pixels of regular flame-colored moving objects, like walking people in red shirts, no rapid changes take place in the pixel values. Therefore, the temporal wavelet coefficients ideally should be zero but due to thermal noise of the camera the wavelet coefficients wiggle around zero. The lower threshold T_1 basically determines a given wavelet coefficient being close to zero. The state defined for the wavelet coefficients below T_1 is $S1$. The second threshold T_2 indicates that the wavelet coefficient is significantly higher than zero. The state defined for the wavelet coefficients above this second threshold T_2 is $S3$. The values between T_1 and T_2 define $S2$. The state $S2$ provides hysteresis and it prevents sudden transitions from $S1$ to $S3$ or vice versa. When the wavelet coefficients fluctuate between values above the higher threshold T_2 and below the lower threshold T_1 in a frequent manner this indicates the existence of flames in the viewing range of the camera.

In flame pixels, the transition probabilities a's should be high and close to each other due to random nature of uncontrolled fire. On the other hand, transition probabilities should be small in constant temperature moving bodies because there is no change or little change in pixel values. Hence we expect a higher probability for b_{00} than any other b value in the non-flame moving pixels model (cf. Fig.4.3), which corresponds to higher probability of being in $S1$. The state $S2$ provides hysteresis and it prevents sudden transitions from $S1$ to $S3$ or vice versa.

The transition probabilities between states for a pixel are estimated during a pre-determined period of time around flame boundaries. In this way, the model not only learns the way flame boundaries flicker during a period of time, but also it tailors its parameters to mimic the spatial characteristics of flame regions. The way the model is trained as such, drastically reduces the false alarm rates.

During the recognition phase, the HMM based analysis is carried out in pixels near the contour boundaries of flame-colored moving regions. The state sequence of length 20 image frames is determined for these candidate pixels and fed to

the flame and non-flame pixel models. The model yielding higher probability is determined as the result of the analysis for each of the candidate pixel. A pixel is called as a flame or a non-flame pixel according to the result of this analysis. A fire mask composing of flame pixels is formed as the output of the method.

The probability of a Markov model producing a given sequence of wavelet coefficients is determined by the sequence of state transition probabilities. Therefore, the flame decision process is insensitive to the choice of thresholds T_1 and T_2, which basically determine if a given wavelet coefficient is close to zero or not. Still, thresholds can be determined using a k-means type algorithm, as well.

2.2.4 Spatial Wavelet Analysis

The fourth step of our fire detection algorithm is the spatial wavelet analysis of moving regions containing *Fire* mask pixels to capture color variations in pixel values. In an ordinary fire-colored object there will be little spatial variations in the moving region as shown in Fig. 2.7 (a). On the other hand, there will be significant spatial variations in a fire region as shown in Fig. 2.8 (a). The spatial wavelet analysis of a rectangular frame containing the pixels of fire-colored moving regions is performed. The images in Figs. 2.7 (b) and 2.8 (b) are obtained after a single stage two-dimensional wavelet transform that is implemented in a separable manner using the same filters explained in Subsection 2.2.3. Absolute values of low-high, high-low and high-high wavelet subimages are added to obtain these images. A decision parameter v_4 is defined for this step, according to the energy of the wavelet subimages:

$$v_4 = \frac{1}{M \times N} \sum_{k,l} |I_{lh}(k,l)| + |I_{hl}(k,l)| + |I_{hh}(k,l)|, \tag{2.12}$$

where $I_{lh}(k,l)$ is the low-high subimage, $I_{hl}(k,l)$ is the high-low subimage, and $I_{hh}(k,l)$ is the high-high subimage of the wavelet transform, respectively, and $M \times N$ is the number of pixels in the fire-colored moving region. If the decision parameter of the fourth step of the algorithm, v_4, exceeds a threshold, then it is likely that this moving and fire-colored region under investigation is a fire region.

(a) (b)

Figure 2.7: (a) A child with a fire-colored t-shirt, and b) the absolute sum of spatial wavelet transform coefficients, $|I_{lh}(k,l)|+|I_{hl}(k,l)|+|I_{hh}(k,l)|$, of the region bounded by the indicated rectangle.

(a) (b)

Figure 2.8: (a) Fire, and (b) the absolute sum of spatial wavelet transform coefficients, $|I_{lh}(k,l)|+|I_{hl}(k,l)|+|I_{hh}(k,l)|$, of the region bounded by the indicated rectangle.

Both the 1-D temporal wavelet analysis described in Subsection 2.2.3 and the 2-D spatial wavelet analysis are computationally efficient schemes because a multiplierless filter bank is used for both 1-D and 2-D wavelet transform computation [34], [45]. Lowpass and highpass filters have weights $\{\frac{1}{4}, \frac{1}{2}, \frac{1}{4}\}$ and $\{\frac{-1}{4}, \frac{1}{2}, \frac{-1}{4}\}$, respectively. They can be implemented by register shifts without performing any multiplications.

The wavelet analysis based steps of the algorithm are very important in fire and flame detection because they distinguish ordinary motion in the video from motion due to turbulent flames and fire.

2.3 Decision Fusion

In this section, we describe a voting based decision fusion strategy. However, other data fusion methods can be also used to combine the decision of four stages of the flame and fire detection algorithm.

Voting schemes include *unanimity voting*, *majority voting*, and *m-out-of-n voting*. In *m-out-of-n voting* scheme, an output choice is accepted if at least m votes agree with the decisions of n sensors [60]. We use a variant of m-out-of-n voting, the so-called T-out-of-v voting in which the output is accepted if $H = \sum_i w_i v_i > T$ where the w_i's are user-defined weights, the v_i's are decisions of the four stages of the algorithm, and T is a user-defined threshold. Decision parameter v_i can take binary values 0 and 1, corresponding to normal case and the existence of fire, respectively. The decision parameter v_1 is 1 if the pixel is a moving pixel, and 0 if it is stationary. The decision parameter v_2 is taken as 1 if the pixel is fire-colored, and 0 otherwise. The decision parameter v_3 is 1 if the probability value of flame model is larger than that of non-flame model. The decision parameter v_4 is defined in Equation (2.12).

In uncontrolled fire, it is expected that the fire region should have a non-convex boundary. To gain a further robustness to false alarms, another step checking the convexity of the fire region is also added to the proposed algorithm.

Convexity of regions is verified in a heuristic manner. Boundaries of the regions in the *Fire* mask are checked for their convexity along equally spaced five vertical and five horizontal lines using a 5×5 grid. The analysis simply consists of checking whether the pixels on each line belong to the region or not. If at least three consecutive pixels belong to the background, then this region violates the convexity condition. A *Fire* mask region which has background pixels on the intersecting vertical and/or horizontal lines, is assumed to have a non-convex boundary. This eliminates false alarms due to match light sources, sun, etc.

2.4 Experimental Results

The proposed method, Method-2.1, is implemented on a PC with an Intel Pentium 4, 2.40 GHz processor. It is tested for a large variety of conditions in comparison with the method utilizing only the color and temporal variation information, which we call Method-2.2, described in [64]. The scheme described in [17] is also implemented for comparison and it is called as Method 3 in the rest of the article. The results for some of the test sequences are presented in Table 2.2.

(a) (b)

Figure 2.9: (a) With the method using color and temporal variation only (Method-2.2) [64], false alarms are issued for the fire colored line on the moving truck and the ground, (b) our method (Method-2.1) does not produce any false alarms.

Method-2.2 is successful in determining fire and does not recognize stationary fire-colored objects such as the sun as fire. However, it gives false alarms when the fire-colored ordinary objects start to move, as in the case of a realistic scenario. An example of this is shown in Fig. 2.9 (a). The proposed method does not give any false alarms for this case (Fig. 2.9 (b)). The fire-colored strip on the cargo truck triggers an alarm in Method-2.2 when the truck starts to move. Similarly, false alarms are issued with Method-2.2 in Movies 3, 7 and 9, although there are no fires taking place in these videos. The moving arm of a man is detected as fire in Movie 7 (Fig. 2.10 (c)), and a red parking car is marked as fire in Movie 9 with Method-2.2 (Fig. 2.10 (d)).

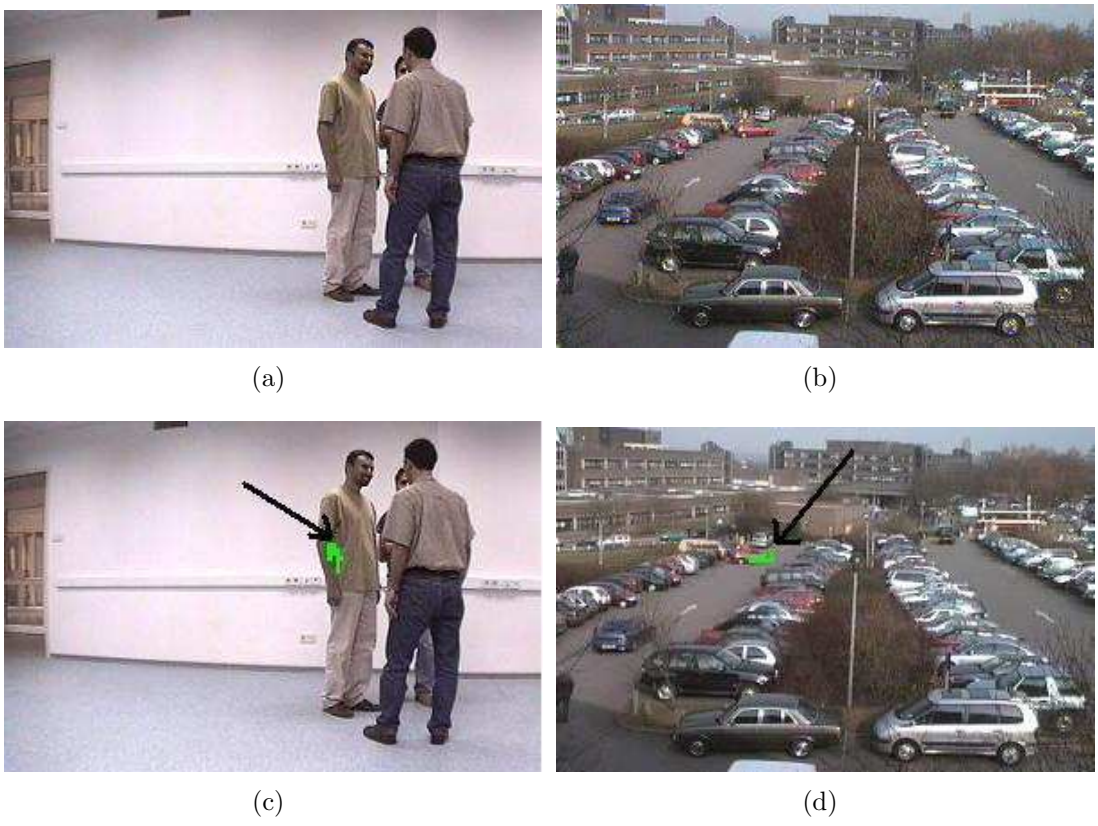

(a) (b)

(c) (d)

Figure 2.10: Sample images (a) and (b) are from Movies 7 and 9, respectively. (c) False alarms are issued for the arm of the man with the method using color and temporal variation only (Method-2.2) [64] and (d) on the fire-colored parking car. Our method does not give any false alarms in such cases (see Table 2.2).

Method-2.3 gives similar detection results for fire. However, it also suffers from inefficient analysis of the motion of fire colored objects. Fire-colored ordinary

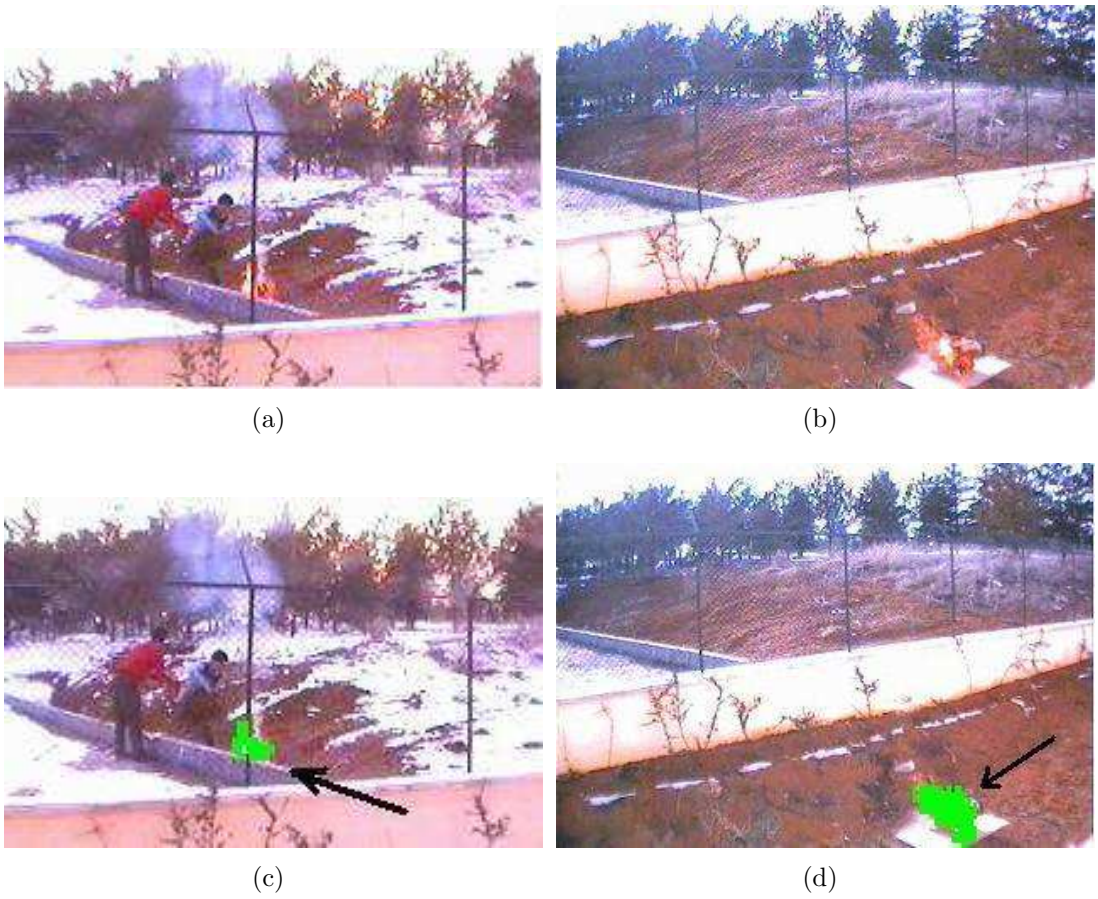

(a) (b)

(c) (d)

Figure 2.11: Sample images (a) and (b) are from Movies 2 and 4, respectively. Flames are successfully detected with our method (Method-2.1) in (c) and (d). In (c), although flames are partially occluded by the fence, a fire alarm is issued successfully. Fire pixels are painted in bright green.

moving objects causes Method-2.3 to give false alarms in Movies 1, 3, 7 and 9. If Method-2.1 is used, moving fire-colored ordinary objects do not cause an alarm to be raised. This is because the cyclic movement of flames is taken into account in our method, as well as the spatial variation in the color/brightness values of the moving fire-colored regions. Method-2.1 successfully detects fire in videos covering various scenarios, including partial occlusion of the flame. Sample images showing the detected regions are presented in Fig. 2.11.

In Movie 11, a man wearing a fire-colored shirt intentionally waves his arms to mimic the quasi-periodic flicker behavior in flames. Although all of the methods produce false alarms in this Movie, Method 1 significantly decreases the number of false positives relative to Methods-2.2 and 2.3.

These methods are also compared to each other in terms of computational cost (as shown in Table 2.3). Movies in Tables 2.2 and 2.3 are all captured at 10 fps with a frame size of 320 by 240 pixels. The average processing times per frame are 17.0 msec, 12.5 msec and 14.5 msec, for our method, Method-2.2, and Method-2.3, respectively. Our method is computationally more demanding due to additional wavelet analysis based steps. Since only shift and add type operations take place when convolving signals with the wavelet filters, additional cost is not high. Our implementation works in real-time for videos with frame size 320 by 240 pixels, captured at 10 fps or higher in a PC.

The video clips that we tested our method contain a total of 83,745 frames in 61 sequences. In 19 of the sequences fire takes place. Our method is successful in detecting fire in all of these sequences. This corresponds to a fire detection rate of 1.0. A fire contour recognition rate of 0.999 is reported in [48], which corresponds to a fire detection rate of 0.999. Our overall false alarm (false positive) rate is 0.001. It is reported that non-fire contour recognition rate is 1.0 in [48] which corresponds to a false alarm rate of 0. The video sequences containing fire in [48] are not publicly available. Therefore we used our own data set. We also test our method with the data set of the EC funded Context Aware Vision using Image-based Active Recognition (CAVIAR) project [8], publicly available at URL: http://homepages.inf.ed.ac.uk/rbf/CAVIAR/. Although there are a lot of

clips with moving fire-colored objects, none of the clips in this data set contains fire. Our method gives no false alarms in any of these sequences.

2.5 Summary

In this chapter, an algorithm for flame detection in visible range video is developed. The algorithm not only uses color and temporal variation information, but also characterizes flicker process in flames using HMMs trained with 1-D temporal wavelet transform coefficients and color variation in fire-colored moving regions using 2-D spatial wavelet transform. Methods based on only color information and ordinary motion detection may produce false alarms in real scenes where no fires are taking place. The experimental results show that false alarms can be drastically reduced by developing a Markovian setting with temporal and spatial wavelet analysis.

The method can be used for detection of fire in movies and video databases, as well as real-time detection of fire. It can be incorporated into a surveillance system monitoring an indoor or outdoor area of interest for early detection of fire.

Table 2.2: Comparison of the proposed method (Method-2.1), the method based on color and temporal variation clues only (Method-2.2) described in [64], and the method proposed in [17] (Method-2.3).

Video sequences	Number of frames with fire	Number of frames detected as fire			Number of false positive frames			Description
		Method			Method			
		2.1	2.2	2.3	2.1	2.2	2.3	
Movie 1	0	0	46	13	0	46	13	A fire-colored moving truck
Movie 2	5	5	5	5	0	0	0	Fire in a garden
Movie 3	0	0	7	5	0	7	5	A car leaving a fire-colored parking lot
Movie 4	37	37	44	47	0	7	10	A burning box
Movie 5	64	64	88	84	0	24	20	A burning pile of wood
Movie 6	41	41	56	50	0	15	9	Fire behind a man with a fire colored shirt
Movie 7	0	0	14	7	0	14	7	Four men walking in a room
Movie 8	18	18	18	18	0	0	0	Fire in a fireplace
Movie 9	0	0	15	5	0	15	5	A crowded parking lot
Movie 10	0	0	0	0	0	0	0	Traffic on a highway
Movie 11	0	2	107	86	2	107	86	Dancing man with fire-colored shirt

Table 2.3: Time performance comparison of Methods 2.1, 2.2, and 2.3 for the movies in Table 2.2. The values are the processing times per frame in milliseconds.

Videos	Method-2.1	Method-2.2	Method-2.3
Movie 1	16	12	14
Movie 2	17	12	14
Movie 3	17	12	14
Movie 4	16	12	14
Movie 5	18	13	15
Movie 6	18	13	15
Movie 7	17	13	15
Movie 8	18	13	15
Movie 9	16	12	14
Movie 10	17	12	14
Movie 11	17	12	14

Chapter 3

Flame Detection in Infra-red (IR) Video

In this chapter, a novel method to detect flames in infra-red (IR) video is described. The chapter begins with the previous work in the literature related with IR video based fire detection. IR cameras produce a single channel video and flames and other hot objects appear as bright objects. Therefore, color information in regular video cannot be used. However, brightness information is an important clue for fire detection. In the subsequent sections, the proposed flame detection method in IR video is presented. The method essentially consists of spatial analysis of flame regions in wavelet domain, and temporal modeling of flame pixels using hidden Markov models (HMMs). In Section 3.2.1, the spatial image analysis and feature extraction method based on wavelet analysis is described. In Section 3.2.2, temporal video analysis and HMM based modeling of the flicker process is presented. Simulation examples are presented in Section 4.3.

3.1 Previous Work

Current fire and flame detection algorithms in regular video [64], [17], [84], [87] use color information in video. They are not robust in outdoor applications,

for example, they may produce false alarms to reddish leaves flickering in the wind and reflections of periodic warning lights. IR cameras can be used to realize robust systems. However IR cameras and systems are more expensive than regular cameras.

A bright-looking object in IR video exhibiting rapid time-varying contours is an important sign of presence of flames in the scene. This time-varying behavior is not only directly observable in the contours of a fire region but also observable as variations of color channel values of the pixels in regular video. On the other hand, entire fire region appears as a flat white region in IR cameras operating in white-hot mode.

As pointed out in Chapter 2, turbulent flames flicker with a frequency of around 10 Hz [14] and [1]. Various other flame flicker values were reported for different fuel types in [5] and [42], such as 11.7 Hz and 12.5 Hz. The flicker process is modeled using Markov models as in regular video. The use of infra-red (IR) cameras instead of a regular camera provides further robustness to imaging based fire detection systems especially for fires with little radiance in visible spectrum, e.g. alcohol and hydrogen fires which are common in tunnel collisions. Unfortunately, the algorithms developed for regular video cannot be used in IR video due to the lack of color information and there is almost no spatial variation or very little texture information in fire regions in IR video as in most hot objects. Therefore, new image analysis techniques have to be developed to automatically detect fire in IR videos.

In IR video, boundaries of moving bright regions are estimated in each IR image frame. It is easier to estimate hot object boundaries in IR video to contour estimation in color video. A one-dimensional curve (1-D) representing the distance to the boundary from the center of mass of the region is extracted for each moving hot region. The wavelet transform of this 1-D curve is computed and the high frequency nature of the contour of the fire region is determined using the energy of the wavelet signal. This spatial domain clue replacing the spatial color variance information in regular video is combined with temporal clues to reach a final decision.

The proposed algorithm is designed for ranges up to 30 meters. After this range, flame flicker is hard to observe and object contours cannot be estimated accurately.

3.2 Fire and Flame Behavior in IR Video

Most IR imaging sensors provide a measure of the heat distribution in the scene in a range of wavelengths and each pixel has a single value. Usually, hot (cold) objects in the scene are displayed as bright (dark) regions in white-hot mode in IR cameras. Therefore fire and flame pixels appear as local maxima in an IR image. If a relatively bright region moves in the captured video then it should be marked as a potential region of fire in the scene monitored by the IR camera. However, an algorithm based on only motion and brightness information will produce many false alarms because vehicles, animals, and people are warmer than the background and they also appear as bright objects. In the proposed approach, in addition to motion and relative brightness information object boundaries are analyzed both spatially (intra-frame) and temporally (inter-frame).

Boundaries of uncontrolled fire regions in an image frame are obviously irregular. On the other hand, almost all regular objects and people have smooth and stationary boundaries. This information is modeled using wavelet domain analysis of moving object contours which is described in the next subsection. One can reduce the false alarms which may be due to ordinary moving hot objects by carrying out temporal analysis around object boundaries to detect random changes in object contours. This analysis is described in Section 3.2.2.

3.2.1 Wavelet Domain Analysis of Object Contours

Moving objects in IR video are detected using the background estimation method developed by Collins et al. [19]. This method assumes that the camera is stationary. Moving pixels are determined by subtracting the current image from the

background image and thresholding. A recursive adaptive threshold estimation is described in [19] as well. Other methods can be also used for moving object estimation. After moving object detection, it is checked whether the object is hotter than the background, i.e., it is verified if some of the object pixels are higher in value than the background pixels.

Hot objects and regions in IR video can be determined in moving cameras as well by estimating local maxima in the image. Contours of these high temperature regions can be determined by region growing.

The next step of the proposed method is to determine the center of mass of the moving bright object. A one-dimensional (1-D) signal $x(\theta)$ is obtained by computing the distance from the center of mass of the object to the object boundary for $0 \leq \theta < 2\pi$. In Fig. 3.1, two FLIR (forward looking infra-red) image frames are shown. Example feature functions for walking man pointed with an arrow and the fire region in Fig. 3.1 are shown in Fig. 4.5 for 64 equally spaced angles $x[l] = x(l\theta_s)$, $\theta_s = \frac{2\pi}{64}$. To determine the high-frequency content of a curve, we use a single scale wavelet transform shown in Fig. 4.2. The feature signal $x[l]$ is fed to a filterbank shown in Fig. 4.2 and the low-band signal

$$c[l] = \sum_m h[2l - m]x[m] \tag{3.1}$$

and the high-band subsignal

$$w[l] = \sum_m g[2l - m]x[m] \tag{3.2}$$

are obtained. Coefficients of the lowpass and the highpass filters are $h[l] = \{\frac{1}{4}, \frac{1}{2}, \frac{1}{4}\}$ and $g[l] = \{-\frac{1}{4}, \frac{1}{2}, -\frac{1}{4}\}$, respectively [34], [11], [45].

The absolute values of high-band (wavelet) $w[l]$ and low-band $c[l]$ coefficients of the fire region and the walking man are shown in Figs. 4.6 and 4.7, respectively. The high-frequency variations of the feature signal of the fire region is clearly distinct from that of the man. Since regular objects have relatively smooth boundaries compared to flames, the high-frequency wavelet coefficients of flame boundary feature signals have more energy than regular objects. Therefore, the

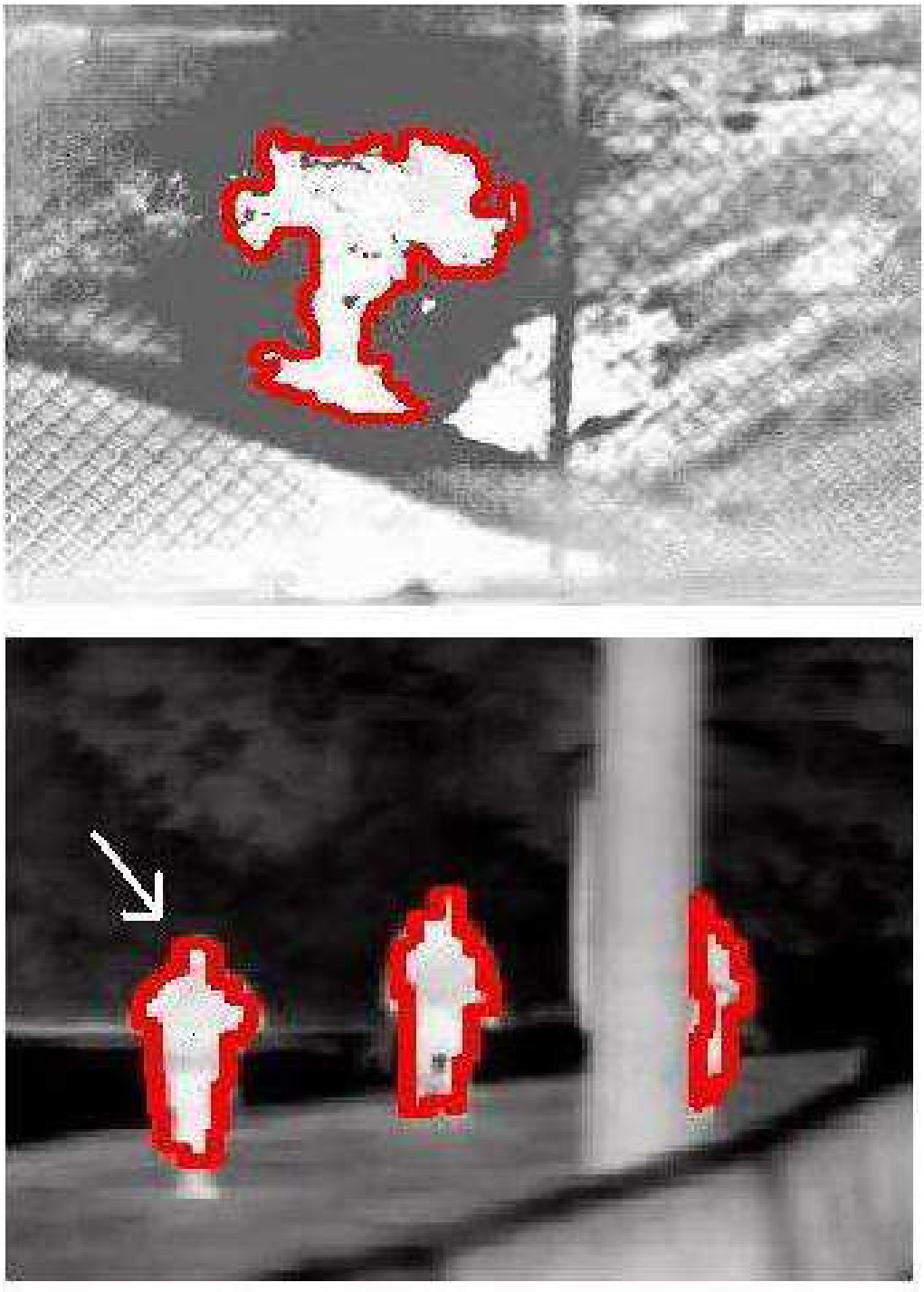

Figure 3.1: Two relatively bright moving objects in FLIR video: a) fire image, and b) a man (pointed with an arrow). Moving objects are determined by the hybrid background subtraction algorithm of [19].

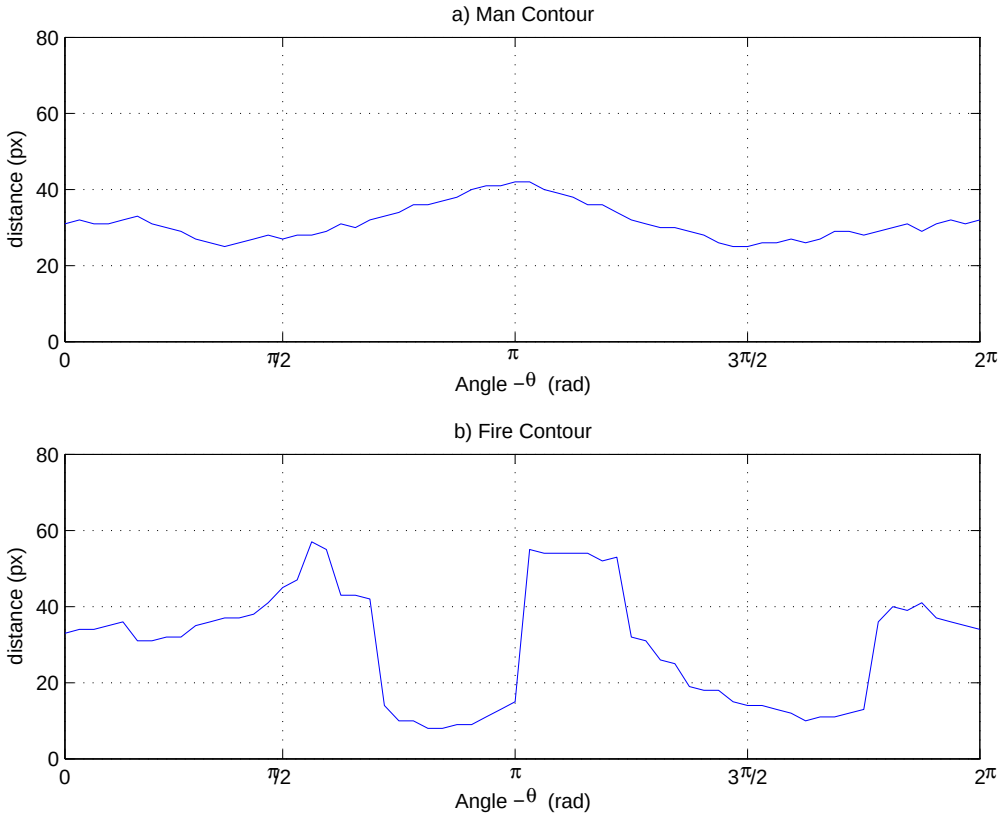

Figure 3.2: Equally spaced 64 contour points of the a) walking man, and b) the fire regions shown in Fig. 3.1.

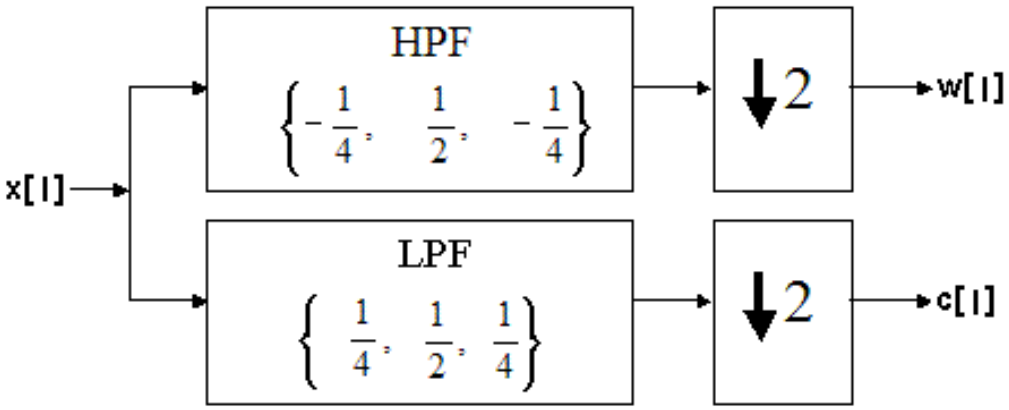

Figure 3.3: Single-stage wavelet filter bank. The high-pass and the low-pass filter coefficients are $\{-\frac{1}{4}, \frac{1}{2}, -\frac{1}{4}\}$ and $\{\frac{1}{4}, \frac{1}{2}, \frac{1}{4}\}$, respectively.

ratio of the wavelet domain energy to the energy of the low-band signal is a good indicator of a fire region. This ratio is defined as

$$\rho = \frac{\sum_l |w[l]|}{\sum_l |c[l]|} \tag{3.3}$$

The likelihood of the moving region to be a fire region is highly correlated with the parameter ρ. Higher the value of ρ, higher the probability of the region belonging to flame regions.

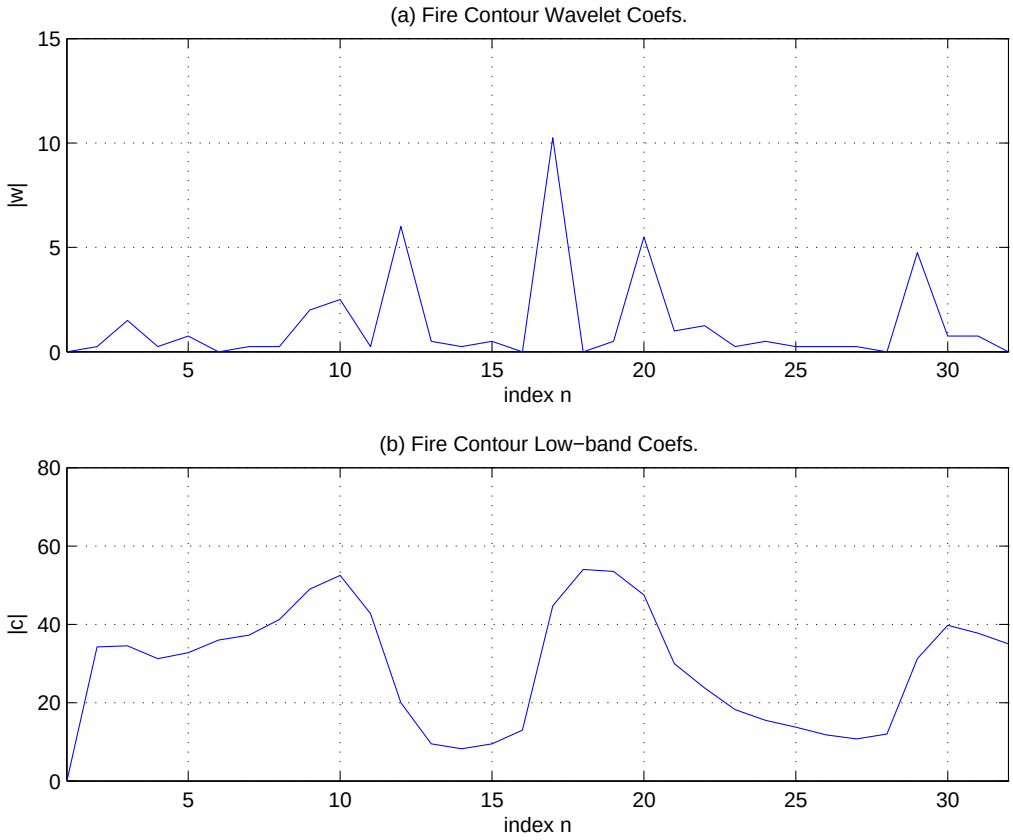

Figure 3.4: The absolute values of a) high-band (wavelet) and b) low-band coefficients for the fire region.

A threshold ρ_T for ρ was experimentally estimated off-line. During real-time analysis, regions for which $\rho > \rho_T$ are first determined. Such regions are possible fire regions. In order not to miss any fire region, a low threshold value for ρ_T is selected. Therefore, temporal flicker analysis should be carried out in these

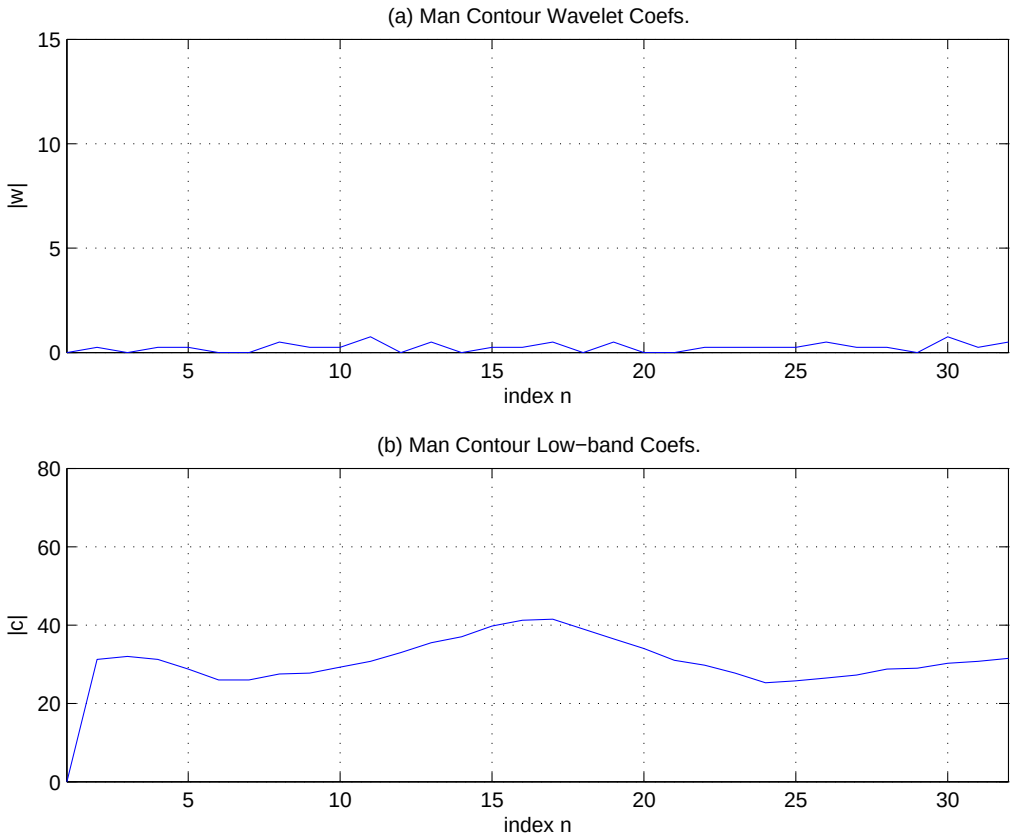

Figure 3.5: The absolute a) high-band (wavelet) and b) low-band coefficients for the walking man.

regions to reach a final decision. Flicker detection process is described in the next subsection.

3.2.2 Modeling Temporal Flame Behavior

It was reported in mechanical engineering literature that turbulent flames flicker with a frequency of 10 Hz [1]. In [48], the shape of fire regions are represented in Fourier domain. Since, Fourier Transform does not carry any time information, FFTs have to be computed in windows of data and temporal window size and the peak or energy around 10 Hz is very critical for flicker detection. If the window size is too long then one may not get enough peaks in the FFT data. If it is too short then one may completely miss flicker and therefore no peaks can be observed in the Fourier domain. Furthermore, one may not observe a peak at 10 Hz but a plateau around it, which may be hard to distinguish from the Fourier domain background.

Another problem is that one may not detect periodicity in fast growing uncontrolled fires because the boundary of fire region simply grows in video. Actually, the fire behavior is a wide-band random activity below 15 Hz and a random process based modeling approach is naturally suited to characterize the rapid time-varying characteristic of flame boundaries. Broadbent [5] and Huang et al. [42] independently reported different flicker frequency distributions for various fuel types. In general, a pixel especially at the edge of a flame becomes part of the fire and disappears in the background several times in one second of a video at random. In fact, we analyzed the temporal characteristics of the red channel value of a pixel at the boundary of a flame region in color-video clips recorded at 10 fps and 25 fps. We also analyzed the temporal characteristics of the intensity value of a pixel at the boundary of a flame region in an IR video clip recorded at 10 fps. We obtained the flicker frequency distributions shown in Fig. 3.6 for 10 fps color video, 25 fps color video and 10 fps IR video, respectively. We assumed that the flame flicker behavior is a wide-band random activity below 15 Hz for all practical purposes. This is the basic reason behind our stochastic model.

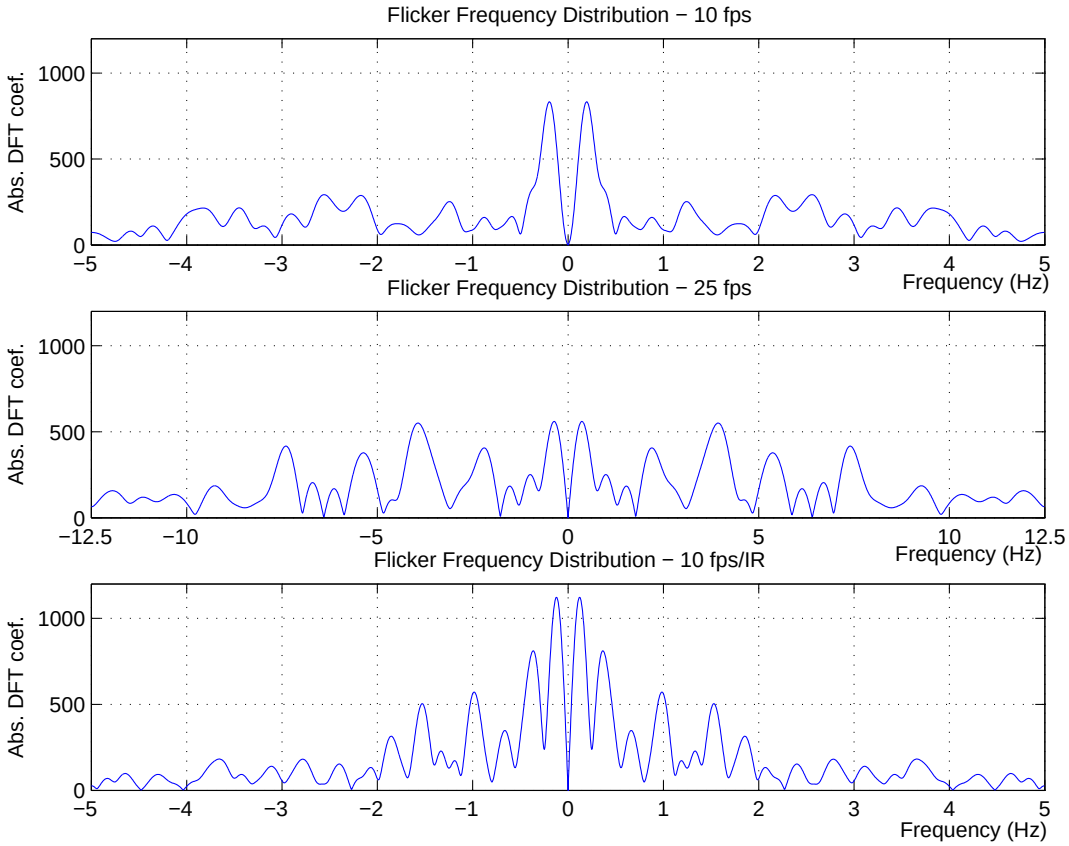

Figure 3.6: Flicker frequency distributions for a) 10 fps color video, b) 25 fps color video and c) 10 fps IR video. These frequency distributions were obtained by analyzing the temporal variations in the red channel value of a pixel at the boundary of a flame region in color-video clips recorded at 10 fps and 25 fps and intensity value of a pixel at the boundary of a flame region in an IR video clip recorded at 10 fps, respectively.

Similar to the discussions in Chapter 2, flame flicker process in IR video is characterized by a random Markov model. As in the previous chapter, three-state Markov models are trained off-line for both flame and non-flame pixels to represent the temporal behavior (cf. Fig. 4.3). These models are trained using a feature signal which is defined as follows: Let $I_k(n)$ be the intensity value of the $k-th$ pixel at frame n. The wavelet coefficients of I_k are obtained by the same structure shown in Fig. 4.2, but filtering is implemented temporally.

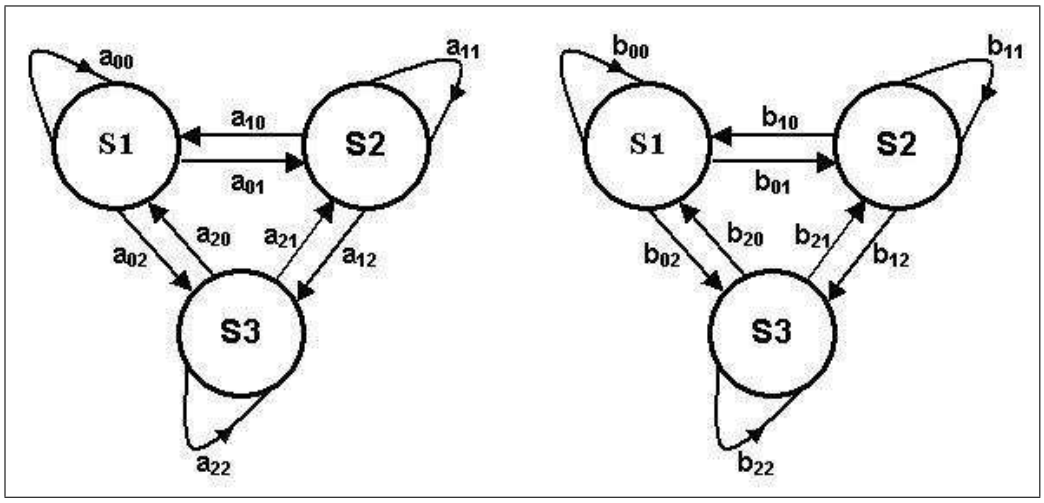

Figure 3.7: Three-state Markov models for a) flame and b) non-flame moving pixels.

The states of HMMs are defined as follows: at time n, if $|w(n)| < T_1$, the state is in $S1$; if $T_1 < |w(n)| < T_2$, the state is $S2$; else if $|w(n)| > T_2$, the state $S3$ is attained. For the pixels of regular hot objects like walking people, engine of a moving car, etc., no rapid changes take place in the pixel values. When the wavelet coefficients fluctuate between values above the higher threshold T_2 and below the lower threshold T_1 in a frequent manner this indicates the existence of flames in the viewing range of the IR camera.

The transition probabilities between states for a pixel are estimated during a pre-determined period of time around flame boundaries. During the recognition phase, the HMM based analysis is carried out in pixels near the contour boundaries of bright moving regions whose ρ values exceed ρ_T. The state sequence of

length 20 image frames is determined for these candidate pixels and fed to the flame and non-flame pixel models. The model yielding higher probability is determined as the result of the analysis for each of the candidate pixel. A pixel is called as a flame or a non-flame pixel according to the result of this analysis. A fire mask composing of flame pixels is formed as the output of the method.

3.3 Experimental Results

The proposed method was implemented in a personal computer with an AMD AthlonXP 2000+ 1.66GHz processor. The HMMs used in the temporal analysis step were trained using outdoor IR video clips with fire and ordinary moving bright objects like people and cars. Video clips have 236577 image frames with 160 by 120 pixel resolution. All of the clips are captured at 10 fps using a cooled long-wave IR camera with a spectral range of 8-12 μm. This camera has a longer range than 30 meters up to which distance the proposed algorithm is developed for. We cannot detect a starting fire in longer distances using the proposed algorithm, because flame flicker cannot be observed in long distances.

There are moving cars and walking people in most of the test video clips. Image frames from some of the clips are shown in Figs. 3.8 and 3.9. To increase the number of videos in experimental studies, black and white video clips are also used.

We used some of our clips for training the Markov models. The fire model was trained with fire videos and the other model was trained with ordinary moving bright objects. The remaining 48 video clips were used for test purposes. Our method yields no false positives in any of the IR test clips.

A modified version of a recent method by Guillemant and Vicente [36] for real-time identification of smoke in black and white video is implemented for comparison. This method is developed for forest fire detection from watch towers. In a forest fire, smoke rises first, therefore, the method was tuned for smoke detection. Guillemant and Vicente based their method on the observation that

Figure 3.8: Image frames from some of the test clips. a), b) and c) Fire regions are detected and flame boundaries are marked with arrows. d), e) and f) No false alarms are issued for ordinary moving bright objects.

Figure 3.9: Image frames from some of the test clips with fire. Pixels on the flame boundaries are successfully detected.

the movements of various patterns like smoke plumes produce correlated temporal segments of gray-level pixels, which they called as *temporal signatures*. For each pixel inside an envelope of possible smoke regions, they recovered its last d luminance values to form a point $P = [x_0, x_1, ..., x_{d-1}]$ in *d-dimensional* "embedding space". Luminance values were quantized to 2^e levels. They utilized fractal indexing using a space-filling Z-curve concept whose fractal rank is defined as:

$$z(P) = \sum_{j=0}^{e-1} \sum_{l=0}^{d-1} 2^{l+jd} x_l^j \tag{3.4}$$

where x_l^j is the $j-th$ bit of x_l for a point P. They defined an instantaneous velocity for each point P using the linked-list obtained according to Z-curve fractal ranks. After this step, they estimated a cumulative velocity histogram (CVH) for each possible smoke region by including the maximum velocity among them and made smoke decisions about the existence of smoke according to the standard deviation, minimum average energy, and shape and smoothness of these histograms [36].

Our aim is to detect flames in manufacturing and power plants, large auditoriums, and other large indoor environments. So, we modified the method in [36] similar to the approach presented in Sec. 2.2. For comparison purposes, we replaced our wavelet-based contour analysis step with the CVH based method and leave the rest of the algorithm as proposed. We formed two three-state Markov models for flame and non-flame bright moving regions. These models were trained for each possible flame region using wavelet coefficients of CVH standard deviation values. States of HMMs were defined as in Sec. 3.2.2.

Comparative detection results for some of the test videos are presented in Table 3.1. The second column lists the number of frames in which flames exist in the viewing range of the camera. The third and fourth columns show the number of frames in which flames were detected by the modified CVH method explained in the above paragraph, and our method, respectively. Our method detected flame boundaries that have irregular shapes both temporally and spatially. Both methods detected fire in video clips V3–V6 and V8–V12 which contain actual fires indoor and outdoor. In video clip V3, flames were behind a wall most of the

time. The distance between the camera and fire ranges between 5 to 50 meters in these video clips. Video clips V1, V2, and V7 do not contain any fire. There are flames and walking people in the remaining clips. Some flame frames are missed by both methods but this is not an important problem at all, because the fire was detected in the next frame or the frame after the next one. The method using CVH detected fire in most of the frames in fire containing videos, as well. However, it yielded false alarms in clips V1, V7 and V9–V12, in which there were a group of people walking by a car and around fire place. Proposed method analyzes the contours of possible fire regions in wavelet domain. This makes it more robust to slight contour changes than the modified method which basically depends on the analysis of motion vectors of possible fire regions.

Flames of various burning materials have similar yet different temporal and spatial characteristics. For example, oil flame has a peak flicker frequency around 15 Hz whereas it is around 5 Hz for coal flame (cf. Fig. 2 in [5]). In fact, flames of the same burning material under different weather/wind conditions have also different temporal and spatial characteristics. What is common among various flame types is the wide-band random nature in them causing temporal and spatial flicker. Our method exploits this stochastic nature. We use wavelet based feature signals obtained from flickering flames to train and test our models in order to get rid of the effects of specific conditions forming the flames. The wavelet domain feature signals capture the condition-independent random nature of flames.

To verify the performance of our method with respect to flames of different materials, we set up the following experiment:

1. We train the model with ‘paper’ fire and test it with both ‘paper’ and ‘paper + alcohol’ fires.

2. We train the model with ‘paper + alcohol’ fire and test it with both ‘paper’ and ‘paper + alcohol’ fires.

The results of this experiment for some of the test clips are presented in Table 3.2. The results show that the method has similar detection rates for different fires when trained with different flame types.

Table 3.1: Detection results for some of the test clips. In the video clip V3, flames are hindered by a wall for most of the time.

Video clips	Number of frames with flames	Number of frames in which flames detected		Number of false positive frames	
		CVH Method	Our Method	CVH Method	Our Method
V1	0	17	0	17	0
V2	0	0	0	0	0
V3	71	42	63	0	0
V4	86	71	85	0	0
V5	44	30	41	0	0
V6	79	79	79	0	0
V7	0	15	0	15	0
V8	101	86	101	0	0
V9	62	52	59	8	0
V10	725	510	718	54	0
V11	1456	1291	1449	107	0
V12	988	806	981	19	0

The proposed method was also tested with regular video recordings in comparison with the modified version of the method in [36] and the fire detection method described in [87]. The method in [87] uses frequency subband analysis to detect 10 Hz flame flicker, instead of using HMMs to capture the random temporal behavior in flames. Results for some of the clips are presented in Table 3.3. The clip V17 does not contain any fire, either. However it leads to false alarms because a man with bright fire colored shirt dances in front of the camera to fool the algorithm. This man would not cause any false alarms if an infrared camera were used instead of a regular visible range camera.

It should also be noted that, the proposed method is computationally more efficient than [36] because it is mostly based on contour analysis of the bright moving objects. Average processing time per frame for the proposed method is 5 msec as shown in Table 3.3.

Table 3.2: Fire detection results of our method when trained with different flame types.

Video clips	Flame type	Number of frames with flames	Number of frames in which flames detected by Our Method trained with	
			Paper fire	Paper+alcohol fire
V9	Paper	62	60	58
V10	Paper	725	722	722
V11	Paper+alcohol	1456	1449	1453
V12	Paper+alcohol	993	988	991
V13	Paper+alcohol	1434	1426	1430
V14	Paper	999	996	995

Table 3.3: Comparison of the proposed method with the modified version of the method in [36] (CVH method) and the fire detection method described in [87] for fire detection using a regular visible range camera. The values for processing times per frame are in milliseconds.

Video clips	Number of frames with flames	Number of frames in which flames detected			Processing time per frame (msec)		
		Our Method	Method in [87]	CVH Method	Our Method	Method in [87]	CVH Method
V15	37	31	37	26	5	16	11
V16	18	13	18	8	5	17	10
V17	0	2	9	7	4	16	10

3.4 Summary

A novel method to detect flames in IR video is developed. The algorithm uses brightness and motion clues along with a temporal and a contour analysis in wavelet domain. The main contribution of the method is the utilization of hidden Markov models trained using temporal wavelet domain information to detect random flicker process. The high frequency behavior of flame region boundaries are analyzed using a wavelet based contour analysis technique. The experimental results indicate that when the fire falls into the viewing range of an IR camera, the proposed method is successful in detecting the flames without producing false

alarms in all the examples that we tried. The method can be used for both indoor and outdoor early fire detection applications.

Chapter 4

Short Range Smoke Detection in Video

Smoldering smoke appears before flames in most fires. In addition, the source of the fire and flames cannot always fall into the field of view of a camera or a sensor monitoring an area of interest. Long Wave Infra-Red (LWIR) cameras and pyro-electric infra-red (PIR) sensors which are used in flame detection are not suitable for smoke detection. Contrary to the common belief, smoke cannot be visualized in $8 - 12\mu$m range LWIR cameras and sensors including Forward Looking Infra-Red (FLIR) cameras and PIR sensors [76, 44]. However, smoke of an uncontrolled fire can be easily observed by a visible range camera even if flames are not visible. This results in early detection of fire before it spreads around. This is vital for fire alarm systems when large and open areas are monitored.

A novel method to detect smoke in video is described in this chapter. The chapter begins with the introduction of the video smoke detection method. In Section 4.3, contour analysis is described. Experimental results are presented in Chapter 4.4.

4.1 Detection Algorithm

The flames of a fire may not always fall into the visible range of the camera monitoring a scene covering large areas like plane hangars or open spaces. Fire detection systems should tackle with such situations by successful detection of smoke without flame. In this chapter, temporal and spatial wavelet analysis as well as an analysis of contours of possible smoke regions are carried out for smoke detection.

Smoke gradually smoothen the edges in an image. This characteristic property of smoke is a good indicator of its presence [52], [10]. Edges in an image correspond to local extrema in wavelet domain. Degradation of sharpness in the edges result in a decrease in the values of these extrema. However, these extrema values corresponding to edges do not totally boil down to zero when there is smoke in the scene. In fact, they simply loose some of their energy but they still stay in their original locations, occluded partially by the semi-transparent smoke.

Independent of the fuel type, smoke naturally decrease the chrominance channels U and V values of pixels. Apart from this, as discussed in the previous chapters, both flame and smoke are turbulent phenomena. Smoke regions have time-varying boundaries similar to flame regions. Smoke partially covers and uncovers background objects especially at the early stages of fire. Therefore, a Markov model based modeling of turbulent smoke behavior is appropriate as in flame detection. However, smoke boundaries move with a lower frequency at the early stages of fire.

In addition to color and turbulent behavior analysis, boundaries of smoke regions are also estimated in each video image frame. A one-dimensional curve (1-D) representing the distance to the boundary from the center of mass of the region is extracted for each smoke region. The wavelet transform of this 1-D curve is computed and the high frequency nature of the contour of the smoke region is determined using the energy of the wavelet signal. This spatial domain clue is also combined with temporal clues to reach a final decision.

Smoke detection algorithm consists of five steps: (i) moving pixels or regions in the current frame of a video are determined, (ii) the decrease in high frequency content corresponding to edges in these regions are checked using spatial wavelet transform. If edges loose their sharpness without vanishing completely (iii) the U and V channel values corresponding to edge pixels are checked, (iv) turbulent behavior analysis is carried out by HMMs which use temporal wavelet transform coefficients. Finally, (v) object contours are analyzed in wavelet domain.

Moving objects in video are detected using the background estimation method developed by Collins et al. [19]. This method assumes that the camera is stationary. Moving pixels are determined by subtracting the current image from the background image and thresholding. A recursive threshold estimation is described in [19].

In order to detect smoke, it is necessary to analyze moving regions in video to determine if the motion is due to smoke or an ordinary moving object. Smoke obstructs the texture and edges in the background of an image. Since edges and texture contribute to the high frequency information of the image, energies of wavelet sub-images drop due to smoke in an image sequence. Based on this fact we monitor wavelet coefficients as in Fig. 4.1 and we detect decreases in local wavelet energy, and detect individual wavelet coefficients corresponding to edges of objects in background whose values decrease over time in video. It is also possible to determine the location of smoke using the wavelet sub-images as shown in Fig. 4.1.

Let $I_v(x,y) = |I_{LH}(x,y)| + |I_{HL}(x,y)| + |I_{HH}(x,y)|$ represent a composite image containing high-frequency information corresponding to the image frame I obtained by a single-level 2-D discrete wavelet transformation operation. In order to make the analysis faster, this sub-band image is divided into small blocks of size (K_1, K_2) and the energy $e_I(l_1, l_2)$ value of each block is computed as $e_I(l_1, l_2) = \sum_{(x,y)\in\mathcal{R}_i} I_v(x + l_1K_1, y + l_2K_2)$ where $\mathcal{R}_i$ represents a block of size (K_1, K_2) in the wavelet sub-image. If the wavelet sub-images are computed from the luminance (Y) image, then there is no need to include the chrominance wavelet images. If wavelet transforms of red (R), green (G), and blue (B) color

Figure 4.1: Image frame with smoke and its single level wavelet sub-images. Blurring in the edges is visible. The analysis is carried out in small blocks.

images are computed, then the energy value, $e(l_1, l_2)$, should be computed using all wavelet sub-images of the R, G, and B color images. In our implementation, sub-images are computed from the luminance image only and the block size is taken as 8 by 8 pixels.

Let B represent a background image built-up in time according to the IIR-type background update filter described in Section 2.2.1. Let $B_v(x, y) = |B_{LH}(x, y)| + |B_{HL}(x, y)| + |B_{HH}(x, y)|$ represent a composite image containing high-frequency information corresponding to the background image B obtained by the same single-level 2-D discrete wavelet transformation operation as for $I_v(x, y)$. In a similar manner, local energy values, $e_B(l_1, l_2)$, of the composite image for the background image can be computed as $e_B(l_1, l_2) = \sum_{(x,y)\in\mathcal{R}_i} B_v(x + l_1K_1, y + l_2K_2)$ where $\mathcal{R}_i$ represents a block of size (K_1, K_2) in the wavelet sub-image of the background.

These local energy values, $e_I(l_1, l_2)$ and $e_B(l_1, l_2)$, corresponding to current and background images are compared with each other. If there is a decrease in energy value $e_B(l_1, l_2)$ of a certain block at location (l_1, l_2), then this means that the texture or edges of the scene monitored by the camera no longer appear as sharp in the current image of the video, as they used to be. Therefore, the image region in the viewing range of the camera corresponding to (l_1, l_2)-th block could be covered with smoke. One can set up thresholds for the comparison. If a certain local background energy value $e_B(l_1, l_2)$ drops below a pre-determined threshold,

a warning may be issued.

It is also well-known that wavelet sub-images contain the edge information of the original image. Edges produce local extrema in wavelet sub-images [10]. Wavelet sub-images LH, HL and HH contains horizontal, vertical and diagonal edges of the original image, respectively. If smoke covers one of the edges of the original image then the edge initially becomes less visible and after some time it may disappear from the scene as smoke gets thicker. Let the wavelet coefficient $I_{HL}(x, y)$ be one of the wavelet coefficients corresponding to the edge covered by smoke. Initially, its value decreases due to the reduced visibility, and in subsequent image frames it becomes either zero or close to zero whenever there is very little visibility due to thick smoke. Therefore locations of the edges of the original image is determined from the significant extrema of the wavelet transform of the background image in the proposed method. Slow fading of a wavelet extrema is an important clue for smoke detection. If the values of a group of wavelet coefficients along a curve corresponding to an edge decrease in value in consecutive frames, then this means that there is less visibility in the scene. In turn, this may be due to the existence of smoke.

An instantaneous disappearance or appearance of a wavelet extremum in the current frame cannot be due to smoke. Such a change corresponds to an ordinary moving object covering an edge in the background or the boundary of a moving object and such changes are ignored.

Color information is also used for identifying smoke in video as the third step. Initially, when smoke starts to expand, it is semi-transparent. Consequently, color values of the pixels within semi-transparent smoke covered image regions decrease with comparable rates. This in turn results in the preservation of the direction of the vector defined by the RGB channel values. This is another clue for differentiating between smoke and an ordinary moving object. By itself, this information is not sufficient because shadows of moving objects also behave similarly. As smoke gets thicker, however, the resemblance of the current image frame and the background image decreases. The chrominance values U and V of the candidate smoke pixels in the current frame gets smaller values than their corresponding

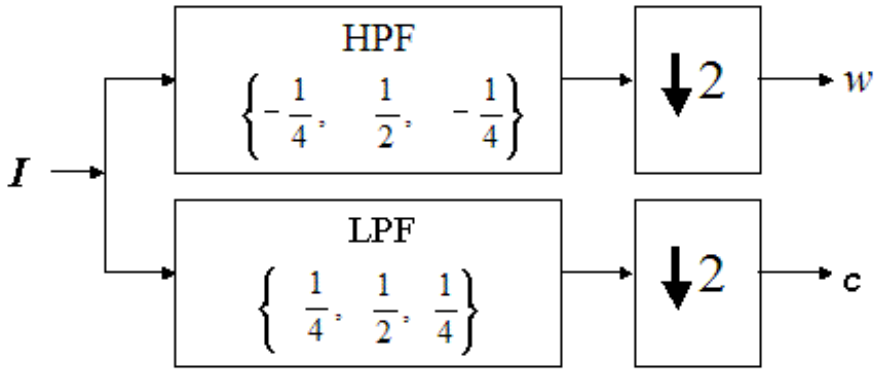

Figure 4.2: Single-stage wavelet filter bank.

values in the background image.

The turbulent characteristic of smoke is also used as an additional information. The candidate regions are checked whether they continuously appear and disappear over time. In general, a pixel especially at the edge of a smoke becomes part of smoke and disappears in the background several times in one second of a video at random. This characteristic behavior is very well suited to be modeled as a random Markov model.

Similar to flame detection methods presented in the previous chapters, three-state Markov models are temporally trained for both smoke and non-smoke pixels (cf.Fig.4.3) using a wavelet based feature signal. These models are trained using a feature signal which is defined as follows: Let $I(x, n)$ be the intensity value of a pixel at location x in the image frame at time step n. The wavelet coefficients of I are obtained by the filter bank structure shown in Fig.4.2. Non-negative thresholds $T1 < T2$ introduced in wavelet domain, define the three states of the hidden Markov models for smoke and non-smoke moving objects. At time n, if $|w(n)| < T1$, the state is in $F1$; if $T1 < |w(n)| < T2$, the state is $F2$; else if $|w(n)| > T2$, the state Out is attained. The transition probabilities between states for a pixel are estimated during a pre-determined period of time around smoke boundaries. In this way, the model not only learns the turbulent behavior of smoke boundaries during a period of time, but also it tailors its parameters to mimic the spatial characteristics of smoke regions.

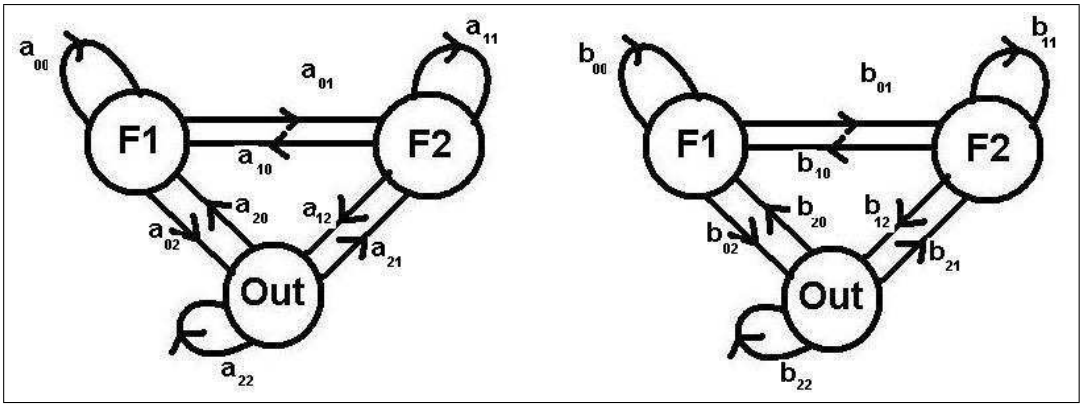

Figure 4.3: Three-state Markov models for smoke(left) and non-smoke moving pixels.

4.2 Wavelet Domain Analysis of Object Contours

In addition to temporal and color analysis, contours of possible smoke regions are further analyzed. For this purpose, the centers of masses of the moving objects are determined. A one dimensional (1-D) signal is obtained by computing the distance from the center of mass of the object to the object boundary for $0 \leq \theta < 2\pi$. In Fig. 4.4, two image frames are shown. Example feature functions of 64 equally spaced angles for moving vehicle and the fire region in Fig. 4.4 are shown in Fig. 4.5. The high-frequency variations of the feature signal of smoke region is clearly distinct from that of the car and lights.

To determine the high-frequency content of a curve, we use a single scale wavelet transform shown in Fig. 4.2. The absolute wavelet (w) and low-band (c) coefficients of smoke region and the moving car are shown in Figs. 4.6 and 4.7, respectively. The ratio of the wavelet domain energy to the energy of the low-band signal is a good indicator of a smoke region. This ratio is defined as $\rho = \frac{\sum_n |w[n]|}{\sum_n |c[n]|}$. The likelihood of the moving region to be a smoke region is highly correlated with the parameter ρ.

Figure 4.4: Two moving objects in video: smoke image (top), and a vehicle (bottom). The object boundaries are determined by the background subtraction algorithm.

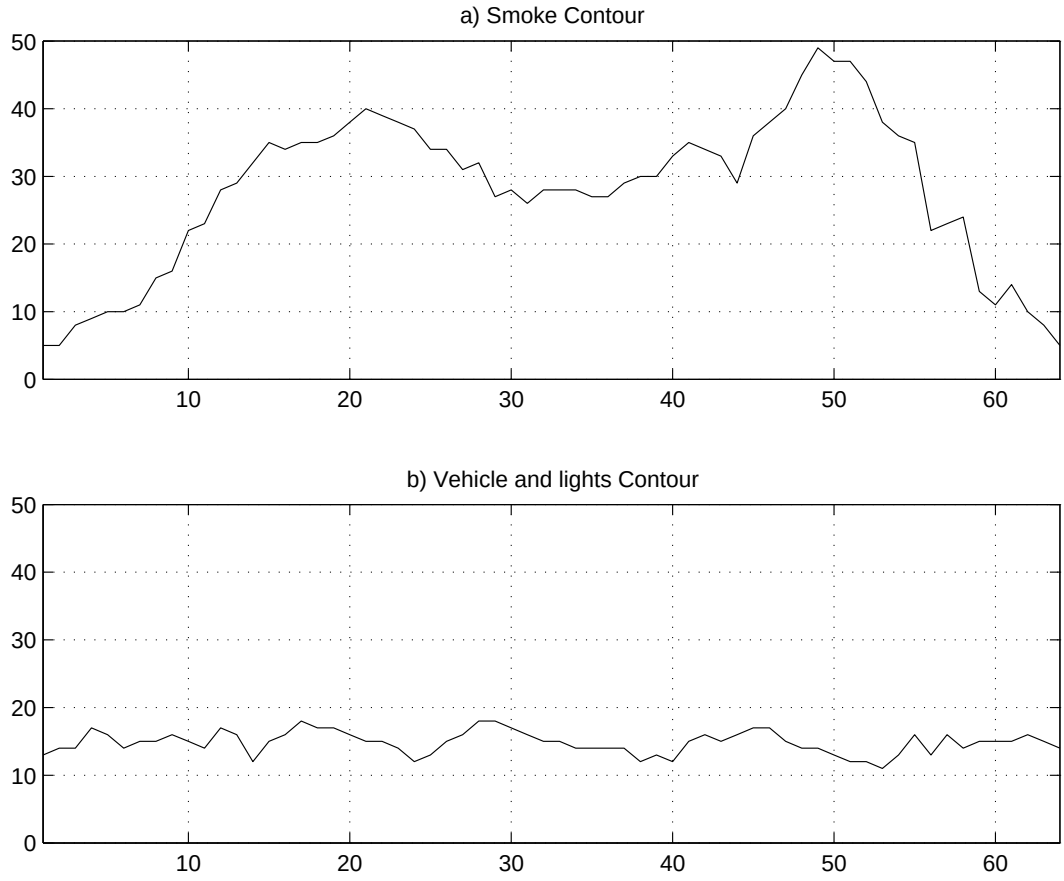

Figure 4.5: Equally spaced 64 contour points of smoke (top) and the vehicle regions (bottom) shown in Fig.4.4.

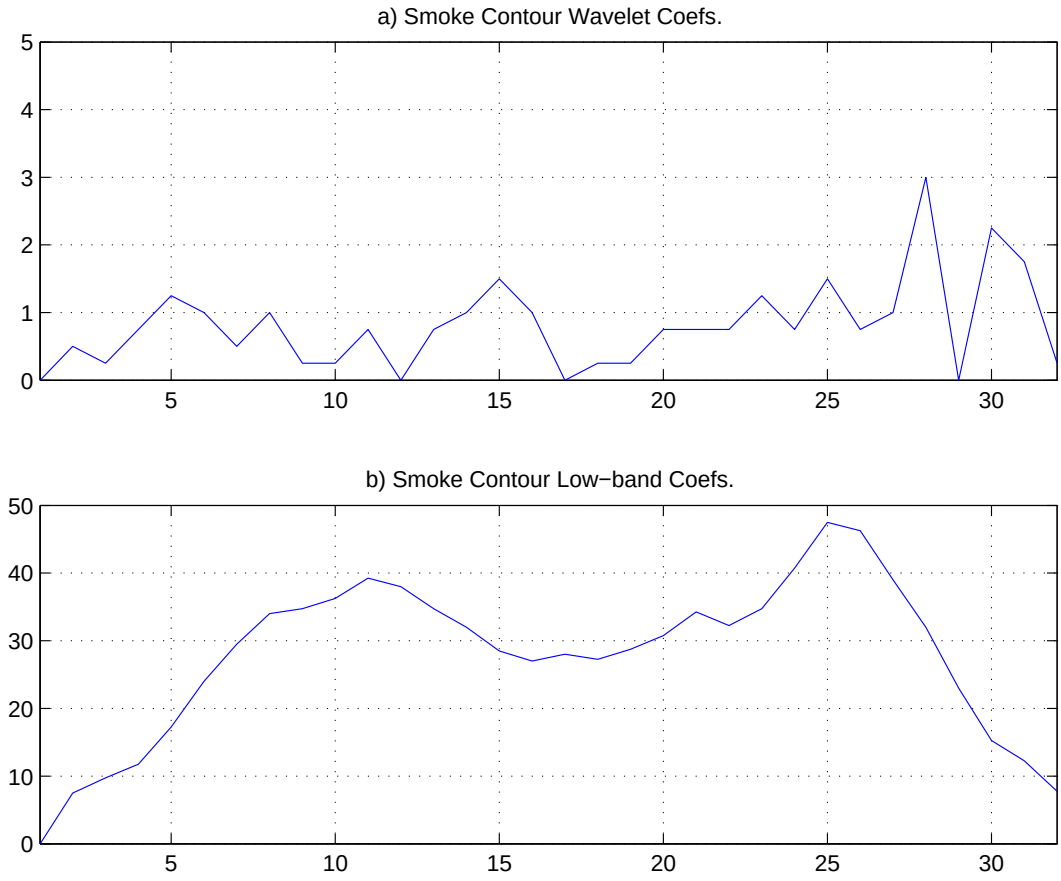

Figure 4.6: The absolute a) wavelet and b) low-band coefficients for the smoke region.

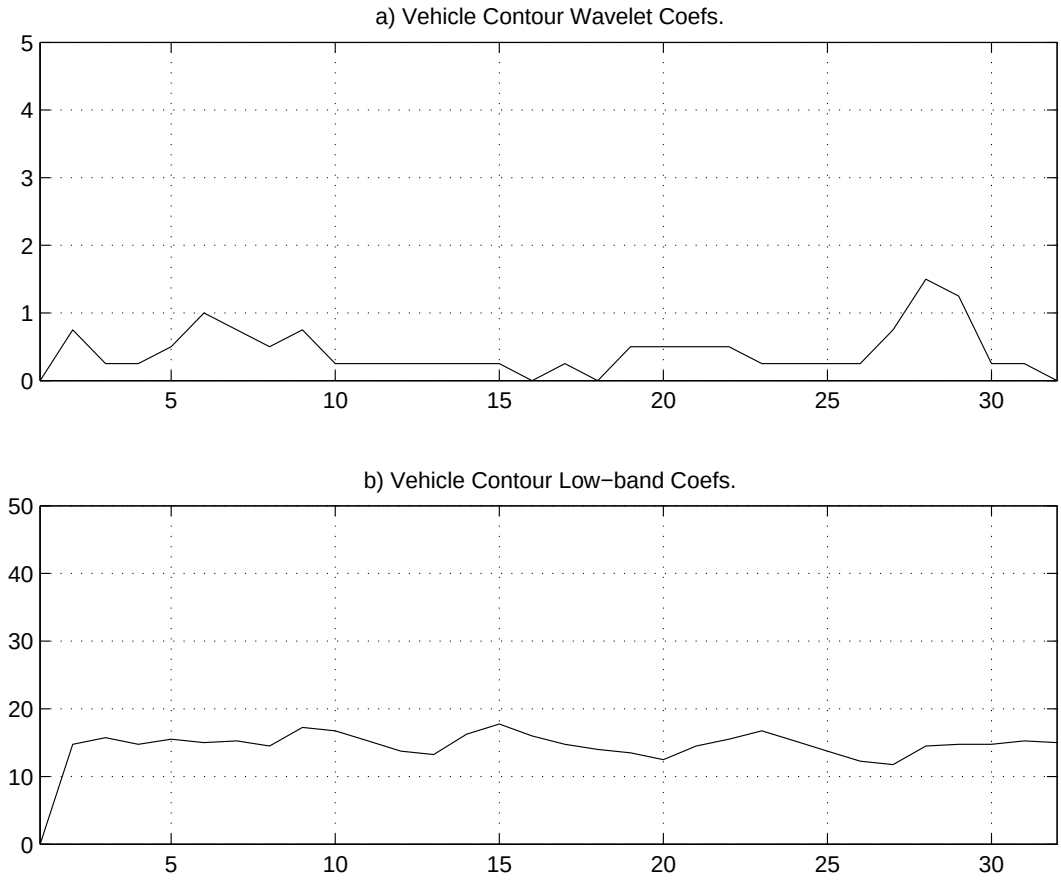

Figure 4.7: The absolute a) wavelet and b) low-band coefficients for the vehicle.

4.3 Experimental Results

The proposed method (Method-4.1) is implemented in a PC with an AMD AthlonXP 2000+ 1.66GHz processor and tested for a large variety of conditions including real-time and off-line videos containing only smoke, both flame and smoke, and videos with no smoke or flame.

It is observed that, the proposed method is suitable for detection of smoke in a range of up to 30m to the camera. This is due to the fact that as the distance increases, the turbulent movements in smoke regions start to disappear and become unobservable after a certain point. It is also hard to estimate the contours of smoke regions at longer distances.

The computational cost of the wavelet transform is low. The filter-bank in Fig. 4.2 have integer coefficient low and high-pass Lagrange filters. The same filters are used for a single level wavelet decomposition of image frames in the spatial wavelet analysis step and also for contour analysis. Smoke detection is achieved in realtime. The processing time per frame is about 5 msec for frames with sizes of 160 by 120 pixels.

Detection results for some of the test sequences are presented in Table 4.1. Smoke is successfully detected in all of the shots containing smoke. No false alarms are issued in live tests and off-line videos recorded in the day time. False alarms are eliminated also for the videos recorded in the night with the help of the contour analysis. A false alarm is issued with the method in [86], Method-4.2, in Movie 9 which is recorded at night. A parking car is captured from its front in this video. The driver intentionally varies the intensity of the front lights of the car. The light beams directed towards the camera at night defines artificial edges around them. These edges appear and disappear continuously as the intensity of the lights change. The U,V channel values of the pixels decrease as the light intensities are lowered, since everywhere in the scene is dark other than the car lights. In this way, car lights at night mimic smoke characteristics in the day time and a false alarm is issued using Method-4.2. However, using the method proposed in this chapter (Method-4.1), this false alarm is eliminated, because

the contour of the moving region defined by the car lights does not possess high frequency characteristics as in a smoke region.

Proposed smoke detection method, Method-4.1, is also compared with the fire detection method presented in [87], Method-4.3, in videos containing both smoke and flame. The comparison results in some of the test sequences are presented in Table 4.2. At the early stages of fire, smoke is released before flames become visible. Method-4.1 successfully detects smoke in such situations earlier than Method-4.3. Hence, early detection of fire is possible with the proposed smoke detection method. In Movies 11 and 12, flames are not in the viewing range of the camera. A fire detection system without smoke detection capability fails in detecting the fire before it spread around.

Table 4.1: Detection results of Method-4.1 and Method-4.2 for some live and off-line videos.

Video Sequences	Number of shots with smoke	Number of Shots detected as Smoke		Description
		Method-4.1	Method-4.2	
Movie 1	0	0	0	Smoke-colored parking car
Movie 2	5	5	5	Fire in a garden
Movie 3	5	5	5	Fire in a garden in snow
Movie 4	7	7	7	A burning box
Movie 5	6	6	6	A burning pile of woods
Movie 6	3	3	3	Fire in a waste-bin in the garden monitored from an indoor camera
Movie 7	0	0	0	Three men walking in a room
Movie 8	8	8	8	Fire in a garden
Movie 9	0	0	1	A parking car in the night

4.4 Summary

In this chapter, a novel method for detecting short range smoke in visible range video is developed. The algorithm is mainly based on determining the edge regions whose wavelet sub-band energies decrease with time and wavelet based

Table 4.2: Smoke and flame detection time comparison of Method-4.1 and Method-4.3, respectively. Smoke is an early indicator of fire. In Movies 11 and 12, flames are not in the viewing range of the camera.

Video Sequences	Method	Detection time (sec.)	Description
Movie 10	Method-4.1	3	Fire in a garden
	Method-4.3	8	
Movie 11	Method-4.1	4	Fire in a trash bin
	Method-4.3	N/A	
Movie 11	Method-4.1	7	Fire at a distance of 30m
	Method-4.3	N/A	

contour analysis of possible smoke regions. These regions are then analyzed along with their corresponding background regions with respect to their RGB and chrominance values. The turbulent behavior of smoke is also modeled with Markov models and set as an additional clue for the final smoke decision.

The method can be used for detection of smoke in movies and video databases as well as real-time detection of smoke. It can be incorporated with a surveillance system monitoring an indoor or an outdoor area of interest for early detection of fire. It can also be integrated with the flame detection method in [87] in order to have a more robust video based fire detection system.

Chapter 5

Flame Detection Using PIR Sensors

In this chapter, a flame detection system based on a pyroelectric (or passive) infrared (PIR) sensor is described. Since the PIR sensor can be visualized as a single-pixel camera, an algorithm similar to the (IR) video flame detection is developed.

The fundamental property that is used in the methods described in Chapters 2 and 3 for is the random flicker of flames. As pointed out in Chapters 2 and 3, flame flicker behavior is a wide-band activity. Similar behavior for flame flicker are also reported in [82] and [7]. As a result, a Markov model based modeling of flame flicker process produces more robust performance compared to frequency domain based methods. In [82], several experiments on the relationship between burner size and flame flicker frequency are presented. Recent research on pyro-IR based combustion monitoring includes [7] in which a monitoring system using an array of PIR detectors is realized.

A regular camera or typical IR flame sensors have a fire detection range of 30 meters. This is due to the fact that flicker in flames cannot be or sensed from longer distances. Therefore, PIR based systems provide a cost-effective solution to the fire detection problem in relatively large rooms as the unit cost of a camera

based system or a regular IR sensor based system is in the order of one thousand dollars.

In this chapter, wavelet domain signal processing is also used, which provides robustness against sensor signal drift due to temperature variations in the observed area. Regular temperature changes due to hot plates and radiators are slow variations compared to the moving objects and flames. Since wavelet subsignals of a waveform are high-pass and band-pass in nature they do not get affected by the slow variations.

Events are classified into two different classes in this approach. The first class represents fire events, on the other hand, the second class represents non-fire events. PIR sensor circuits are designed for detecting the movement of hot objects. Therefore, we include regular human motion events such as walking or running in the non-fire event class.

The PIR sensor can be considered as a single-pixel camera without loss of generality. Therefore, the proposed PIR based fire detection algorithm is obtained simply by removing the spatial analysis steps of the video flame detection methods developed in Chapters 2 and 3.

Data acquisition and the PIR systems are described in the next Section. The proposed algorithm and the experiments are presented in Sections 5.2 and 5.3, respectively.

5.1 PIR Sensor System and Data Acquisition

Commercially available PIR sensor read-out circuits produce binary outputs. However, it is possible to capture a continuous time analog signal indicating the strength of the received signal in time. The corresponding circuit for capturing an analog signal output is shown in Fig. 5.1.

The circuit consists of 4 operational amplifiers (op amps), IC1A, IC1B, IC1C and IC1D. IC1A and B constitute a two stage amplifier circuit whereas IC1C

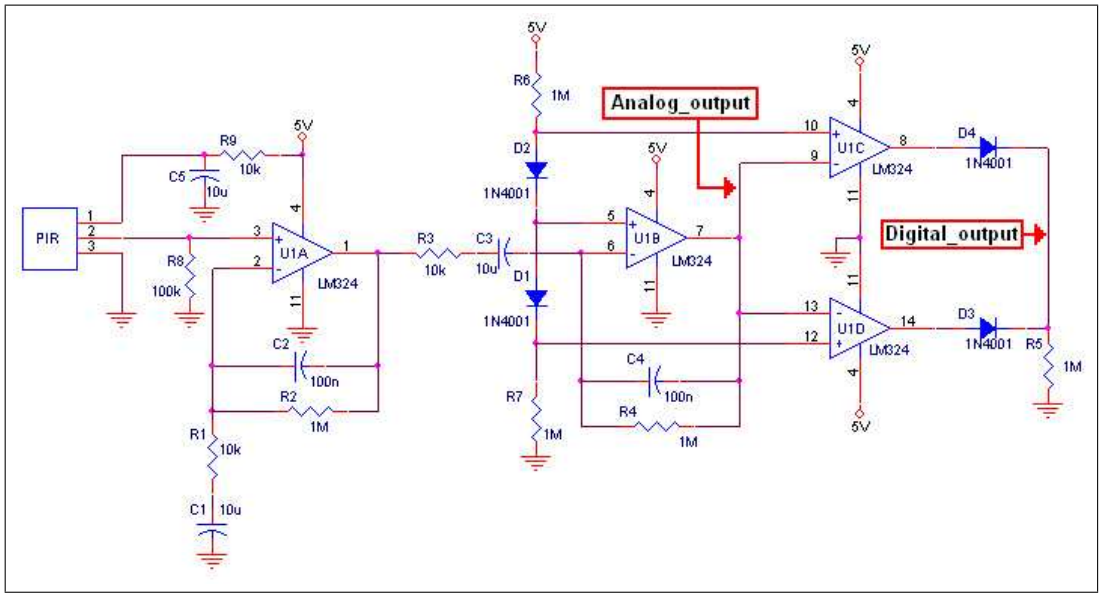

Figure 5.1: The circuit diagram for capturing an analog signal output from a PIR sensor.

and D couple behaves as a comparator. The very-low amplitude raw output at the 2^{nd} pin of the PIR sensor is amplified through the two stage amplifier circuit. The amplified signal at the output of IC1B is fed into the comparator structure which outputs a binary signal, either 0 V or 5 V. Instead of using binary output in the original version of the PIR sensor read-out circuit, we directly measure the analog output signal at the output of the 2^{nd} op amp, IC1B.

In order to capture the flame flicker process the analog signal is sampled with a sampling frequency of $f_s = 50Hz$ because the highest flame flicker frequency is 13Hz [1] and $f_s = 50Hz$ is well above $2 \times 13Hz$. In Fig. 5.2, a frequency distribution plot corresponding to a flickering flame of an uncontrolled fire is shown. It is clear that the sampling frequency of 50Hz is sufficient. Typical sampled signal for no activity case using 8 bit quantization is shown in Fig. 5.3. Other typical received signals from a moving person and flickering fire are presented in Fig. 5.4.

The strength of the received signal from a PIR sensor increases when there is motion due to a hot body within its viewing range. In fact, this is due to the fact that pyroelectric sensors give an electric response to a rate of change

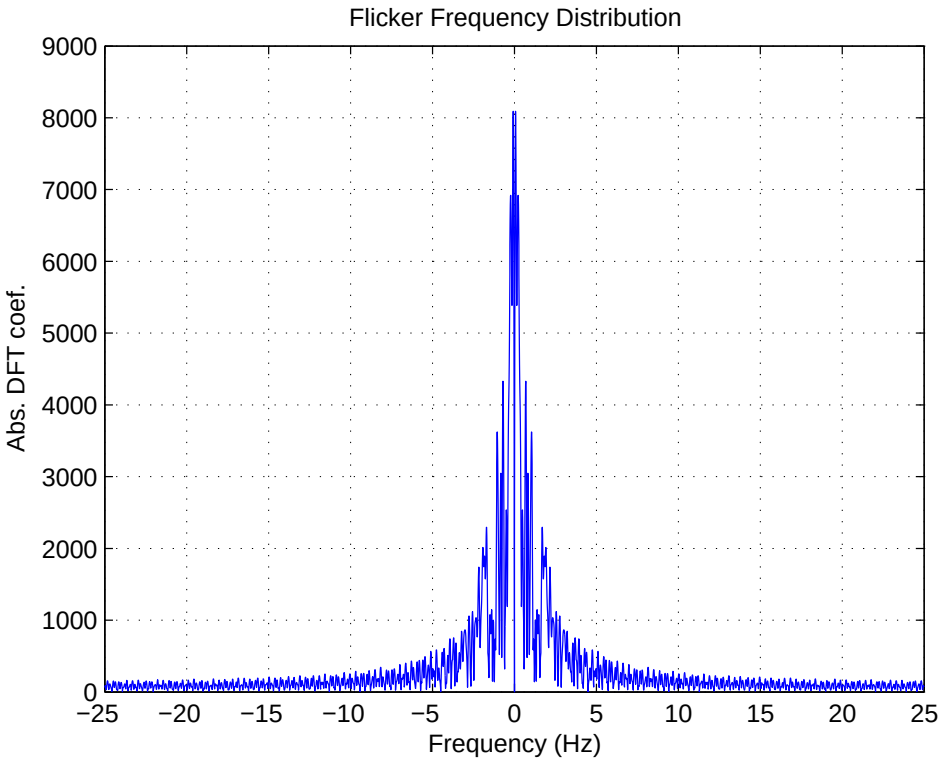

Figure 5.2: Flame flicker spectrum distribution. PIR signal is sampled with 50 Hz.

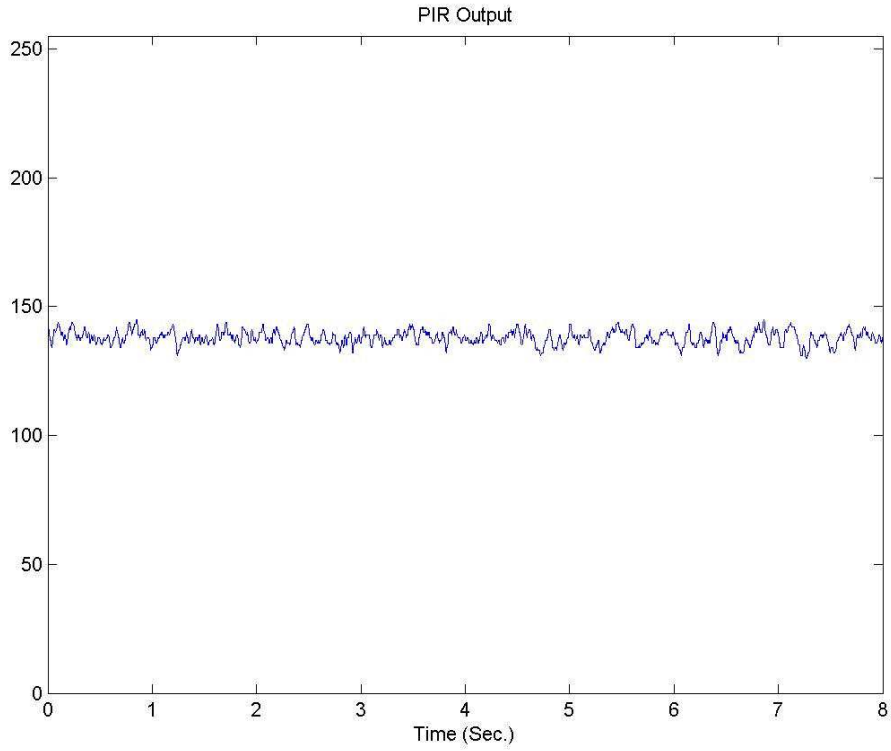

Figure 5.3: A typical PIR sensor output sampled at 50 Hz with 8 bit quantization when there is no activity within its viewing range.

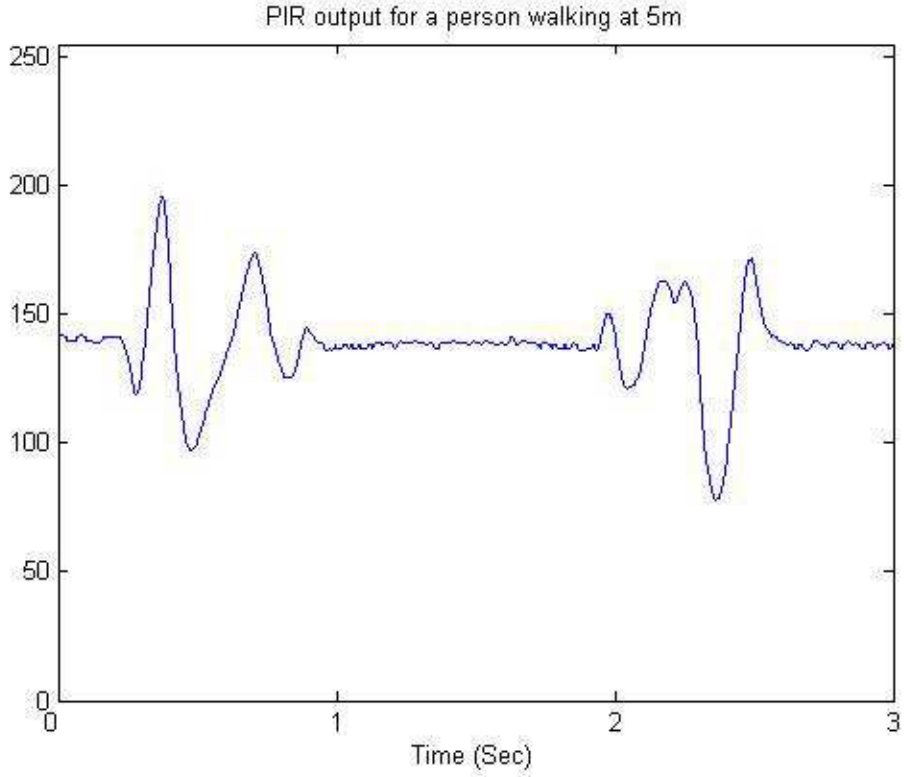

(a)

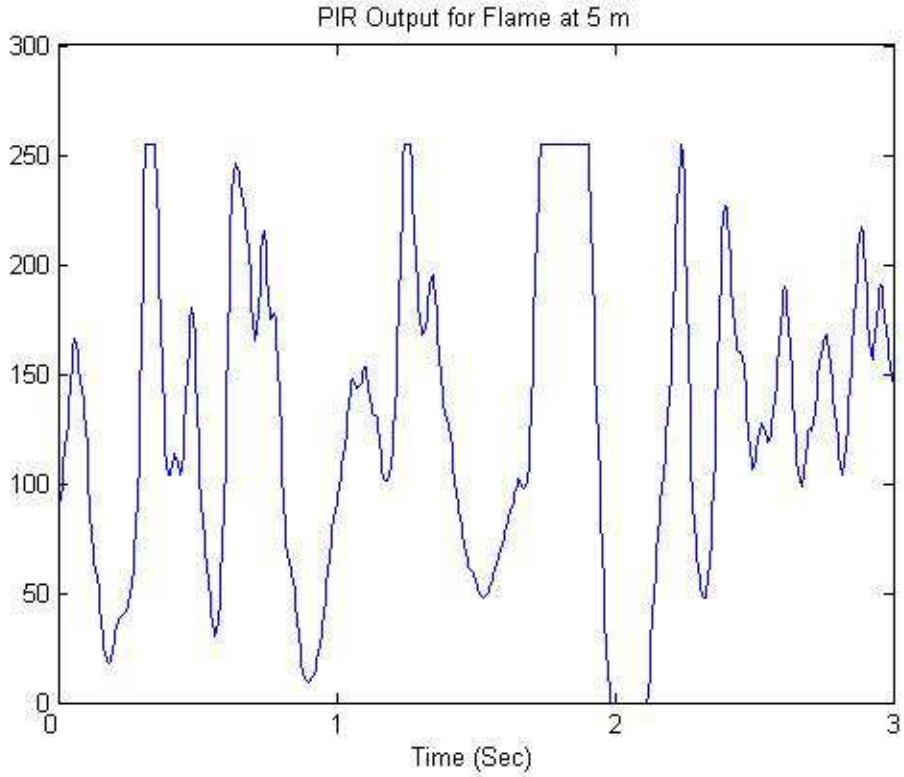

(b)

Figure 5.4: PIR sensor output signals recorded at a distance of 5m for a (a) walking person, and (b) flame.

of temperature rather than temperature itself. On the other hand, the motion may be due to human motion taking place in front of the sensors or flickering flame. In this chapter the PIR sensor data is used to distinguish the flame flicker from the motion of a human being like running or walking. Typically the PIR signal frequency of oscillation for a flickering flame is higher than that of PIR signals caused by a moving hot body. In order to keep the computational cost of the detection mechanism low, we decided to use Lagrange filters for obtaining the wavelet transform coefficients as features instead of using a direct frequency approach, such as FFT based methods.

5.2 Sensor Data Processing and HMMs

There is a bias in the PIR sensor output signal which changes according to the room temperature. Wavelet transform of the PIR signal removes this bias. Let x[n] be a sampled version of the signal coming out of a PIR sensor. Wavelet coefficients obtained after a single stage subband decomposition, w[k], corresponding to [12.5 Hz, 25 Hz] frequency band information of the original sensor output signal x[n] are evaluated with an integer arithmetic high-pass filter corresponding to Lagrange wavelets [13] followed by decimation. The filter bank of a biorthogonal wavelet transform is used in the analysis. The lowpass filter has the transfer function:

$$H_l(z) = \frac{1}{2} + \frac{1}{4}(z^{-1} + z^{1}) \tag{5.1}$$

and the corresponding high-pass filter has the transfer function

$$H_h(z) = \frac{1}{2} - \frac{1}{4}(z^{-1} + z^{1}) \tag{5.2}$$

The term HMM is defined as “hidden-state” Markov model in Rabiner [67]. However, the term HMM is also used in a relaxed manner when several Markov models are used to classify events. The term “hidden” refers to the fact that the model producing the observed data is unknown.

An HMM based classification is carried out for fire detection. Two three-state Markov models are used to represent fire and non-fire events (cf. Fig. 6.2). In these Markov models, state $S1$ corresponds to no activity within the viewing range of the PIR sensor. The system remains in state $S1$ as long as there is not any significant activity, which means that the absolute value of the current wavelet coefficient, $|w[k]|$, is below a non-negative threshold $T1$. A second threshold $T2$ is also defined in wavelet domain which determines the state transitions between $S2$ and $S3$. If $T1 < |w[k]| < T2$, then state $S2$ is attained. In case of $|w[k]| > T2$, state $S3$ is acquired.

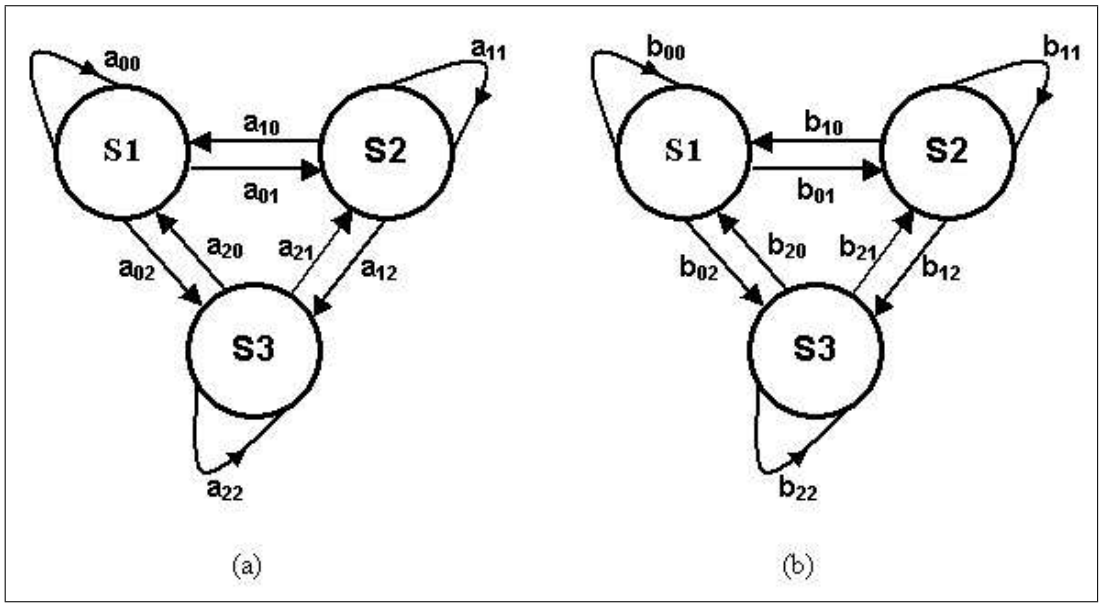

Figure 5.5: Two three-state Markov models are used to represent (a) 'fire' and (b) 'non-fire' classes, respectively.

The first step of the HMM based analysis consists of dividing the wavelet coefficient sequences in windows of 25 samples. For each window, a corresponding state transition sequence is determined. An example state transition sequence of size 5 may look like

$$C = (S2, S1, S3, S2, S1) \tag{5.3}$$

Since the wavelet signal captures the high frequency information in the signal, we expect that there will be more transitions occurring between states when

monitoring fire compared to human motion.

5.2.1 Threshold Estimation for State Transitions

The thresholds $T1$ and $T2$ in the wavelet domain determine the state transition probabilities for a given sensor signal. In the training step, the task is to find optimal values for $T1$ and $T2$. Given $(T1, T2)$ and ground-truth fire and non-fire wavelet training sequences, it is possible to calculate the transition probabilities for each class. Let a_{ij} denote the transition probabilities for the 'fire' class and b_{ij} denote the transition probabilities for the 'non-fire' class.

The decision about the class affiliation of a state transition sequence C of size L is done by calculating the two joint probabilities $P_a(C)$ and $P_b(C)$ corresponding to fire and non-fire classes, respectively:

$$P_a(C) = \prod_i p_a(C_{i+1}|C_i) = \prod_i a_{C_i,C_{i+1}} \tag{5.4}$$

and

$$P_b(C) = \prod_i p_b(C_{i+1}|C_i) = \prod_i b_{C_i,C_{i+1}} \tag{5.5}$$

where $p_a(C_{i+1}|C_i) = a_{C_i,C_{i+1}}$, and $p_b(C_{i+1}|C_i) = \prod_i b_{C_i,C_{i+1}}$, and $i = 1, ..., L$.

In case of $P_a(C) > \xi P_b(C)$, for $\xi > 0$, the class affiliation of state transition sequence C will be declared as 'fire', otherwise it is declared as 'non-fire'. In our implementation, we take $\xi = 1$ without loss of generality.

Given N_a training sequences $A_1, ..., A_{N_a}$ from 'fire' class and N_b training sequences $B_1, ..., B_{N_b}$ from 'non-fire' class, the task of the training step is to find the tuple (T1, T2) which maximizes the dissimilarity D = $(S_a - S_b)^2$, where $S_a = \sum_i P_a(B_i)$ and $S_b = \sum_i P_b(A_i)$.

This means that, for each given tuple $(T1, T2)$, there is a specific value of the dissimilarity D, so that D is a function of $(T1, T2)$

$$D = D(T1, T2) \tag{5.6}$$

Figure 5.6 shows a typical plot of the dissimilarity function $D(T1, T2)$. It can be seen from this figure that the cost function D is multi-modal and and non-differentiable. Therefore, we solve this maximization problem using a Genetic Algorithm (GA) having the objective function $D(T1, T2)$.

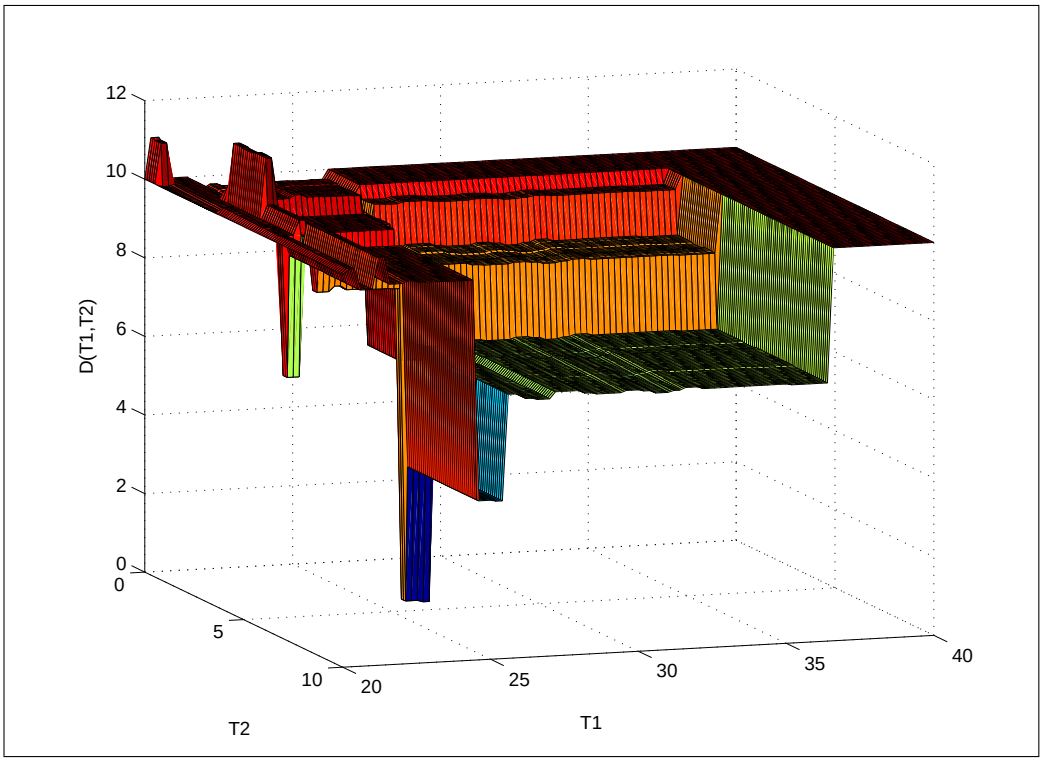

Figure 5.6: A typical plot of the dissimilarity function D(T1,T2)x10^{-4}. It is multi-modal and non-differentiable.

For the training of the HMMs, the state transition probabilities for human motion and flame are estimated from 250 consecutive wavelet coefficients covering a time frame of 10 seconds.

During the classification phase a state history signal consisting of 50 consecutive wavelet coefficients are computed from the received sensor signal. This state sequence is fed to fire and non-fire models in running windows. The model yielding highest probability is determined as the result of the analysis of PIR sensor data.

For flame sequences, the transition probabilities $a's$ should be high and close to each other due to random nature of uncontrolled fire. On the other hand, transition probabilities should be small in constant temperature moving bodies like a walking person because there is no change or little change in PIR signal values. Hence we expect a higher probability for b_{00} than any other b value in the non-fire model which corresponds to higher probability of being in $S1$. The state $S2$ provides hysteresis and it prevents sudden transitions from $S1$ to $S3$ or vice versa.

5.3 Experimental Results

The analog output signal is sampled with a sampling frequency of 50 Hz and quantized at 8 bits. Real-time analysis and classification methods are implemented with C++ running on a PC. Digitized output signal is fed to the PC via RS-232 serial port.

The detection range of a PIR sensor based system is 5 meters but this is enough to cover most rooms with high ceilings. In our experiments we record fire and non-fire sequences at a distance of 5m to the sensor, as well. For fire sequences, we burn paper and alcohol, and record the output signals. For the non-fire sequences, we record walking and running person sequences. The person within the viewing range of the PIR sensor walks or runs on a straight line which is tangent to the circle with a radius of 5m and the sensor being at the center.

The training set consists of 90 fire and 90 non-fire recordings with durations varying between three to four seconds. The test set for fire class is 198 and that of non-fire set is 558. Our method successfully detects fire for 195 of the sequences in the fire test set. It does not trigger fire alarm for any of the sequences in the non-fire test set. This is presented in Table 5.3.

The false negative alarms, 3 out of 198 fire test sequences, are issued for the recordings where a man was also within the viewing range of the sensor along with a fire close to diminish inside a waste-bin. The test setting where false alarms

Table 5.1: Results with 198 fire, 588 non-fire test sequences. The system triggers an alarm when fire is detected within the viewing range of the PIR sensor.

	No. of Sequences	No. of False Alarms	No. of Alarms
Fire Test Sequences	198	3	195
Non-Fire Test Sequences	588	0	0

are issued is presented in Fig. 5.7.

5.4 Summary

In this chapter, a method for flame detection using PIR sensors is proposed. Analog signal from a PIR sensor is sampled with a sampling frequency of 50 Hz and quantized with 8 bits. Single level wavelet coefficients of the output signal are used as feature vectors for flame detection.

PIR sensor output recordings containing various human movements and flames of paper and alcohol fire at a range of 5m are used for training the HMMs corresponding to different events. Thresholds for defining the states of HMMs are estimated using an evolutionary algorithm, since the underlying cost function to be minimized has proved to be multi-modal and non-differentiable. Flame detection results of the proposed algorithm show that the single-pixel assumption for PIR sensor proves to be a correct one.

This thesis demonstrates that low-cost PIR sensors which are commonly used as indoor and outdoor motion detectors, can be utilized as fire sensors when coupled with appropriate processing. The main advantage of a PIR based fire detection system over conventional particle sensors is its ability to detect the presence of fire from a distance which results in a faster response time.

Figure 5.7: The PIR sensor is encircled. The fire is close to die out completely. A man is also within the viewing range of the sensor.

Chapter 6

Wildfire Detection

In this chapter, a computer vision based algorithm for wildfire detection is developed. The main detection algorithm is composed of four sub-algorithms detecting (i) slow moving objects, (ii) smoke-colored regions, (iii) rising regions, and (iv) shadows. Each sub-algorithm yields its own decision as a zero-mean real number, representing the confidence level of that particular sub-algorithm. Confidence values are linearly combined with weights determined according to a novel active fusion method based on the least-mean-square (LMS) algorithm which is a widely used technique in adaptive filtering. Weights are updated on-line using the LMS method in the training (learning) stage. The error function of the LMS based training process is defined as the difference between the weighted sum of decision values and the decision of an oracle, who is the security guard of the forest look-out tower. Simulation results are presented.

6.1 Related Work

Manned lookout posts are widely available in forests all around the world to detect wild fires. Surveillance cameras can be placed on to these surveillance towers to monitor the surrounding forestal area for possible wild fires. Furthermore, they can be used to monitor the progress of the fire from remote centers.

In this chapter, a computer vision based method for wildfire detection is presented. Currently, average fire detection time is five minutes in manned lookout towers in Turkey. Guards have to work 24 hours in remote locations under difficult circumstances. They may get tired or leave the lookout tower for various reasons. Therefore, computer vision based video analysis systems capable of producing automatic fire alarms are necessary to reduce the average forest fire detection time.

There are several approaches on automatic detection of forest fires in the literature. Some of the approaches are directed towards detection of the flames using infra-red and/or visible-range cameras and some others aim at detecting the smoke due to wildfire [22] [46], [4] [36]. There are also recent papers on sensor based detection of forest fires [39], [70]. Infrared cameras and sensor based systems have the ability to capture the rise in temperature however they are much more expensive compared to regular pan-tilt-zoom (PTZ) cameras.

It is almost impossible to view flames of a wildfire from a camera mounted on a forest watch tower unless the fire is very near to the tower. However, smoke rising up in the forest due to a fire is usually visible from long distances. A snapshot of a typical wildfire smoke captured by a look-out tower camera from a distance of 5 Km is shown in Fig. 6.1.

Guillemant and Vicente based their method on the observation that the movements of various patterns like smoke plumes produce correlated temporal segments of gray-level pixels. They utilized fractal indexing using a space-filling Z-curve concept along with instantaneous and cumulative velocity histograms for possible smoke regions. They made smoke decisions about the existence of smoke according to the standard deviation, minimum average energy, and shape and smoothness of these histograms [36].

Smoke at far distances ($> 100m$ to the camera) exhibits different spatio-temporal characteristics than nearby smoke and fire [84], [23], [87]. This demands specific methods explicitly developed for smoke detection at far distances rather than using nearby smoke detection methods described in [86]. This approach is in accordance with the 'weak' Artificial Intelligence (AI) framework [61] introduced

Figure 6.1: Snapshot of a typical wildfire smoke captured by a forest watch tower which is 5 km away from the fire (rising smoke is marked with an arrow).

by Hubert L. Dreyfus as opposed to 'generalized' AI. According to this framework each specific problem in AI should be addressed as an individual engineering problem with its own characteristics [25], [26].

The proposed automatic video based wildfire detection algorithm is based on four sub-algorithms: (i) slow moving video object detection, (ii) smoke-colored region detection, (iii) rising video object detection, (iv) shadow detection and elimination. Each sub-algorithm decides on the existence of smoke in the viewing range of the camera separately. Decisions from sub-algorithms are combined together by an adaptive active fusion method. Initial weights of the sub-algorithms

are determined from actual forest fire videos and test fires. They are updated using the least-mean-square (LMS) algorithm during initial installation. The LMS algorithm was initially developed by Widrow in 1960's together with neural networks [91]. The error function in the LMS adaptation is defined as the difference between the overall decision of the compound algorithm and the decision of an oracle. In our case, the oracle is the security guard. The compound decision algorithm will obviously produce false alarms. The system asks the guard to verify its decision whenever an alarm occurs. In this way, the user actively participate in the learning process.

The chapter is organized as follows: Section 6.2 describes briefly each one of the four sub-algorithms which make up the compound (main) wildfire detection algorithm. Adaptive active fusion method is described in Section 6.3. In Section 6.4, experimental results are presented and the proposed online active fusion method is compared with the universal linear predictor and the weighted majority algorithms. Finally, conclusions are drawn in Section 6.5.

6.2 Building Blocks of Wildfire Detection Algorithm

Wildfire detection algorithm is developed to recognize the existence of wildfire smoke within the viewing range of the camera monitoring forestal areas. The proposed wildfire smoke detection algorithm consists of four main sub-algorithms: (i) slow moving object detection in video, (ii) smoke-colored region detection, (iii) rising video object detection, (iv) shadow detection and elimination of shadow regions, with decision functions, $D_1(x,n)$, $D_2(x,n)$, $D_3(x,n)$ and $D_4(x,n)$, respectively, for each pixel at location x of every incoming image frame at time step n. Computationally efficient sub-algorithms are selected in order to realize a real-time wildfire detection system working in a standard PC.

Decision functions $D_i, \quad i = 1, ..., M$ of sub-algorithms do not produce binary values 1 (correct) or -1 (false), but they produce zero-mean real numbers for

each incoming sample x. If the number is positive (negative), then the individual algorithm decides that there is (not) smoke due to forest fire in the viewing range of the camera. Output values of decision functions express the confidence level of each sub-algorithm. Higher the value, the more confident the algorithm.

6.2.1 Detection of Slow Moving Objects

Video objects at far distances to the camera seem to move slower (px/sec) in comparison to the nearby objects moving at the same speed. Assuming the camera is fixed, two background images, $B^{fast}(x,n)$ and $B^{slow}(x,n)$ corresponding to the scene with different update rates are estimated [9], [65], where x is the location of the pixel at frame number n.

In [19] a background image $B(x,n+1)$ at time instant $n+1$ is recursively estimated from the image frame $I(x,n)$ and the background image $B(x,n)$ of the video as follows:

$$B(x,n+1) = \begin{cases} aB(x,n) + (1-a)I(x,n) & \text{if } x \text{ is stationary} \\ B(x,n) & \text{if } x \text{ is a moving pixel} \end{cases} \tag{6.1}$$

where $I(x,n)$ represent the intensity value of the pixel at location x in the n^{th} video frame I, and a is a parameter between 0 and 1. Initially, $B^{fast}(x,0)$ and $B^{slow}(x,0)$ can be taken as $I(x,0)$. Stationary and moving pixel definitions are given in [19]. Background images $B^{fast}(x,n)$ and $B^{slow}(x,n)$ are updated as in Eq. 6.1 with different update rates. In our implementation, $B^{fast}(x,n)$ is updated at every frame and $B^{slow}(x,n)$ is updated once in a second with $a = 0.7$ and 0.9, respectively.

Slow moving objects within the viewing range of the camera are detected by comparing background images, B^{fast} and B^{slow} [83], [9], [65]. If there exists a substantial difference between the two images for some period of time, then an alarm for slow moving region is raised, and the region is marked.

The decision value indicating the confidence level of the first sub-algorithm is determined by the difference between background images. The decision function

$D_1(x,n)$ is defined as:

$$D_1(x,n) = \begin{cases} -1 & \text{if } |B^{fast}(x,n) - B^{slow}(x,n)| \leq T_{low} \\ 2\frac{|B^{fast}(x,n) - B^{slow}(x,n)| - T_{low}}{T_{high} - T_{low}} - 1 & \text{if } T_{low} \leq |B^{fast}(x,n) - B^{slow}(x,n)| \leq T_{high} \\ 1 & \text{if } T_{high} \leq |B^{fast}(x,n) - B^{slow}(x,n)| \end{cases} \tag{6.2}$$

where $0 < T_{low} < T_{high}$ are experimentally determined threshold values. In our implementation, T_{low} (T_{high}) is taken as 10 (30) on the luminance (Y) component of video.

Confidence value is 1 (-1), if the difference $|B^{fast}(x,n) - B^{slow}(x,n)|$ is higher (lower) than threshold T_{high} (T_{low}). The decision function $D_1(x,n)$ takes real values in the range [-1,1] if the difference is in between the two threshold values.

Smoke due to forest fires at further distances ($>$ 5km) to the camera seem to move even slower. Therefore, smoke regions at these distances appear neither in B^{fast} nor B^{slow} images. This results in lower difference values between background images B^{slow} and B^{fast}. In order to have substantial difference values and detect smoke at distances further than 5km to the camera, B^{fast} terms in Eq. 6.2 are replaced by the current image I.

6.2.2 Detection of Smoke-Colored Regions

Whenever a slow moving region is detected, its color content is analyzed. Smoke due to forest fires is mainly composed of carbon dioxide, water vapor, carbon monoxide, particulate matter, hydrocarbons and other organic chemicals, nitrogen oxides, trace minerals and some other compounds [2]. The grayish color of the rising plume is primarily due to water vapor and carbon particles in the output fire composition. Such regions can be identified by setting thresholds in the YUV color space. Also, luminance value of smoke regions should be high especially at the initial phases of a wildfire, as shown in Fig. 6.1. On the other hand, the chrominance values should be very low in a smoke region. Confidence value corresponding to this sub-algorithm should account for these characteristics.

The decision function $D_2(x,n)$ takes values between 1 and -1 depending on the values of the $Y(x,n)$, $U(x,n)$ and $V(x,n)$ channel values. The decision function $D_2(x,n)$ is defined as:

$$D_2(x,n) = \begin{cases} 1 - \frac{|U(x,n)-128|+|V(x,n)-128|}{128}, & \text{if } Y(x,n) > T_I \\ -1, & \text{otherwise} \end{cases} \tag{6.3}$$

where $Y(x,n)$, $U(x,n)$ and $V(x,n)$ are the luminance and chrominance values of the pixel at location x of the input image frame at time step n, respectively. The luminance component Y takes real values in the range $[0, 255]$ in an image and the mean values of chrominance channels, U and V are increased to 128 so that they also take values between 0 and 255. The threshold T_I is an experimentally determined value and taken as 100 on the luminance (Y) component in this work. The confidence level of $D_2(x,n)$ is -1 if $Y(x,n)$ is below T_I. The reason that we have the threshold T_I is to eliminate dark regions which also have low chrominance values. Since wildfire smoke regions are mostly colorless, having very low chrominance values, the decision value approaches to 1 as the chrominance values $U(x,n)$ and $V(x,n)$ are around the mean value of 128 for pixels whose luminance values are greater than T_I. Confidence value drops down to -1 for pixels with high chrominance values.

6.2.3 Detection of Rising Regions

Wildfire smoke regions tend to rise up into the sky at the early stages of the fire. This characteristic behavior of smoke plumes is modeled with three-state Hidden Markov Models (HMM) in this chapter. Temporal variation in row number of the upper-most pixel belonging to a slow moving region is used as a one dimensional (1-D) feature signal, $F = f(n)$, and fed to the Markov models shown in Fig.6.2. One of the models (λ_1) corresponds to genuine wildfire smoke regions and the other one (λ_2) corresponds to regions with clouds and cloud shadows. Transition probabilities of these models are estimated off-line from actual wildfires and test fires, and clouds. The state S1 is attained, if the row value of the upper-most pixel in the current image frame is smaller than that of the previous frame (rise-up). If the row value of the upper-most pixel in the current image frame is larger than

that of the previous frame, then S2 is attained and this means that the region moves-down. No change in the row value corresponds to S3.

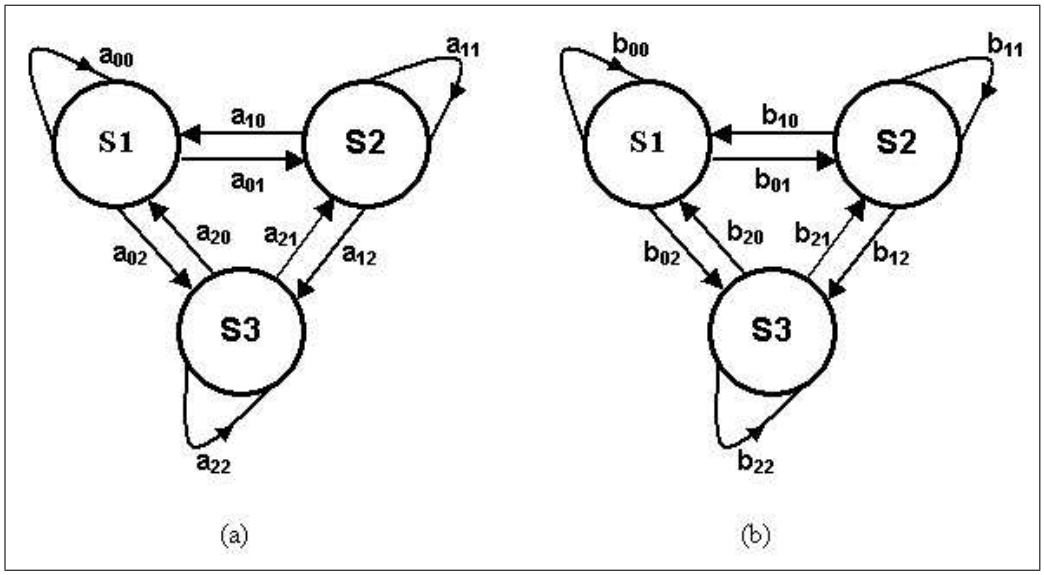

Figure 6.2: Markov model λ_1 corresponding to wildfire smoke (left) and the Markov model λ_2 of clouds (right). Transition probabilities a_{ij} and b_{ij} are estimated off-line.

A slow moving region is classified as a rising region when the probability of obtaining the observed feature signal $F = f(n)$ given the probability model λ_1 is greater than the probability of obtaining the observed feature signal $F = f(n)$ given the probability model λ_2, i.e., when the upper-most pixel belonging to a slow moving region tends to exhibit a rising characteristic:

$$p_1 = P(F|\lambda_1) > p_2 = P(F|\lambda_2) \tag{6.4}$$

where F is the observed feature signal, λ_1 and λ_2 represent the Markov models for wildfire smoke and clouds, respectively.

As the probability p_1 (p_2) gets a larger value than p_2 (p_1), the confidence level of this sub-algorithm increases (decreases). Therefore, the zero-mean decision function $D_3(x, n)$ is determined by the normalized difference of these probabilities:

$$D_3(x, n) = \frac{p_1 - p_2}{p_1 + p_2} \tag{6.5}$$

When a slow moving region is classified as a rising region, i.e., $p_1 \gg p_2$, $D_3(x,n)$ is close to 1. Otherwise, the decision function $D_3(x,n)$ is close to -1.

6.2.4 Shadow Detection and Removal

Shadows of slow moving clouds are major source of false alarms for video based wildfire smoke detection systems. Unfortunately, shadows of clouds have very low U and V values, similar to smoke regions due to wildfires.

The decision function for shadow regions are defined based on the shadow detection method described in [41]. Average RGB values are calculated for slow moving regions both in the current and the background images. Let $S(n)$ represent a slow moving region in the image I at frame number n. The average color vector, $\vec{c_{I,S}}(n)$, of this region in the image I at frame number n is calculated as follows:

$$\vec{c_{I,S}}(n) = \frac{1}{A_{S(n)}}\Big(\sum_{x\in S(n)} r_I(x,n), \sum_{x\in S(n)} g_I(x,n), \sum_{x\in S(n)} b_I(x,n)\Big) \tag{6.6}$$

where $A_{S(n)}$ is the area of the slow moving region $S(n)$, and $r_I(x,n)$, $g_I(x,n)$, and $b_I(x,n)$ are the red, green and blue channel values of the pixel at location x in the $n-th$ image frame I. Similarly, average color vector, $\vec{c_{B,S}}$, of the same region in the background image, B, is calculated as follows:

$$\vec{c_{B,S}}(n) = \frac{1}{A_{S(n)}}\Big(\sum_{x\in S(n)} r_B(x,n), \sum_{x\in S(n)} g_B(x,n), \sum_{x\in S(n)} b_B(x,n)\Big) \tag{6.7}$$

where $r_B(x,n)$, $g_B(x,n)$, and $b_B(x,n)$ are the red, green and blue channel values of the pixel at location x in the background image frame B at frame number n. We used the background image B^{slow} as the background image in our implementation.

In shadow regions, the angle, $\theta(x)$, between the average color vectors, $\vec{c_{I,S}}$ and $\vec{c_{B,S}}$, should be small and the magnitude of the vector in the current image should be smaller than that of the vector in the background image, i.e., $|\vec{c_{I,S}}(n)| < |\vec{c_{B,S}}(n)|$ [41]. This is because shadow regions retain the color and the underlying texture to some extent.

The confidence value of this sub-algorithm is defined according to the angle and magnitudes of average color vectors, $c_{I,S}^{\vec{}}(n)$ and $c_{B,S}^{\vec{}}(n)$. The decision function $D_4(x,n)$ corresponding to this sub-algorithm for a pixel in the $n-th$ image and background frames is given by:

$$D_4(x,n) = \begin{cases} \frac{4|\theta(x)|}{\pi} - 1, & \text{if } |c_{I,S}^{\vec{}}(n)| < |c_{B,S}^{\vec{}}(n)| \\ -1, & \text{if } |c_{I,S}^{\vec{}}(n)| > |c_{B,S}^{\vec{}}(n)| \end{cases} \tag{6.8}$$

where $\theta(x)$ is the angle between the two color vectors. When the angle between the two color vectors are close to each other, the function $D_4(x,n)$ is close to -1 which corresponds to shadow regions. Similar decision functions for shadow detection can be defined according to other color spaces including the YUV space.

There are other shadow detection algorithms in the literature [66]. However, we selected the algorithm described in this section, because of its low computational complexity. Our aim is to realize a wildfire detection system working in real-time.

The threshold values in all of the decision functions described in this section are chosen in such a way that they produce positive values for all of the wild fire video recordings that we have. Still, one can define other sets of decision functions with different threshold values representing various threat/security levels. In the standard monitoring mode without any fires in the viewing range of the cameras, the security level may be kept as 'low'. Once a fire is detected, the system can automatically switch to security level 'high' and increase the probability of detecting possible fires that may follow the initial one, by lowering the thresholds in the decision functions.

Decision results of four sub-algorithms, D_1, D_2, D_3 and D_4 are linearly combined to reach a final decision on a given pixel whether it is a pixel of a smoke region or not. Equal weights could be assigned to each sub-algorithm, however, this would yield a non-adaptive algorithm without any learning capability. On the other hand, wildfire detection is actually a dynamic process. There may be wild variations between forestal areas and substantial temporal changes may occur within the same forestal region. An adaptive combination of different sub-algorithms would be more appropriate for robust wildfire detection. In the next

section the adaptive active learning algorithm will be discussed.

6.3 Adaptation of Sub-algorithm Weights

Cameras, once installed, operate at forest watch towers throughout the fire season for about six months. There is usually a guard in charge of the cameras, as well. The guard can supply feed-back to the detection algorithm after the installation of the system. Whenever an alarm is issued, she/he can verify it or reject it. In this way, she/he can participate the learning process of the adaptive algorithm. The proposed active fusion algorithm can be also used in other supervised learning problems.

As described in the previous section, the main wildfire detection algorithm is composed of four sub-algorithms. Each algorithm has its own decision function yielding a zero-mean real number for slow moving regions at every image frame of a video sequence. Decision values from sub-algorithms are linearly combined and weights of sub-algorithms are adaptively updated in our approach. Sub-algorithm weights are updated according to the least-mean-square (LMS) algorithm which is by far the most widely used adaptive filtering method [37], [93]. It also finds applications in general classification and pattern recognition problems [27]. However, to the best of our knowledge, this thesis is the first example of an LMS based approach introduced in an online active learning framework. Due to the tracking capability of the algorithm, the proposed framework for online active decision fusion may find applications in problems with drifting concepts.

Another innovation that we introduced in this chapter is that individual decision algorithms do not produce binary values 1 (correct) or -1 (false), but they produce a zero-mean real number. If the number is positive (negative), then the individual algorithm decides that there is (not) smoke due to forest fire in the viewing range of the camera. Higher the absolute value, the more confident the sub-algorithm.

Let the compound algorithm be composed of M-many detection algorithms:

$D_1, ..., D_M$. Upon receiving a sample input x, each algorithm yields a zero-mean decision value $D_i(x) \in \mathbb{R}$. The type of the sample input x may vary depending on the algorithm. It may be an individual pixel, or an image region, or the entire image depending on the sub-algorithm of the computer vision problem. In the wildfire detection problem the number of sub-algorithms, M=4 and each pixel at the location x of incoming image frame is considered as a sample input for every detection algorithm.

Let $\mathbf{D}(x,n) = [D_1(x,n)...D_M(x,n)]^T$, be the vector of confidence values of the sub-algorithms for the pixel at location x of input image frame at time step n, and $\mathbf{w}(n) = [w_1(n)...w_M(n)]^T$ be the current weight vector.

We define

$$\hat{y}(x,n) = \mathbf{D^T}(x,n)\mathbf{w}(n) = \sum_i w_i(n)D_i(x,n) \tag{6.9}$$

as an estimate of the correct classification result $y(x,n)$ of the oracle for the pixel at location x of input image frame at time step n, and the error $e(x,n)$ as $e(x,n) = y(x,n) - \hat{y}(x,n)$. Weights are updated by minimizing the mean-square-error (MSE):

$$\min_{w_i} E[(y(x,n) - \hat{y}(x,n))^2], \quad i = 1, ..., M \tag{6.10}$$

where E represents the expectation operator. Taking the derivative with respect to weights:

$$\frac{\partial E}{\partial w_i} = -2E[(y(x,n) - \hat{y}(x,n))D_i(x,n)] = -2E[e(x,n)D_i(x,n)], \quad i = 1, ..., M \tag{6.11}$$

and setting the result to zero:

$$-2E[e(x,n)D_i(x,n)] = 0, \quad i = 1, ..., M \tag{6.12}$$

a set of M equations is obtained. The solution of this set of equations is called the Wiener solution [37], [93]. Unfortunately, the solution requires the computation of cross-correlation terms in Eq. 6.12. The gradient in Eq. 6.11 can be used in a steepest descent algorithm to obtain an iterative solution to the minimization problem in Eq. 6.10 as follows:

$$\mathbf{w}(n+1) = \mathbf{w}(n) + \lambda E[e(x,n)\mathbf{D}(x,n)] \tag{6.13}$$

where λ is a step size. In the well-known LMS algorithm, the ensemble average $E[e(x,n)\mathbf{D}(x,n)]$ is estimated using the instantaneous value $e(x,n)\mathbf{D}(x,n)$ or it can be estimated from previously processed pixels as follows:

$$\hat{e}(x,n)\hat{\mathbf{D}}(x,n)] = \frac{1}{L}\sum_{x,n} e(x,n)\mathbf{D}(x,n) \tag{6.14}$$

where L is the number of previously processed pixels which is equal to the number of terms inside the summation. The LMS algorithm is derived by noting that the quantity in Eq. 6.13 is not available but its instantaneous value is easily computable, and hence the expectation is simply replaced by its instantaneous value [73]:

$$\mathbf{w}(n+1) = \mathbf{w}(n) + \lambda e(x,n)\mathbf{D}(x,n) \tag{6.15}$$

Eq. 6.15 is a computable weight-update equation. Whenever the oracle provides a decision, the error $e(x,n)$ is computed and the weights are updated according to Eq. 6.15. Note that, the oracle does not assign her/his decision to each and every pixel one by one. She/he actually selects a window on the image frame and assigns a "1" or "-1" to the selected window.

Convergence of the LMS algorithm can be analyzed based on the MSE surface:

$$E[e^2(x,n)] = P_y(x,n) - 2\mathbf{w}^T\mathbf{p} - \mathbf{w}^T\mathbf{R}\mathbf{w} \tag{6.16}$$

where $P_y = E[y^2(x,n)]$, $\mathbf{p} = E[y(x,n)\mathbf{D}(x,n)]$, and $\mathbf{R} = E[\mathbf{D}(x,n)\mathbf{D}^T(x,n)]$, with the assumption that $y(x,n)$ and $\mathbf{D}(x,n)$ are wide-sense-stationary random processes. The MSE surface is a function of the weight vector $\mathbf{w}$. Since $E[e^2(x,n)]$ is a quadratic function of $\mathbf{w}$, it has a single global minimum and no local minima. Therefore, the steepest descent algorithm of Eqs. 6.13 and 6.15 is guaranteed to converge to the Wiener solution, $\mathbf{w}^*$ [73] with the following condition on the step size λ [93]:

$$0 < \lambda < \frac{1}{\alpha_{max}} \tag{6.17}$$

where α_{max} is the largest eigenvalue of $\mathbf{R}$.

In Eq. 6.15, the step size λ can be replaced by

$$\frac{\mu}{||\mathbf{D}(x,n)||^2} \tag{6.18}$$

as in the normalized LMS algorithm, which leads to:

$$\mathbf{w}(n+1) = \mathbf{w}(n) + \mu \frac{e(x,n)}{||\mathbf{D}(x,n)||^2}\mathbf{D}(x,n) \tag{6.19}$$

where the μ is an update parameter and the normalized LMS algorithm converges for $0 < \mu < 2$ to the Wiener solution, $\mathbf{w}^*$ with the wide-sense-stationarity assumption. Initially the weights can be selected as $\frac{1}{M}$. The adaptive algorithm converges, if $y(x,n)$ and $D_i(x,n)$ are wide-sense stationary random processes and when the update parameter μ lies between 0 and 2 [92]. The update algorithm is summarized in Fig. 6.5.

The sub-algorithms described in the previous section are devised in such a way that each of them yields non-negative decision values, D_i's, for pixels inside smoke regions, in all of the wild fire video recordings that we have. The final decision which is nothing but the weighted sum of individual decisions must also take a non-negative value when the decision functions yield non-negative values. This implies that, in the weight update step of the active decision fusion method, weights, $w_i(n) \geq 0$, should also be non-negative. In the proposed method, the weights are updated according to Eq. 6.19. If any one of the weights happens to be negative then it is set to zero complying with the non-negative weight constraint.

Unfortunately, the wide-sense-stationarity assumption is not a valid assumption in natural images, as in many signal processing applications. Nevertheless, the LMS algorithm is successfully used in many telecommunication and signal processing problems. Wide-sense-stationarity assumption may be valid in some parts of a sequence in which there are no spatial edges and temporal changes.

The main advantage of the LMS algorithm compared to other related methods, such as the weighted majority algorithm [47], is the controlled feedback mechanism based on the error term. Weights of the algorithms producing incorrect (correct) decision is reduced (increased) according to Eq. 6.19 in a controlled and fast manner. In weighted majority algorithm, conflicting weights with the oracle are simply reduced by a factor of two [47], [58]. Another advantage of the LMS algorithm is that it does not assume any specific probability distribution about the data.

6.3.1 Set Theoretic Analysis of the Weight Update Algorithm

The weight update algorithm summarized in Fig. 6.5 can be also analyzed in a vector space framework without using stochastic signal processing concepts.

Ideally, weighted decision values of sub-algorithms should be equal to the decision value of $y(x,n)$ the oracle:

$$y(x,n) = \mathbf{D}^T(x,n)\mathbf{w} \tag{6.20}$$

which represents a hyperplane in the M-dimensional space, $\mathbf{w} \in \mathbb{R}^M$. A hyperplane is a close and convex set in $\mathbb{R}^M$. At time instant n, $\mathbf{D}^T(x,n)\mathbf{w}(n)$ may not be equal to $y(x,n)$. The next set of weights are determined by projecting the current weight vector $\mathbf{w}(n)$ onto the hyperplane represented by Eq. 6.20. This process is geometrically depicted in Fig. 6.4. The orthogonal projection $\mathbf{w}(n+1)$ of the vector of weights $\mathbf{w}(n) \in \mathbb{R}^M$ onto the hyperplane $y(x,n) = \mathbf{D}^T(x,n)\mathbf{w}$ is the closest vector on the hyperplane to the vector $\mathbf{w}(n)$ (cf. Fig 6.3).

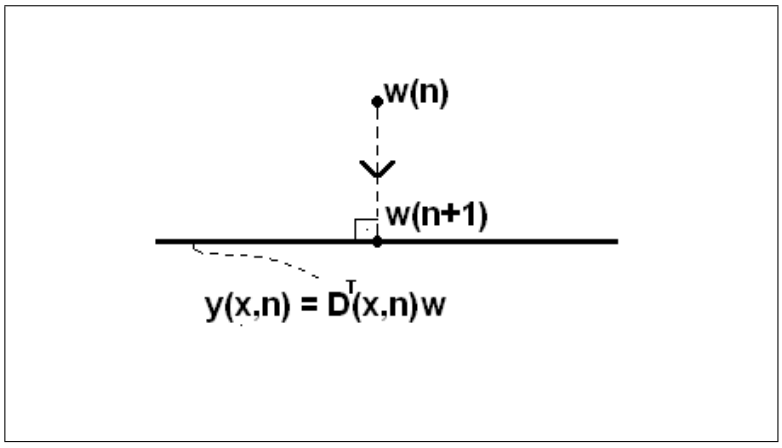

Figure 6.3: Orthogonal Projection: Find the vector $\mathbf{w}(n+1)$ on the hyperplane $y(x,n) = \mathbf{D}^T(x,n)\mathbf{w}$ minimizing the distance between $\mathbf{w}(n)$ and the hyperplane.

Let us formulate the problem as a minimization problem:

$$\mathbf{w}(n+1) = \arg\min_{\mathbf{w}} ||\mathbf{w} - \mathbf{w}(n)|| \tag{6.21}$$

$$s.t. \quad \mathbf{D}^T(x,n)\mathbf{w} = y(x,n) \tag{6.22}$$

Solution can be obtained by using Lagrange multipliers:

$$\mathcal{L} = \sum_i (w_i(n) - w_i)^2 + \lambda(\mathbf{D}^T(x,n)\mathbf{w} - y(x,n)) \tag{6.23}$$

Taking partial derivatives with respect to w_i:

$$\frac{\partial \mathcal{L}}{\partial w_i} = 2(w_i(n) - w_i) + \lambda D_i(x,n), \quad i = 1, ..., M \tag{6.24}$$

and setting the result to zero:

$$2(w_i(n) - w_i) + \lambda D_i(x,n) = 0, \quad i = 1, ..., M \tag{6.25}$$

a set of M equations is obtained:

$$\mathbf{w}(n+1) = \mathbf{w}(n) + \frac{\lambda}{2}\mathbf{D}(x,n) \tag{6.26}$$

The Lagrange multiplier, λ, can be obtained from the condition equation:

$$\mathbf{D}^T(x,n)\mathbf{w} - y(x,n) = 0 \tag{6.27}$$

as follows:

$$\lambda = 2\frac{y(x,n) - \hat{y}(x,n)}{||\mathbf{D}(x,n)||^2} = 2\frac{e(x,n)}{||\mathbf{D}(x,n)||^2} \tag{6.28}$$

where the error, $e(x,n)$, is defined as $e(x,n) = y(x,n) - \hat{y}(x,n)$ and $\hat{y}(x,n) = \mathbf{D}^T(x,n)\mathbf{w}(n)$. Plugging this into Eq. 6.26

$$\mathbf{w}(n+1) = \mathbf{w}(n) + \frac{e(x,n)}{||\mathbf{D}(x,n)||^2}\mathbf{D}(x,n) \tag{6.29}$$

is obtained. Note that this is identical to Eq. 6.30

The projection vector $\mathbf{w}(n+1)$ is calculated as follows:

$$\mathbf{w}(n+1) = \mathbf{w}(n) + \frac{e(x,n)}{||\mathbf{D}(x,n)||^2}\mathbf{D}(x,n) \tag{6.30}$$

This equation is the same as the NLMS equation, Eq. 6.19, with $\mu = 1$.

Whenever a new input arrives, another hyperplane based on the new decision values $\mathbf{D}(x,n)$ of sub-algorithms, is defined in $\mathbb{R}^M$

$$y(x,n+1) = \mathbf{D}^T(x,n+1)\mathbf{w} \tag{6.31}$$

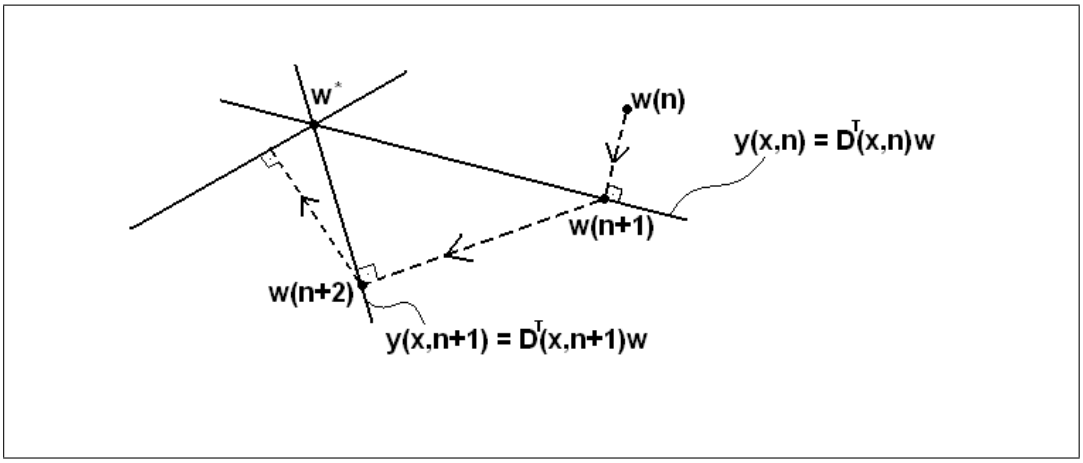

Figure 6.4: Geometric interpretation: Weight vectors corresponding to decision functions at each frame are updated as to satisfy the hyperplane equations defined by the oracle's decision $y(x,n)$ and the decision vector $\mathbf{D}(x,n)$. Lines in the figure represent hyperplanes in $\mathbb{R}^M$.

This hyperplane will probably not be the same as $y(x,n) = \mathbf{D}^T(x,n)\mathbf{w}(n)$ hyperplane as shown in Fig. 6.4. The next set of weights, $\mathbf{w}(n+2)$, are determined by projecting $\mathbf{w}(n+1)$ onto the hyperplane in Eq. 6.31. Iterated weights converge to the intersection of hyperplanes [10], [20] for $0 < \mu < 2$ according to the projections onto convex sets (POCS) theory [13], [95], [56].

If the intersection of hyperplanes is an empty set, then the updated weight vector simply satisfies the last hyperplane equation. In other words, it tracks decisions of the oracle by assigning proper weights to the individual subalgorithms.

Another weight update algorithm can be developed by defining hyperslabs in $\mathbb{R}^M$ as follows:

$$y(x,n) - \epsilon \leq \mathbf{D}^T(x,n)\mathbf{w} \leq y(x,n) + \epsilon \tag{6.32}$$

where $\epsilon > 0$ is an artificially introduced positive number such that hyperslabs defined at different time instants produce a nonempty intersection set. In Eq. 6.32, if $y(x,n) = 1$ then $y(x,n) - \epsilon \geq 0$ and if $y(x,n) = -1$ then $y(x,n) + \epsilon < 0$.

Furthermore, when $y(x,n) = 1$, the upper bound can be simply removed and projections can be performed onto the half-spaces. A half-space can be defined

as follows:

$$\mathbf{D}^T(x,n)\mathbf{w} \geq 0 \tag{6.33}$$

In other words, weighted combination of decision values of sub-algorithms must be greater than 0, because the oracle states that $y(x,n) = 1$.

Weights, $w_i(n) \geq 0$, are kept non-negative in the weight update step to detect smoke. Each $w_i(n) \geq 0$ corresponds to a half-space which are closed and convex. Therefore, the POCS theory can be applied to this case as well. Whenever a weight happens to be negative, its projection onto the half-space $w_i(n) \geq 0$ is taken as 0.

For $y(x,n) = -1$, we have

$$\mathbf{D}^T(x,n)\mathbf{w} < 0 \tag{6.34}$$

In this case, the weight update equation for $y(x,n) = 1$ will be

$$\mathbf{w}(n+1) = \begin{cases} \mathbf{w}(n), & \text{if } \mathbf{D}^T(x,n)\mathbf{w} > 0 \\ \mathbf{w}(n) + \mu \frac{e(x,n)}{||\mathbf{D}(x,n)||^2}\mathbf{D}(x,n), & \text{otherwise} \end{cases} \tag{6.35}$$

where $e(x,n) = \Gamma - \mathbf{D}^T(x,n)\mathbf{w}(n)$ and Γ is any positive number. With this choice, $\mathbf{w}(n+1)$ satisfies $\mathbf{D}^T(x,n)\mathbf{w}(n+1) > 0$ (for $\Gamma = 0$, the weights correspond to projection onto the hyperplane $\mathbf{D}^T(x,n)\mathbf{w}(n+1) = 0$).

For $y(x,n) = -1$, the weight update equation will be

$$\mathbf{w}(n+1) = \begin{cases} \mathbf{w}(n), & \text{if } \mathbf{D}^T(x,n)\mathbf{w} < 0 \\ \mathbf{w}(n) + \mu \frac{e(x,n)}{||\mathbf{D}(x,n)||^2}\mathbf{D}(x,n), & \text{otherwise} \end{cases} \tag{6.36}$$

where $e(x,n) = \Upsilon - \mathbf{D}^T(x,n)\mathbf{w}(n)$ and Υ is any positive number.

It is almost impossible to know whether hyperplanes have a nonempty intersection set for this computer vision application. However, half-spaces defined by Eqs. 6.33 and 6.34 and they probably have a nonempty intersection set. As a result, weight updates do not diverge [95].

This set theoretic framework with tracking capability is especially useful when the on-line active learning problem is of dynamic nature with drifting concepts [72]. In this problem, the nature of forestal recordings vary over time due

Active Decision Fusion(x,n)
for $i = 1$ to M **do**
  $w_i(0) = \frac{1}{M}, Initialization$
end for
$\hat{y}(x,n) = \sum_i w_i(n) D_i(x,n)$
if $\hat{y}(x,n) \geq 0$ **then**
  return 1
else
  return -1
end if
$e(x,n) = y(x,n) - \hat{y}(x,n)$
for $i = 1$ to M **do**
  $w_i(n) \leftarrow w_i(n) + \mu \frac{e(x,n)}{||\mathbf{D}(x,n)||^2} D_i(x,n)$
end for

Figure 6.5: The pseudo-code for the active decision fusion algorithm

to weather conditions and changes in illumination which makes it necessary to deploy an adaptive wildfire detection system. It is not feasible to develop one strong fusion model with fixed weights in this setting with drifting nature. An ideal on-line active learning mechanism should keep track of drifts in video and adapt itself accordingly. The projections in Eqs. 6.19, 6.30, 6.35, and 6.36 adjust the importance of individual sub-algorithms by updating the weights according to the decisions of the oracle.

6.4 Experimental Results

The proposed wildfire detection scheme with LMS based active learning method is implemented on a PC with an Intel Core Duo CPU 1.86GHz processor and tested with forest surveillance recordings captured from cameras mounted on top of forest watch towers near Antalya and Mugla regions in Turkey. *The installed system successfully detected three forest fires in the summer of 2008.*

The proposed active decision fusion strategy is compared with the universal linear predictor (ULP) scheme proposed by Oza [58], [59], and Singer and Feder [74] for online active learning. In the ULP scheme, decisions of individual

Universal Predictor(x,n)
for $i = 1$ to M **do**
  $w_i(0) = \frac{1}{M}, Initialization$
end for
$\hat{y}_u(x,n) = \sum_i v_i(n) D_i(x,n)$
if $\hat{y}_u(x,n) \geq 0$ **then**
  return 1
else
  return -1
end if
for $i = 1$ to M **do**
  $v_i(n+1) = \frac{exp(-\frac{1}{2c}\ell(y(x,n),D_i(x,n)))}{\sum_j exp(-\frac{1}{2c}\ell(y(x,n),D_j(x,n)))}$
  $\ell(y(x,n), D_i(x,n)) = [y(x,n) - D_i(x,n)]^2$
end for

Figure 6.6: The pseudo-code for the universal predictor

algorithms are linearly combined similar to Eq. 6.9 as follows:

$$\hat{y}_u(x,n) = \sum_i v_i(n) D_i(x,n) \tag{6.37}$$

where the weights, $v_i(n)$, are updated according to the ULP algorithm, which assumes that the data (or confidence values $D_i(x,n)$, in our case) is governed by some unknown probabilistic model P [74]. The objective of a universal predictor is to minimize the expected cumulative loss. An explicit description of the weights, $v_i(n)$, of the ULP algorithm is given as follows:

$$v_i(n+1) = \frac{exp(-\frac{1}{2c}\ell(y(x,n), D_i(x,n)))}{\sum_j exp(-\frac{1}{2c}\ell(y(x,n), D_j(x,n)))} \tag{6.38}$$

where c is a normalization constant and the loss function for the i-th decision function is:

$$\ell(y(x,n), D_i(x,n)) = [y(x,n) - D_i(x,n)]^2 \tag{6.39}$$

The constant c is taken as 4 as indicated in [74]. The universal predictor based algorithm is summarized in Fig. 6.6.

We also implemented the Weighted Majority Algorithm (WMA) as the decision fusion step [47]. The WMA is summarized in Fig. 6.7 [58]. In WMA, as opposed to our method, individual decision values from sub-algorithms are

Weighted Majority(x,n)
for $i = 1$ to M **do**
  $w_i(0) = \frac{1}{M}$, Initialization
end for
if $\sum_{i:d_i(x,n)=1} w_i(n) \geq \sum_{i:d_i(x,n)=-1} w_i(n)$ **then**
  return 1
else
  return -1
end if
for $i = 1$ to M **do**
  if $d_i(x,n) \neq y$ **then**
    $w_i(n+1) \leftarrow \frac{w_i(n)}{2}$
  end if
end for

Figure 6.7: The pseudo-code for the Weighted Majority Algorithm

binary, i.e., $d_i(x,n) \in \{-1,1\}$, which are simply the quantized version of real valued $D_i(x,n)$ defined in Section 6.2. In the WMA, the weights of sub-algorithms yielding contradictory decisions with that of the oracle are reduced by a factor of two in an un-controlled manner, unlike the proposed LMS based algorithm and the ULP scheme. Initial weights for WMA are taken as $\frac{1}{M}$, as in the proposed LMS based scheme.

The LMS based scheme, the ULP based scheme, the WMA based scheme, and the non-adaptive approach with fixed weights are compared with each other in the following experiments. In Tables 6.1 and 6.2, 6-hour-long forest surveillance recordings containing actual forest fires and test fires as well as video sequences with no fires are used.

We have 7 actual forest fire videos and 5 test fire videos ranging from 2 km to 8 km captured in Antalya and Mugla regions in Turkey, in the summers of 2007 and 2008. All of the above mentioned decision fusion methods detect forest fires within 8 seconds, as shown in Table 6.1. The detection rates of the methods are comparable to each other. On the other hand, the proposed adaptive fusion strategy significantly reduces the false alarm rate of the system by integrating the feedback from the guard (oracle) into the decision mechanism within the active learning framework described in Section 6.3. In Fig. 6.8 a typical false alarm

issued for shadows of clouds by an untrained algorithm with decision weights equal to $\frac{1}{4}$ is presented as a sequence of snapshots taken at seconds 1, 7, 13 and 18 from the clip $V15$. The proposed algorithm does not produce a false alarm in this video.

When a false alarm is issued by the compound algorithm, the learning process is much faster for the LMS based scheme in comparison to the ULP and WMA based methods. This is reflected in Fig. 6.9, in which the average squared error functions $\bar{E}_{LMS}(n)$, $\bar{E}_{ULP}(n)$ and $\bar{E}_{WMA}(n)$ at image frame n, for the LMS, ULP and the WMA based methods are shown, respectively. The average squared error values are computed over all x in the image frame n, and defined as:

$$\bar{E}(n) = \frac{1}{N_I} \sum_{x} (e(x,n))^2 \tag{6.40}$$

where N_I is the total number of pixels in the image frame, $e(x,n) = y(x,n) - \hat{y}(x,n)$ and $\hat{y}(x,n) = \sum_i w_i D_i(x,n)$. The average squared error values $\bar{E}_{LMS}(n)$, $\bar{E}_{ULP}(n)$ and $\bar{E}_{WMA}(n)$ are computed after the first false alarm is issued. The average squared error value $\bar{E}_{LMS}(n)$ corresponding to the LMS based scheme decays fast reaching around 0 within 5 frames of video which is about 1 sec. It takes about 3 sec and 6 sec for the average squared error values $\bar{E}_{ULP}(n)$ and $\bar{E}_{WMA}(n)$ corresponding to the ULP and the WMA based schemes to converge.

The proposed LMS based method produces the lowest number of false alarms in our data set. A set of video clips containing moving cloud shadows is used to generate Table 6.2. These video clips are especially selected. Number of image frames in which false alarms are issued by different methods are presented in Table 6.2. Total number of false alarms for the clips in Table 6.2 issued by the methods (a) the LMS based scheme, (b) the ULP based scheme, (c) the WMA based scheme and (d) the non-adaptive approach with fixed weights are 5, 93, 240 and 612, respectively.

The software is currently being used in 10 forest watch towers in Antalya and Mugla regions. We tested the system live and monitored the number of false alarms for two days in September 2008. The current system produces 0.25 false alarms per hour. This is an acceptable rate for a look-out tower.

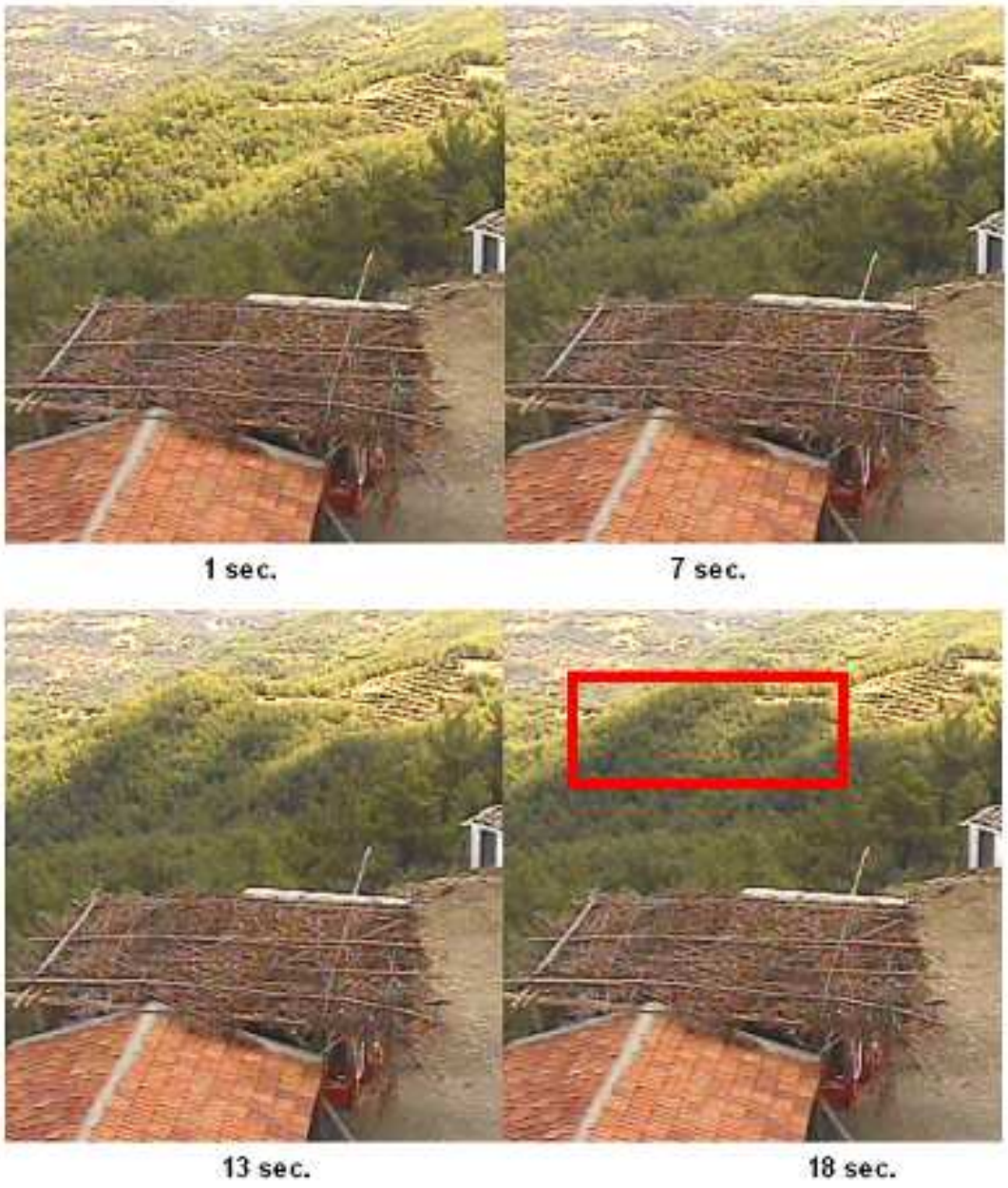

Figure 6.8: Sequence of frames excerpted from clip $V15$. Within 18 seconds of time, cloud shadows cover forestal area which results in a false alarm in an untrained algorithm with decision weights equal to $\frac{1}{4}$ depicted as a bounding box. The proposed algorithm does not produce a false alarm in this video.

Table 6.1: Frame numbers at which an alarm is issued with different methods for wildfire smoke captured at various ranges and fps. It is assumed that the smoke starts at frame 0.

Video Sequence	Range (km)	Capture Frame Rate (fps)	Frame number at which an alarm is issued			
			LMS Based	Universal	WMA Based	Fixed Weights
V1	4	7	24	22	28	20
V2	8	7	44	48	40	51
V3	2	7	28	35	38	29
V4	3	5	33	38	26	37
V5	5	10	58	67	69	41
V6	6	10	40	41	38	32
V7	6	10	38	36	30	35
V8	6	10	53	57	56	47
V9	6	10	67	71	56	71
V10	3	5	28	34	32	35
V11	5	7	42	40	36	39
V12	5	7	51	55	54	44

6.5 Summary

An automatic wildfire detection algorithm using an LMS based active learning capability is developed. The compound algorithm comprises of four sub-algorithms yielding their own decisions as confidence values in the range $[-1, 1] \in \mathbb{R}$. The LMS based adaptive decision fusion strategy takes into account the feedback from guards of forest watch towers. Experimental results show that the learning duration is decreased with the proposed online active learning scheme. It is also observed that false alarm rate of the proposed LMS based method is the lowest in our data set, compared to universal linear predictor (ULP) and weighted majority algorithm (WMA) based schemes.

The tracking capability of the LMS algorithm is analyzed using a set theoretic framework. The proposed framework for decision fusion is suitable for problems with concept drift. At each stage of the LMS algorithm, the method tracks the changes in the nature of the problem by performing an orthogonal projection onto a hyperplane describing the decision of the oracle.

Table 6.2: The number of false alarms issued by different methods to video sequences without any wildfire smoke.

Video Sequence	Frame Rate (fps)	Video Duration (sec.)	Number of frames with false alarm			
			LMS Based	Universal	WMA Based	Fixed Weights
V13	7	100	0	16	37	73
V14	10	100	0	11	48	172
V15	10	100	0	13	28	116
V16	5	100	0	9	19	41
V17	5	100	2	6	24	59
V18	7	100	1	15	32	67
V19	7	100	2	23	52	84

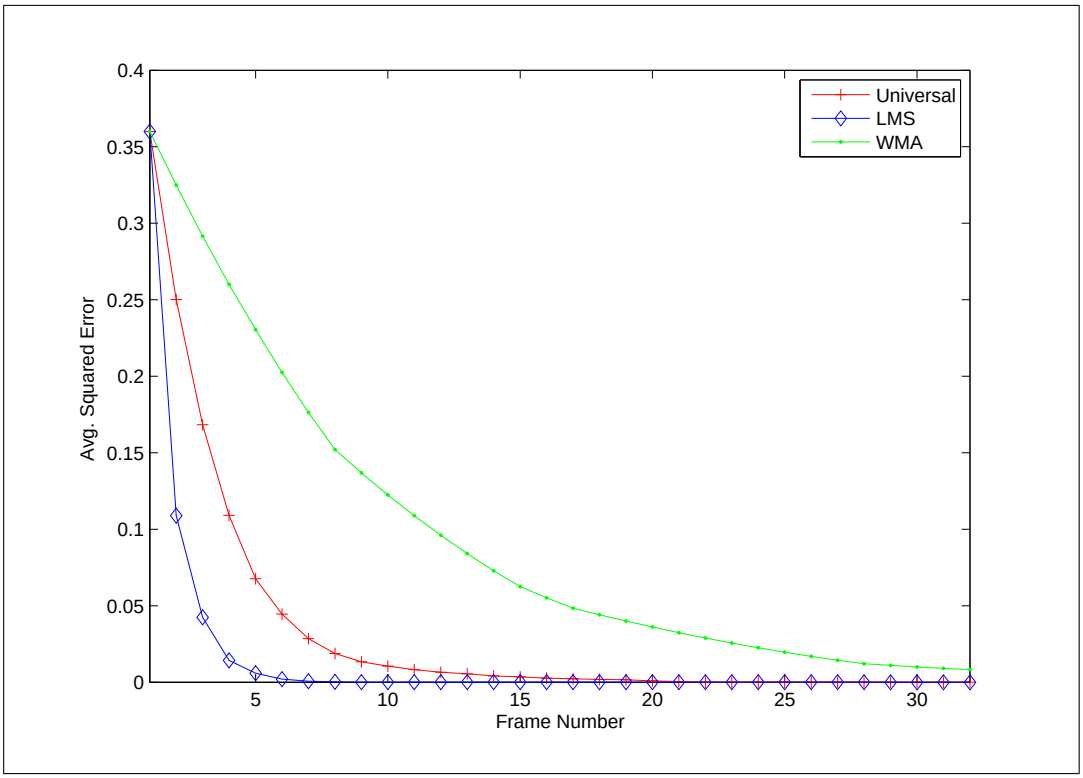

Figure 6.9: The average error curves for the LMS, universal predictor, and the WMA based adaptation algorithms in clip $V13$. All of the algorithms converge to the same average error value in this case, however the convergence rate of the LMS algorithm is faster than both the universal predictor and the WMA algorithm.

Chapter 7

Conclusion and Future Work

Fire detection systems are vital in saving people's lives, and preventing hazards before they get out of control. Particle based detectors are commonly used in such systems. These sensors are sensitive to produced during fire. An alarm is issued only if these chemicals physically reach the sensor and their presence is detected by either ionization or photometry. This requirement makes these sensors dependent on the distance to fireplace as well as their location. Besides, these sensors cannot be used outdoors. Image and video based systems can be an alternative to particle sensors for fire detection.

In this thesis, we developed novel signal and image analysis techniques for automatic fire detection using cameras and infra-red sensors. Fire detection problem can be also viewed as a problem of recognition of a specific dynamic texture type in video. Dynamic texture and flame and smoke behavior can be modeled using stochastic methods. In this thesis, we used Markov models which are tailored for flame and smoke detection. We developed specific methods for flame, smoke and wildfire smoke which have various spatio-temporal characteristics.

We developed dedicated methods for various aspects of fire using different types of sensors. We explicitly developed real-time methods for

- short-range ($< 30m$) flame detection in visible range video,

- short-range ($< 30m$) flame detection in long-wave infra-red (LWIR) video,

- short-range smoke detection in visible range video,

- short-range flame detection using pyro-electric infra-red (PIR) sensor, and

- long-range ($> 100m$) smoke detection in visible range video.

Each type of sensor has its own advantages and disadvantages on visualizing different aspects of fire. Flames are visible when viewed by visible and IR sensors. Although flame flicker becomes hard to observe as distance to the location of fire increases. As a result, methods for short-range flame detection by IR and visible sensors are proposed. Gradual increase in temperature can be monitored with IR cameras and PIR sensors which can be helpful to take precautions even before a fire starts. However, smoke, which is an early indicator of smoldering fires, is transparent for LWIR cameras and PIR sensors. Consequently, smoke detection is not possible using IR sensors. Smoke detection, both short and long-range, is only possible with visible range cameras. Since long-range smoke has different spatio-temporal characteristics than nearby smoke, separate algorithms are developed for each case.

One common novelty that is introduced in all of the methods developed for fire detection using several types of sensors is that flicker process in fire is characterized using Markov models trained with wavelet based feature signals. Flicker was not thoroughly characterized by previous studies on video based fire detection, which resulted in higher false alarm rates. Flicker modeling in a Markovian setting suits well with the stochastic nature of fire. Besides, sub-band analysis (or wavelet analysis) extracts non-stationarity inherent in flames and smoke. The use of wavelet transform based feature signals, leads to the development of computationally efficient algorithms that work in real-time running on a standard PC.

Another important contribution of the thesis is the introduction of a novel set theoretic framework for decision fusion and on-line active learning. As described throughout the thesis, all of the proposed algorithms are composed of several sub-algorithms yielding their own decisions and confidence values about the observed

phenomenon. In the last stage of each detection algorithm, individual decisions from sub-algorithms are combined together to reach a final decision. A least-mean-square (LMS) based active decision fusion strategy is proposed and this framework is successfully applied in the decision fusion step of the long-range wildfire detection method.

The LMS adaptive decision fusion framework takes into account the feedback from an oracle (security-guard) whose decisions are taken as the ground-truth. Individual sub-algorithm weights are updated in such a way that the final decision tracks the classification results of the oracle at each time step. At each stage of the LMS algorithm, the method tracks the changes in the nature of the problem by performing an orthogonal projection onto a hyperplane describing the decision of the oracle. Therefore, the proposed framework for decision fusion may provide insight in problems with drifting concepts belonging to many other research areas in machine learning applications including computer vision.

The proposed wildfire detection method is integrated into forest fire early warning systems which are installed in ten forest watch towers in Turkey. Our system successfully did not miss any smoke due to test fires. It also detected three forest fires in their early stages in Antalya and Aksehir regions in the summer of 2008. The system is developed to assist the guard in fire detection. The Directorate of Forestry and Ministry of Environment and Forestry of Turkey will install the system to other forestal areas under high risk of fire in upcoming years.

In this thesis, we developed signal and image processing algorithms for fire detection dedicated to sensing modalities like visible range and LWIR cameras, and PIR senors. In the proposed setting, just a single type of sensor is assumed to monitor an area of interest for each sensing modality.

A natural future direction pertains to extending both the number and types of sensors covering an indoor or an outdoor area of interest. This extension requires the development of algorithms that efficiently extract useful information from multitude of sensors and interpret them to reach a final decision. The same analysis algorithms may be used for each sensor. However, overall decision can be given by linearly combining sensor outputs that define confidence levels for

each sensor. The proposed set theoretic framework can be used to actively adapt individual sensor weights in accordance with the feedback from an oracle.

Bibliography

[1] B. Albers and A. Agrawal. Schlieren analysis of an oscillating gas-jet diffusion. *Combustion and Flame*, 119:84–94, 1999.

[2] H. Ammann, R. Blaisdell, M. Lipsett, S. Stone, S. Therriault, J. W. P. Jenkins, and K. Lynch. Wildfire smoke - A guide for public health officials, `http://depts.washington.edu/wildfire/pubhlthguidev.9.0.pdf`, Accessed at December 2008.

[3] M. Bagci, Y. Yardimci, and A. Cetin. Moving object detection using adaptive subband decomposition and fractional lower order statistics in video sequences. *Signal Processing*, pages 1941–1947, 2002.

[4] I. Bosch, S. Gomez, L. Vergara, and J. Moragues. Infrared image processing and its application to forest fire surveillance. In *Proceedings of the IEEE Conference on Advanced Video and Signal Based Surveillance (AVSS)*, pages 283–288, 2007.

[5] J. A. Broadbent. Fundamental flame flicker monitoring for power plant boilers. In *Proceedings of the IEE Seminar on Advanced Sensors and Instrumentation Systems for Combustion Processes*, pages 4/1–4/4, 2000.

[6] H. Bunke and T. C. (Eds.). *HMMs Applications in Computer Vision*. World Scientific, 2001.

[7] F. Carter and N. Cross. Combustion monitoring using infrared array-based detectors. *Measurement Science and Technology*, 14:1117–1122, 2003.

[8] CAVIAR: Context Aware Vision using Image-based Active Recognition. Test Case Scenarios - EC Funded CAVIAR project/IST 2001 37540, `http://homepages.inf.ed.ac.uk/rbf/caviar/`, Accessed at December 2008.

[9] A. Cetin, M. Akhan, B. Toreyin, and A.Aksay. Characterization of motion of moving objects in video. *US Patent No. 20040223652, pending*, 2004.

[10] A. Cetin and R. Ansari. Signal recovery from wavelet transform maxima. *IEEE Transactions on Signal Processing*, 42:194–196, 1994.

[11] A. Cetin and R. Ansari. Signal recovery from wavelet transform maxima. *IEEE Transactions on Signal Processing*, 42:194–196, 1994.

[12] A. Cetin and D. Chetverikov. Dynamic Texture Detection in Video Showcase, Multimedia Understanding through Semantics and Learning, EC Sponsored Network of Excellence, MUSCLE-NoE, `http://www.muscle-noe.org/content/view/145/64/`, Accessed at December 2008.

[13] E. Cetin. Reconstruction of Signals from Fourier Transform Samples. *Signal Processing*, 16:129–148, 1989.

[14] D. Chamberlin and A. Rose. The flicker of luminous flames. In *Proceedings of the First International Symposium on Combustion*. The Combustion Institute, 1928.

[15] A. Chan and N. Vasconcelos. Layered dynamic textures. In *Proceedings of the Conference on Neural Information Processing Systems (NIPS)*, pages 203–210, December 2005.

[16] A. Chan and N. Vasconcelos. Modeling, clustering, and segmenting video with mixtures of dynamic textures. *IEEE Transactions on Pattern Analysis and Machine Intelligence*, 30(5):909–926, 2008.

[17] T. Chen, P. Wu, and Y. Chiou. An early fire-detection method based on image processing. In *Proceedings of the IEEE International Conference on Image Processing (ICIP)*, pages 1707–1710, 2004.

[18] D. Chetverikov and R. Peteri. A brief survey of dynamic texture description and recognition. In *Proceedings of the Fourth International Conference on Computer Recognition Systems (CORES)*, pages 17–26, 2005.

[19] R. Collins, A. Lipton, and T. Kanade. A system for video surveillance and monitoring. In *Proceedings of the 8-th International Topical Meeting on Robotics and Remote Systems*. American Nuclear Society, April 1999.

[20] P. L. Combettes. The foundations of set theoretic estimation. *Proceedings of the IEEE*, 81(2):182–208, 1993.

[21] J. Davis and A. Bobick. The representation and recognition of action using temporal templates. In *Proceedings of the IEEE Conference on Computer Vision and Pattern Recognition (CVPR)*, pages 928–934, 1997.

[22] J. M. de Dios, B. Arrue, A. Ollero, L. Merino, and F. Gomez-Rodriguez. Computer vision techniques for forest fire perception. *Image and Vision Computing*, 26(4), 2008.

[23] Y. Dedeoglu, B. Töreyin, U. Gudukbay, and A. Cetin. Real-time fire and flame detection in video. In *Proceedings of the IEEE International Conference on Acoustics, Speech and Signal Processing (ICASSP)*, pages 669–672, 2005.

[24] Y. Dedeoglu, B. Töreyin, U. Gudukbay, and A. Cetin. *Multimodal Processing and Interaction: Audio, Video, and Text*, chapter 6 - Surveillance Using Both Video and Audio, pages 143–155. P. Maragos, A. Potamianos, P. Gros. (Eds.) Springer Science+Business Media, LLC, 2008.

[25] H. Dreyfus. *What Computers Can't Do*. 1972.

[26] H. Dreyfus. *What Computers Still Can't Do: A Critique of Artificial Reason*. MIT Press, 1992.

[27] R. O. Duda, P. E. Hart, and D. G. Stork. *Pattern Classification*. Wiley-Interscience Publication, 2000.

[28] R. Fablet and P. Bouthemy. Motion recognition using nonparametric image motion models estimated from temporal and multiscale co-occurrence statistics. *IEEE Transactions on Pattern Analysis and Machine Intelligence*, 25:1619–1624, 2003.

[29] S. Fazekas and D. Chetverikov. Analysis and performance evaluation of optical flow features for dynamic texture recognition. *Signal Processing:Image Communication*, 22(7-8):680–691, 2007.

[30] R. Fisher (Ed.). CVonline: The Evolving, Distributed, Non-Proprietary, On-Line Compendium of Computer Vision, `http://homepages.inf.ed.ac.uk/rbf/cvonline/`, Accessed at December 2008.

[31] G. L. Foresti, C. S. Regazzoni, and P. K. V. (Eds.). *Multisensor Surveillance Systems - The Fusion Perspective*. Kluwer Academic Publishers, 2003.

[32] D. Forsyth and J.Ponce. *Computer Vision: A Modern Approach*. Prentice Hall, 2002.

[33] K. Fujita and S. Nayar. Recognition of dynamic textures using impulse responses of state variables. In *Proceedings of the Third International Workshop on Texture Analysis and Synthesis (Texture)*, pages 31–36, 2003.

[34] O. N. Gerek and A. E. Cetin. Adaptive polyphase subband decomposition structures for image compression. *IEEE Transactions on Image Processing*, 9:1649–1659, October 2000.

[35] A. Ghoreyshi and R. Vidal. Segmenting Dynamic Textures with Ising Descriptors, ARX Models and Level Sets. In *Proceedings of the European Conference on Computer Vision / Dynamical Vision Workshop (ECCV/DV)*, 2006.

[36] P. Guillemant and J. Vicente. Real-time identification of smoke images by clustering motions on a fractal curve with a temporal embedding method. *Optical Engineering*, 40:554–563, 2001.

[37] S. Haykin. *Adaptive Filter Theory*. Prentice Hall, 2002.

[38] G. Healey, D. Slater, T. Lin, B. Drda, and A. Goedeke. A system for real-time fire detection. In *Proceedings of the IEEE Conference on Computer Vision and Pattern Recognition (CVPR)*, pages 15–17, 1993.

[39] M. Hefeeda and M. Bagheri. Wireless sensor networks for early detection of forest fires. In *Proceedings of the International Workshop on Mobile Ad hoc and Sensor Systems for Global and Homeland Security (MASS-GHS)*, October 2007.

[40] F. Heijden. *Image Based Measurement Systems: Object Recognition and Parameter Estimation*. Wiley, 1996.

[41] T. Horprasert, D. Harwood, and L. Davis. A statistical approach for real-time robust background subtraction and shadow detection. In *Proceedings of the IEEE International Conference on Computer Vision/FRAME-RATE Workshop (CVPR/FR)*, 1999.

[42] H. Huang, Y. Yan, G. Lu, and A. Reed. On-line flicker measurement of gaseous flames by imaging processing and spectral analysis. *Measurement Science and Technology*, 10:726–733, 1999.

[43] O. Javed and M. Shah. Tracking and object classification for automated surveillance. In *Proceedings of the European Conference on Computer Vision (ECCV)*, pages 343–357, 2002.

[44] S. Khare and S. Negi. Thermal (infrared) imaging sensors. *Defence Science Journal*, 57(3):173–183, 2007.

[45] C. Kim, R. Ansari, and A. Cetin. A class of linear-phase regular biorthogonal wavelets. In *Proceedings of the IEEE International Conference on Acoustics, Speech and Signal Processing (ICASSP)*, pages 673–676, 1992.

[46] J. Li, Q. Qi, X. Zou, H. Peng, L. Jiang, and Y. Liang. Technique for automatic forest fire surveillance using visible light image. In *Proceedings of the International Geoscience and Remote Sensing Symposium*, volume 5, pages 31–35, 2005.

[47] N. Littlestone and M. Warmuth. The weighted majority algorithm. *Information and Computation*, 108:212261, 1994.

[48] C. Liu and N. Ahuja. Vision based fire detection. In *Proceedings of the International Conference on Pattern Recognition (ICPR)*, volume 4, 2004.

[49] C.-B. Liu, R.-S. Lin, and N. Ahuja. Modeling dynamic textures using subspace mixtures. In *Proceedings of the IEEE International Conference on Multimedia and Expo (ICME)*, 2005.

[50] C.-B. Liu, R.-S. Lin, N. Ahuja, and M.-H. Yang. Dynamic textures synthesis as nonlinear manifold learning and traversing. In *Proceedings of the 17th British Machine Vision Conference (BMVC)*, pages 859–868, 2006.

[51] Z. Lu, W. Xie, J. Pei, and J. Huang. Dynamic texture recognition by spatio-temporal multiresolution histogram. In *Proceedings of the IEEE Workshop on Motion and Video Computing (WACV/MOTION)*, volume 2, pages 241–246, 2005.

[52] S. Mallat and S. Zhong. Characterization of signals from multiscale edges. *IEEE Transactions on Pattern Analysis and Machine Intelligence*, 14(7):710–732, 1992.

[53] R. Q. N. Haering and M. Sezan. Approach and its application to detecting hunts in wildlife video. *IEEE Transactions on Circuits and Systems for Video Technology*, 10(6):857–868, 2000.

[54] M. Naphade, T. Kristjansson, B. Frey, and T. Huang. Multimedia Objects (Multijects): A Novel Approach to Video Indexing and Retrieval in Multimedia Systems. In *Proceedings of the IEEE International Conference on Image Processing (ICIP)*, pages 536–540, 1998.

[55] R. Nelson and R. Polana. Qualitative recognition of motion using temporal texture. *Computer Vision, Graphics and Image Processing (CVGIP): Image Understanding*, 56:78–89, July 1992.

[56] U. Niesen, D. Shah, and G. Wornell. Adaptive alternating minimization algorithms. In *Proceedings of the IEEE International Symposium on Information Theory (ISIT)*, pages 1641–1645, June 2007.

[57] K. Otsuka, T. Horikoshi, S. Suzuki, and M. Fujii. Feature extraction of temporal texture based on spatiotemporal motion trajectory. In *Proceedings of the International Conference on Pattern Recognition (ICPR)*, volume 2, pages 1047–1051, 1998.

[58] N. Oza. *Online Ensemble Learning*. PhD thesis, Electrical Engineering and Computer Sciences, University of California, September 2001.

[59] N. Oza. Online bagging and boosting. In *Proceedings of the IEEE International Conference on Systems, Man and Cybernetics*, volume 3, pages 2340–2345, October 2005.

[60] B. Parhami. Voting algorithms. *IEEE Transactions on Reliability*, 43(4):617–629, 1994.

[61] T. Pavlidis. Computers versus Humans, `http://www.theopavlidis.com/comphumans/comphuman.htm`, Accessed at December 2008.

[62] C. Peh and L.-F. Cheong. Synergizing spatial and temporal texture. *IEEE Transactions on Image Processing*, 11:11791191, 2002.

[63] R. Peteri, M. Huiskes, and S. Fazekas. DynTex-A comprehensive database of Dynamic Textures `http://old-www.cwi.nl/projects/dyntex/`, Accessed at December 2008.

[64] W. Phillips, M. Shah, and N. Lobo. Flame recognition in video. *Pattern Recognition Letters*, 23:319–327, 2002.

[65] F. Porikli, Y. Ivanov, and T. Haga. Robust abandoned object detection using dual foregrounds. *EURASIP Journal on Advances in Signal Processing*, 2008(1):1–10, 2008.

[66] A. Prati, I. Mikic, M. Trivedi, and R. Cucchiara. Detecting moving shadows: Algorithms and evaluation. *IEEE Transactions on Pattern Analysis and Machine Intelligence*, 25:918923, 2003.

[67] L. Rabiner and B.-H. Juang. *Fundamentals of Speech Recognition*. Prentice-Hall Inc., 1993.

[68] A. Rahman and M. Murshed. Real-time temporal texture characterisation using block-based motion co-occurrence statistics. In *Proceedings of the IEEE International Conference on Image Processing (ICIP)*, pages 1593–1596, 2004.

[69] D. Reynolds and R. Rose. Robust text-independent speaker identification using gaussian mixture speaker models. *IEEE Transactions on Speech and Audio Processing*, 3(1):72–83, 1995.

[70] Y. Sahin. Animals as mobile biological sensors for forest fire detection. *Sensors*, 7(12):3084–3099, 2007.

[71] P. Saisan, G. Doretto, Y. Wu, and S. Soatto. Dynamic texture recognition. In *Proceedings of the IEEE Conference on Computer Vision and Pattern Recognition (CVPR)*, volume 2, pages 58–63, December 2001.

[72] J. Schlimmer and R. Granger. Incremental learning from noisy data. *Machine Learning, 1*, page 317354, 1986.

[73] B. Schnaufer and W. Jenkins. New data-reusing LMS algorithms for improved convergence. In *Proceedings of the Asilomar Conference, Pacific Groves, CA*, pages 1584–1588, 1993.

[74] A. Singer and M. Feder. Universal linear prediction by model order weighting. *IEEE Transactions on Signal Processing*, 47-10:2685–2699, 1999.

[75] J. Smith, C.-Y. Lin, and M. Naphade. Video texture indexing using spatiotemporal wavelets. In *Proceedings of the IEEE International Conference on Image Processing (ICIP)*, volume 2, pages 437–440, 2002.

[76] L. St-Laurent, D. Prvost, and X. Maldague. Thermal imaging for enhanced foreground-background segmentation. In *Proceedings of the 8-th International Conference on Quantitative InfraRed Thermography*, 2006.

[77] C. Stauffer and W. Grimson. Adaptive background mixture models for real-time tracking. In *Proceedings of the IEEE Conference on Computer Vision and Pattern Recognition (CVPR)*, volume 2, 1999.

[78] W. Straumann, D. Rizzotti, and N. Schibli. *Method and Device for Detecting Fires Based on Image Analysis*. European Patent EP 1,364,351, 2002.

[79] M. Szummer and R. W. Picard. Temporal texture modeling. In *Proceedings of the IEEE International Conference on Image Processing (ICIP)*, volume 3, pages 823–826, 1996.

[80] Y. Takatoshi. *Fire Detecting Device*. Japanese Patent 11,144,167, 1999.

[81] M. Thuillard. *Method and Device for Detecting Fires Based on Image Analysis*. US Patent 6,011,464, 1998.

[82] M. Thuillard. A new flame detector using the latest research on flames and fuzzy-wavelet algorithms. *Fire Safety Journal*, 37:371–380, 2002.

[83] B. Töreyin. Moving object detection and tracking in wavelet compressed video. Master's thesis, Bilkent University, Department of Electrical and Electronics Engineering, Ankara, Turkey, 2003.

[84] B. Töreyin, Y. Dedeoglu, and A. Cetin. Flame detection in video using hidden markov models. In *Proceedings of the IEEE International Conference on Image Processing (ICIP)*, pages 1230–1233, 2005.

[85] B. Töreyin, Y. Dedeoglu, and A. Cetin. HMM Based Falling Person Detection Using Both Audio and Video. In *Proceedings of the IEEE International Workshop on Human-Computer Interaction (HCI)*, volume 3766, pages 211–220, 2005.

[86] B. Töreyin, Y. Dedeoglu, and A. Cetin. Wavelet based real-time smoke detection in video. In *Proceedings of the 13-th European Signal Processing Conference (EUSIPCO)*, 2005.

[87] B. Töreyin, Y. Dedeoglu, U. Gudukbay, and A. Cetin. Computer vision based system for real-time fire and flame detection. *Pattern Recognition Letters*, 27:49–58, 2006.

[88] B. Töreyin, E. Soyer, I. Onaran, and A. Cetin. Falling person detection using multi-sensor signal processing. *EURASIP Journal on Advances in Signal Processing*, 2008(1):1–10, 2008.

[89] R. Vidal and A. Ravichandran. Optical flow estimation and segmentation of multiple moving dynamic textures. In *Proceedings of the IEEE Conference on Computer Vision and Pattern Recognition (CVPR)*, volume 2, pages 516–521, 2005.

[90] L.-Y. Wei and M. Levoy. Fast texture synthesis using tree-structured vector quantization. In *Proceedings of the 27-th International Conference on Computer Graphics and Interactive Techniques (ACM SIGGRAPH)*, pages 479–488, 2000.

[91] B. Widrow and M. Hoff. Adaptive switching circuits. In *Proceedings of the IRE WESCON (New York Convention Record)*, volume 4, pages 96–104, 1960.

[92] B. Widrow, J. McCool, M. Larimore, and C. Johnson. Stationary and nonstationary learning characteristics of the LMS adaptive filter. *Proceedings of the IEEE*, 64(8):1151–1162, 1976.

[93] B. Widrow and S. Stearns. *Adaptive Signal Processing*. Prentice Hall, 1985.

[94] Z. Xiong, R. Caballero, H. Wang, A. Finn, M. Lelic, and P.-Y. Peng. Video based Smoke Detection: Possibilities, Techniques, and Challenges, available at `http://vision.ai.uiuc.edu/~wanghc/papers/smoke_detection.pdf`, Accessed at December 2008.

[95] D. Youla and H. Webb. Image restoration by the method of convex projections, Part I-Theory. *IEEE Transactions on Medical Imaging*, MI-I-2:81–94, 1982.

[96] J. Zhong and S. Sclaroff. Segmenting foreground objects from a dynamic textured background via a robust kalman filter. In *Proceedings of the International Conference on Computer Vision (ICCV)*, pages 44–50, 2003.